Provided for non-commercial research and education use.
Not for reproduction, distribution or commercial use.

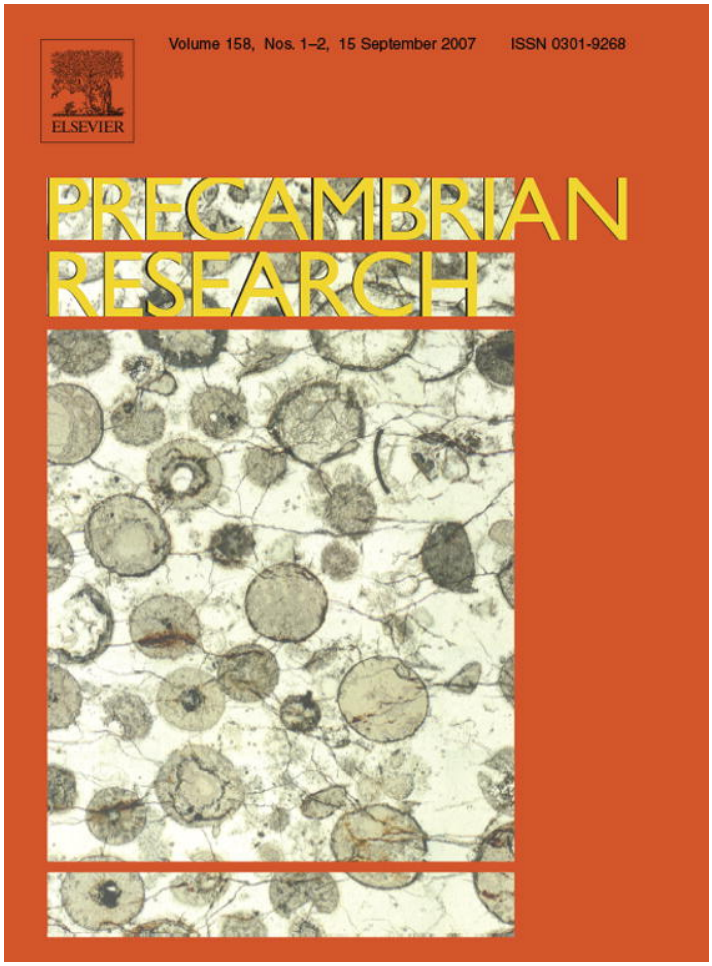

This article was published in an Elsevier journal. The attached copy is furnished to the author for non-commercial research and education use, including for instruction at the author's institution, sharing with colleagues and providing to institution administration.

Other uses, including reproduction and distribution, or selling or licensing copies, or posting to personal, institutional or third party websites are prohibited.

In most cases authors are permitted to post their version of the article (e.g. in Word or Tex form) to their personal website or institutional repository. Authors requiring further information regarding Elsevier's archiving and manuscript policies are encouraged to visit:

http://www.elsevier.com/copyright

Author's personal copy

Available online at www.sciencedirect.com
ScienceDirect
Precambrian Research 158 (2007) 17–50
Precambrian Research
www.elsevier.com/locate/precamres

Geology and metallogeny of the Ar Rayn terrane, eastern Arabian shield: Evolution of a Neoproterozoic continental-margin arc during assembly of Gondwana within the East African orogen

Jeff L. Doebrich [a,*], Abdullah M. Al-Jehani [b], Alim A. Siddiqui [b], Timothy S. Hayes [c], Joseph L. Wooden [d], Peter R. Johnson [b]

[a] *U.S. Geological Survey, 913 National Center,12201 Sunrise Valley Dr., Reston, VA 20192, USA*
[b] *Saudi Geological Survey, P.O. Box 54141, Jiddah 21514, Saudi Arabia*
[c] *U.S. Geological Survey, 520 N. Park Ave., Suite 355, Tucson, AZ 85719, USA*
[d] *U.S. Geological Survey, Mail Stop 937, 345 Middlefield Road, Menlo Park, CA 94025, USA*

Received 13 October 2006; received in revised form 11 April 2007; accepted 23 April 2007

Abstract

The Neoproterozoic Ar Rayn terrane is exposed along the eastern margin of the Arabian shield. The terrane is bounded on the west by the Ad Dawadimi terrane across the Al Amar fault zone (AAF), and is nonconformably overlain on the east by Phanerozoic sedimentary rocks. The terrane is composed of a magmatic arc complex and syn- to post-orogenic intrusions. The layered rocks of the arc, the Al Amar group (>689 Ma to ~625 Ma), consist of tholeiitic to calc-alkaline basaltic to rhyolitic volcanic and volcaniclastic rocks with subordinate tuffaceous sedimentary rocks and carbonates, and are divided into an eastern and western sequence. Plutonic rocks of the terrane form three distinct lithogeochemical groups: (1) low-Al trondhjemite-tonalite-granodiorite (TTG) of arc affinity (632–616 Ma) in the western part of the terrane, (2) high-Al TTG/adakite of arc affinity (689–617 Ma) in the central and eastern part of the terrane, and (3) syn- to post-orogenic alkali granite (607–583 Ma). West-dipping subduction along a trench east of the terrane is inferred from high-Al TTG/adakite emplaced east of low-Al TTG.

The Ar Rayn terrane contains significant resources in epithermal Au–Ag–Zn–Cu-barite, enigmatic stratiform volcanic-hosted Khnaiguiyah-type Zn–Cu–Fe–Mn, and orogenic Au vein deposits, and the potential for significant resources in Fe-oxide Cu–Au (IOCG), and porphyry Cu deposits. Khnaiguiyah-type deposits formed before or during early deformation of the Al Amar group eastern sequence. Epithermal and porphyry deposits formed proximal to volcanic centers in Al Amar group western sequence. IOCG deposits are largely structurally controlled and hosted by group-1 intrusions and Al Amar group volcanic rocks in the western part of the terrane. Orogenic gold veins are largely associated with north-striking faults, particularly in and near the AAF, and are presumably related to amalgamation of the Ar Rayn and Ad Dawadimi terranes.

Geologic, structural, and metallogenic characteristics of the Ar Rayn terrane are analogous to the Andean continental margin of Chile, with opposite subduction polarity. The Ar Rayn terrane represents a continental margin arc that lay above a west-dipping subduction zone along a continental block represented by the Afif composite terrane. The concentration of epithermal, porphyry Cu and IOCG mineral systems, of central arc affiliation, along the AAF suggests that the AAF is not an ophiolitic suture zone, but originated as a major intra-arc fault that localized magmatism and mineralization. West-directed oblique subduction and ultimate collision with a land mass from the east (East Gondwana?) resulted in major transcurrent displacement along the AAF, bringing the eastern part of the arc terrane to its present exposed position, juxtaposed across the AAF against a back-arc basin assemblage

* Corresponding author. Tel.: +1 703 648 6103; fax: +1 703 648 6057.
E-mail address: doebrich@usgs.gov (J.L. Doebrich).

0301-9268/$ – see front matter © 2007 Elsevier B.V. All rights reserved.
doi:10.1016/j.precamres.2007.04.003

Author's personal copy

represented by the Abt schist of the Ad Dawadimi terrane. Our findings indicate that arc formation and accretionary processes in the Arabian shield were still ongoing into the latest Neoproterozoic (Ediacaran), to about 620–600 Ma, and lead us to conclude that evolution of the Ar Rayn terrane (arc formation, accretion, syn- to postorogenic plutonism) defines a final stage of assembly of the Gondwana supercontinent along the northeastern margin of the East African orogen.
© 2007 Elsevier B.V. All rights reserved.

Keywords: Neoproterozoic; Arabian shield; Metallogeny; East African orogen; Ar Rayn terrane; Continental margin

1. Introduction

The Ar Rayn terrane (Delfour, 1981; Calvez et al., 1984; Johnson and Vranas, 1984; Stoeser and Camp, 1985) is exposed along the eastern margin of the Arabian shield (Fig. 1) and is defined by Neoproterozoic rocks east of the Al Amar fault (AAF) and west of an unconformity with Paleozoic epicratonic sedimentary rocks

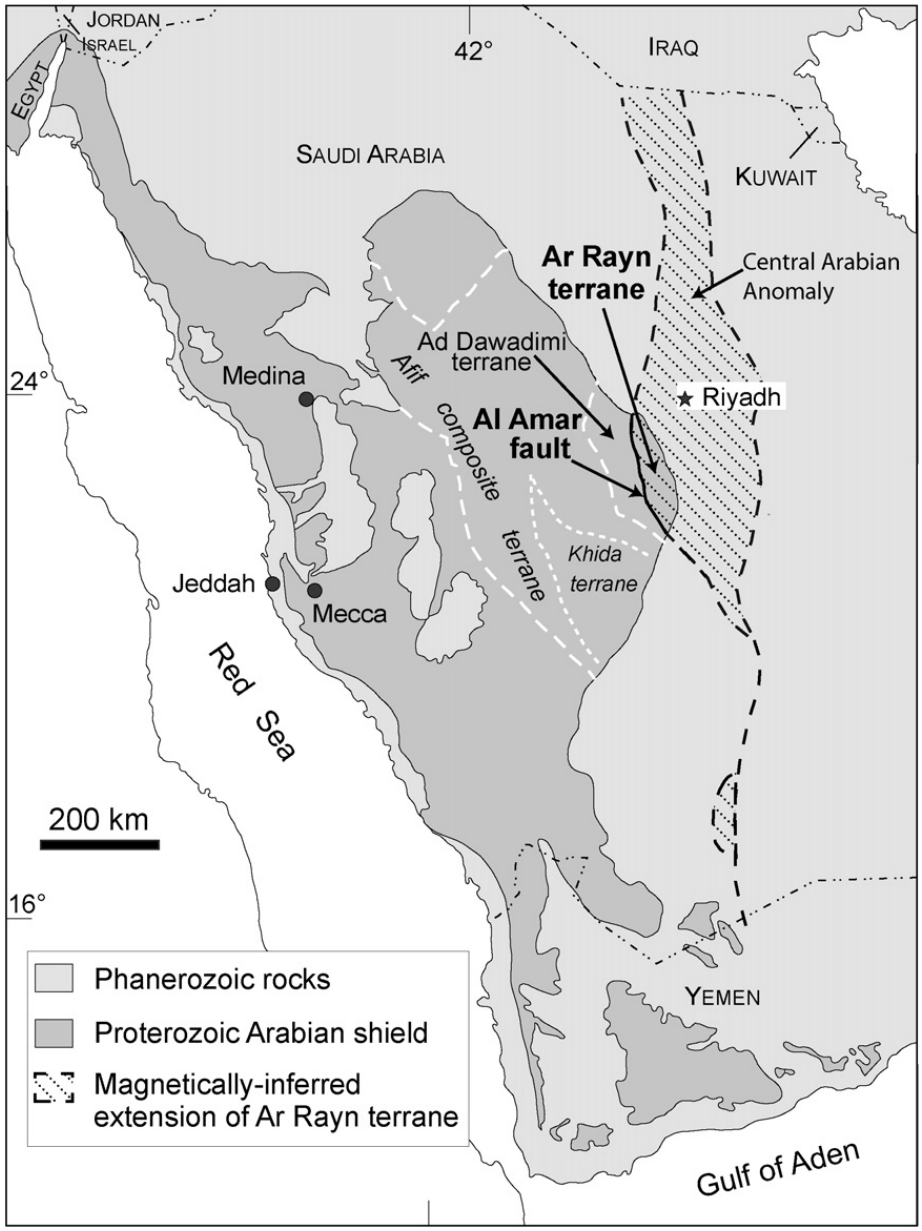

Fig. 1. Index map of the western part of the Arabian Peninsula showing the extent of the Arabian shield, the location of the Ar Rayn, Ad Dawadimi, and Afif composite terranes, and magnetically inferred margin of Neoproterozoic crust continuing beneath Phanerozoic cover (modified from Johnson and Stewart, 1995). Khida terrane from Stoeser et al. (2004), Stoeser and Frost (2006).

Author's personal copy

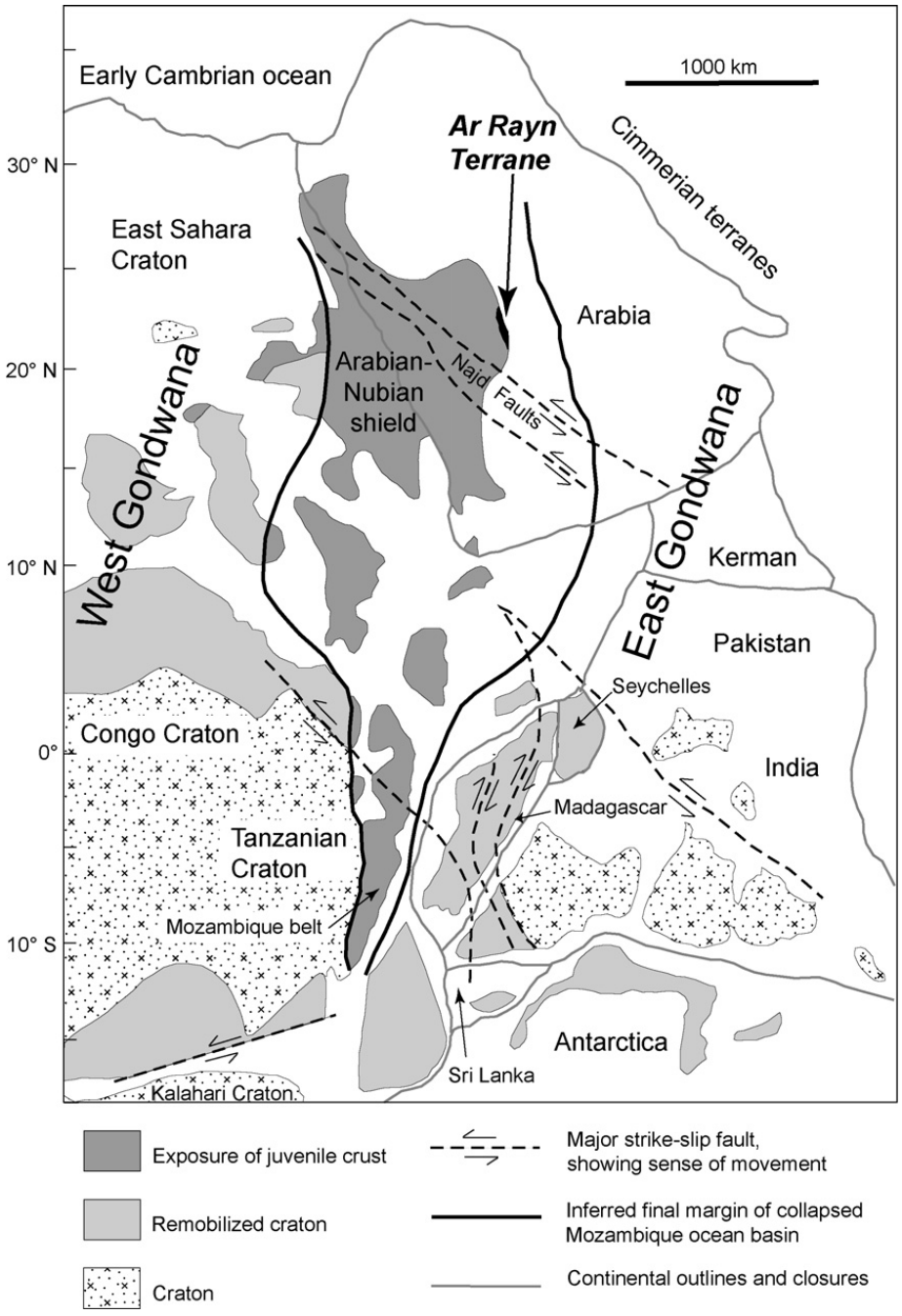

Fig. 2. Generalized map of the East African orogen (after Stern, 1994). Inferred boundary of collapsed Mozambique ocean basin based on geologic, isotopic, and magnetic data. Continental blocks are configured for the end of the Precambrian.

(Fig. 1). The AAF is a serpentinite- and listwaenite-bearing fault zone that separates the Abt schist of the Ad Dawadimi terrane to the west from the Ar Rayn terrane to the east (Fig. 1).

The Ar Rayn terrane represents the exposed part of a larger feature, perhaps a composite terrane, which is characterized by anomalously high magnetic values and is referred to as the central Arabian anomaly (Johnson and Stewart, 1995) (Fig. 1). This north-trending magnetic anomaly extends for hundreds of kilometers beneath Phanerozoic rocks east of the Arabian shield and is interpreted to represent the eastern margin of the Neoproterozoic East African orogen (Figs. 1 and 2; Stern, 1994; Johnson and Stewart, 1995). The East African orogen represents an accretionary collage of arc and microcontinental terranes that formed during the Neoproterozoic closure of the Mozambique Ocean during convergence and suturing of West and East Gondwana (Stern, 1994; Unrug, 1996; Fig. 2). The region is transected by a series of northwest-trending sinistral faults

Author's personal copy

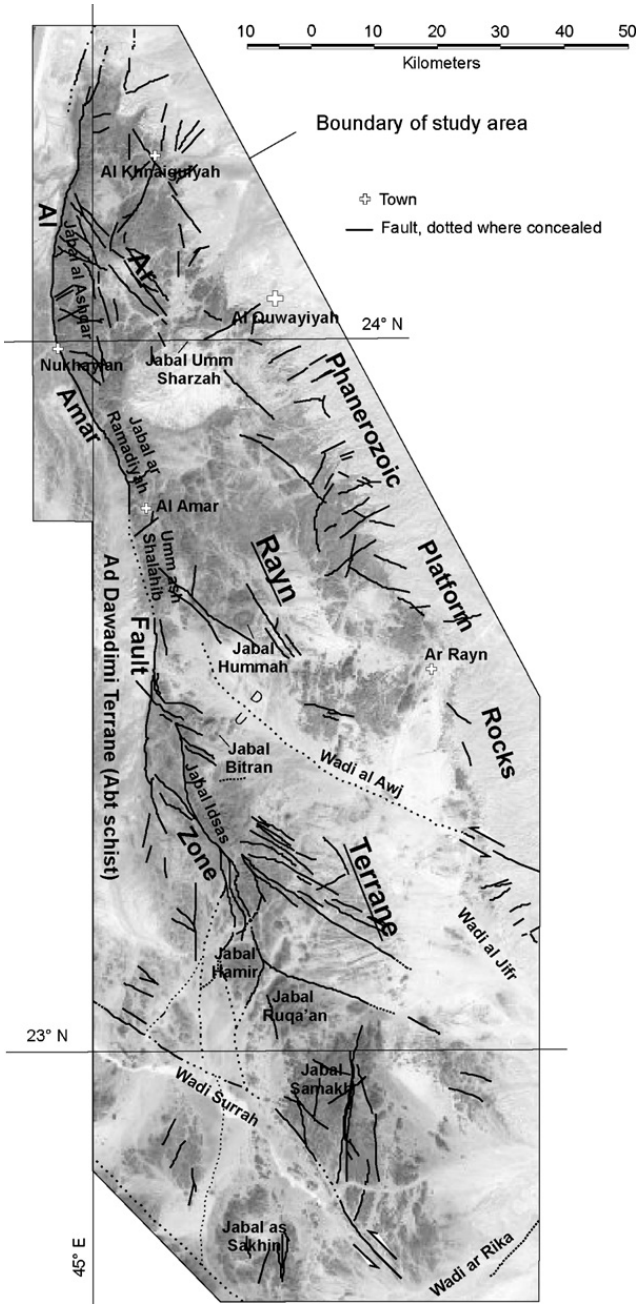

Fig. 3. Index map of the Ar Rayn terrane, with a Landsat 7 image base, showing selected towns and geographic features, and major regional faults.

(Najd faults; Figs. 2 and 3) that locally offset the Al Amar fault and other magnetically-inferred terrane boundaries. The Najd late- to post-orogenic transcurrent faulting event affected large areas of the northern and eastern Arabian shield between 630 and 530 Ma (Fleck et al., 1976; Stacey and Agar, 1985), and perhaps as early as 680 Ma (Johnson, 1996).

Despite its small area of exposure relative to other terranes of the Arabian shield, the Ar Rayn terrane has been the subject of considerable exploration and research since the 1950s (Doebrich et al., 2005). This is primarily because of its rich endowment in a variety of metallic mineral resources, which include the Al Amar Au–Ag–Zn–Cu-barite deposit, the Khnaiguiyah Zn–Cu–Fe–Mn deposits, the Jabal Idsas magnetite prospects, and many other precious- and base-metal prospects.

This paper is the culmination of recent geologic and mineral resource studies in the terrane that have generated new lithogeochemical, geochronologic, and mineral deposit data. This new data, when combined and interpreted with the wealth of existing data, provides the basis for an interpretation of the geotectonic setting of the eastern margin of the Arabian shield and East African orogen (Stern, 1994) and provides new constraints on the timing of Neoproterozoic assembly of Gondwana.

2. Terrane geology

The Neoproterozoic Ar Rayn terrane is composed of a volcanic arc complex, the Al Amar group (Calvez et al., 1984), and three distinct suites of plutonic rocks, all of which have undergone low-grade greenschist metamorphism. The Al Amar group consists of tholeiitic to calc-alkaline basaltic to rhyolitic volcanic and volcaniclastic rocks with subordinate tuffaceous sedimentary rocks and carbonates. The three suites of plutonic rocks were originally defined by Le Bel and Laval (1986) to represent arc-related (group-1), synorogenic (group-2) and postorogenic (group-3) intrusions. Additional data collected during this study confirms the three distinct groups based on lithogeochemistry. However, with new geochronologic data, we present petrogenetic interpretations for the groups that differ from Le Bel and Laval (1986).

2.1. Al Amar group rocks

The Al Amar group was divided by Vaslet et al. (1983) and Manivit et al. (1985b) into the Sidriyah and Shalahib formations. The Sidriyah formation is described as basaltic and andesitic volcanic and volcaniclastic rocks with subordinate marble and siltstone, whereas the Shalahib formation contains more felsic volcanic and volcaniclastic rocks, including rhyolite and dacite flows, tuffs, and ignimbrites with interlayered carbonate and cherty sedimentary rocks. The Sidriyah formation mainly underlies the Shalahib formation, however stratigraphic relationships are not always clear because of rapid lateral facies changes near volcanic centers. Ignimbrite in the Shalahib formation indicates emergent subaerial periods (Vaslet et al., 1983) and suggests that

Author's personal copy

the volcanic arc formed in fluctuating shallow marine and subaerial environments.

Vaslet et al. (1983) and Manivit et al. (1985b) noted a more metamorphosed eastern sequence and less metamorphosed and monoclinal western sequence of the Al Amar group rocks. This east-west variation in metamorphic and structural fabric also was noted during this study and is used as criteria to divide the rocks of the Al Amar group into distinct sequences. We maintain the use of the terms eastern and western sequence and abandon the use of Sidriyah and Shalahib formations (Vaslet et al., 1983; Manivit et al., 1985b) to subdivide the Al Amar group rocks into more clearly defined and mapable units. The eastern sequence rocks are exposed as septa and pendants throughout the central and eastern parts of the terrane, whereas the western sequence rocks are exposed as a narrow semi-continuous belt along the western margin of the terrane, and bounded on the west by the Al Amar fault (Fig. 4).

Rocks of both the eastern and western sequences of the Al Amar group range in composition from basalt to rhyolite (Fig. 5A). For purposes of comparing lithogeochemistry we have classified samples from each sequence as felsic extrusive rock, mafic-intermediate extrusive rock, and porphyritic felsic intrusions based on silica contents (Fig. 5A). Eastern and western sequence felsic volcanic rocks can be distinguished by their Rb, Sr, and Na contents (Fig. 5B). Eastern sequence felsic volcanic rocks have higher Rb and Sr, and lower Na contents than western sequence felsic volcanic rocks. This may be a function of deuteric or hydrothermal alteration (addition of Na and removal of Rb and Sr) of western sequence rocks. However, eastern sequence felsic volcanic rocks are also enriched in immobile trace elements (e.g., Y, Zr, Yb, and La; Fig. 6C and D) relative to equivalent western sequence rocks though REE geochemistry generally does not discriminate felsic volcanic rock of the two sequences (Fig. 7B). Differences in immobile trace-element lithogeochemistry, metamorphic grade and deformation style, and possible alteration of one sequence versus the other suggests that the two sequences formed separately in time and space.

The porphyritic felsic intrusions of the Al Amar group are trondhjemitic (Fig. 5C) and correspond to soda rhyolite and keratophyre protrusions and flow domes as defined by Felenc (1983a,b), Felenc et al. (1983), and Vadala et al. (1994). They are almost exclusively found in the northern half of the belt of western sequence rocks and display a lithogeochemical affinity to Al Amar group felsic volcanic rocks in general (Fig. 7B and C) and western sequence felsic volcanic rocks in particular (Fig. 5B, 6C and D). Based on lithogeochemical affinity and spatial distribution, these intrusions are interpreted to be hypabyssal subvolcanic phases of Al Amar group western sequence felsic extrusive rocks. They have played an important role in the metallogeny of the terrane, as they are spatially and presumed genetically related to epithermal-style Au–Ag–Zn–Cu-barite mineralization in the belt of western sequence rocks.

Minor- and trace-element compositions of volcanic and subvolcanic rocks of the Al Amar group indicate that they range from tholeiitic to calc-alkaline (Fig. 6). However, Fig. 6 emphasizes how different classification schemes can yield variable results, particularly for the mafic-intermediate volcanic rocks. Such classification diagrams are not fool-proof but should be used as one tool among others to best characterize the petrogenesis of these rocks.

Six samples of felsic volcanic and subvolcanic intrusive rocks of the Al Amar group, collected during this study, failed to yield zircon or other datable minerals. The lower age limit of the Al Amar group is constrained by the intrusion at Jabal Umm Sharzah (Figs. 3 and 4), which is dated in this study at 689 ± 10 Ma (see below). A 651 ± 43 Ma whole-rock Rb–Sr age reported by Calvez and Delfour (1986) for Al Amar group rhyolite from the Umm ash Shalahib area is not considered robust as subsequent heating events would have affected the Rb–Sr systematics (Table 1).

2.2. *Hamir group rocks*

Hamir group rocks are named after Jabal Hamir, (Fig. 3; Vaslet et al., 1983) and are present in small elongated fault-bounded blocks along the Al Amar fault zone (Fig. 4). The Al Amar fault zone splays as it progresses south along the western margin of the terrane and thus Hamir group rocks are more abundant in the south as the Hamir depositional basins were apparently larger and more abundant. The Hamir group lies unconformably on Al Amar group, group-1, and group-2 intrusive rocks. The Hamir group reaches a thickness of 150 m and typically consists of a basal polymict conglomerate overlain by sandstone, siltstone, wacke, dolomitic limestone, and andesitic volcanic and volcaniclastic rocks. Although only two Hamir group volcanic rock samples are included in this study (dacite and andesite, Fig. 5A), both samples tend to be more calc-alkaline than equivalent felsic and mafic-intermediate Al Amar group rocks (Fig. 6) and the Hamir andesite displays a distinct REE fractionation pattern relative to other mafic-intermediate Al Amar group rocks (Fig. 7A).

Author's personal copy

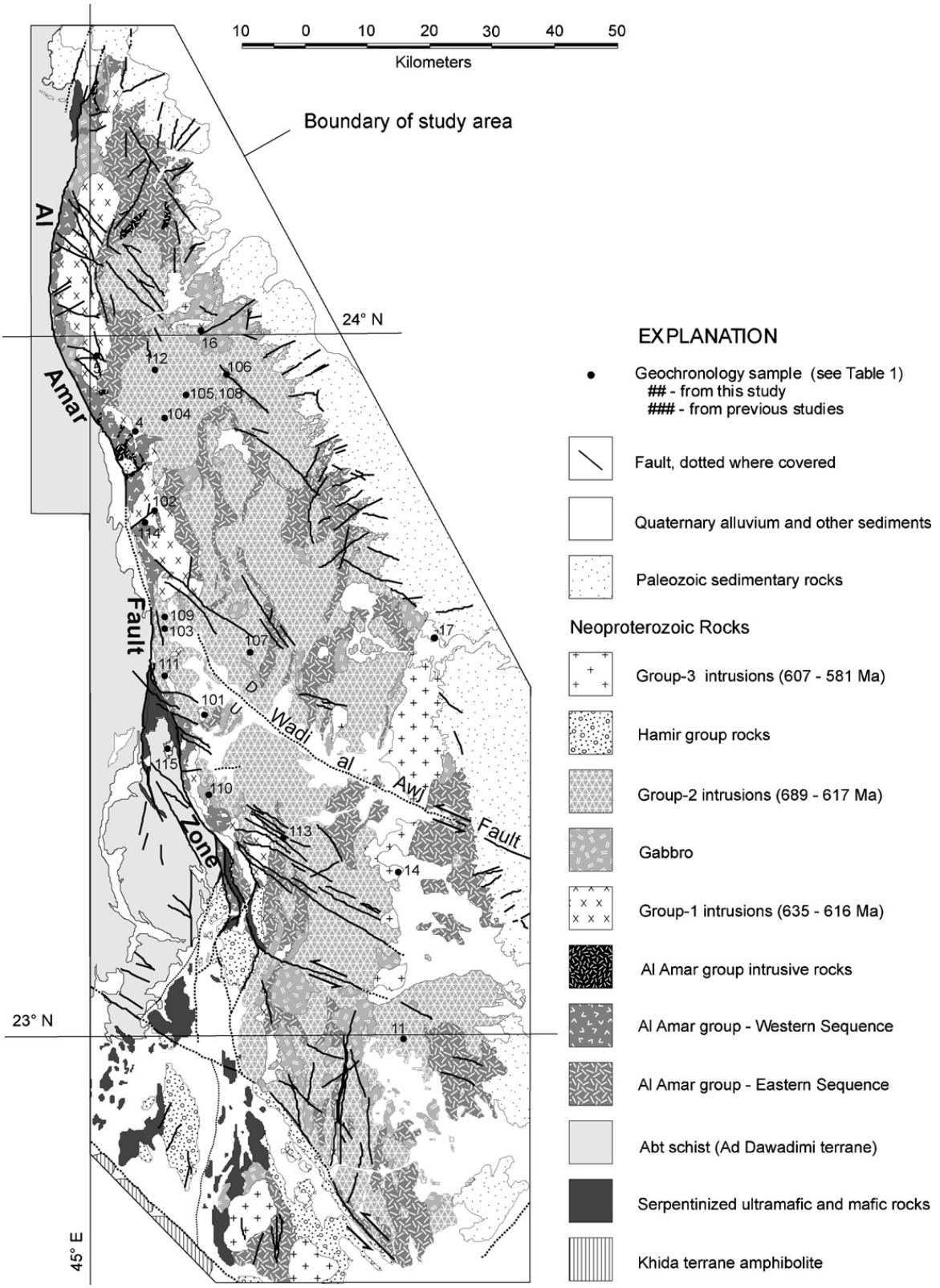

Fig. 4. Generalized geologic map of the Ar Rayn terrane. Modified from Delfour (1979), Delfour et al. (1982), Vaslet et al. (1983), and Manivit et al. (1985a,b).

Author's personal copy

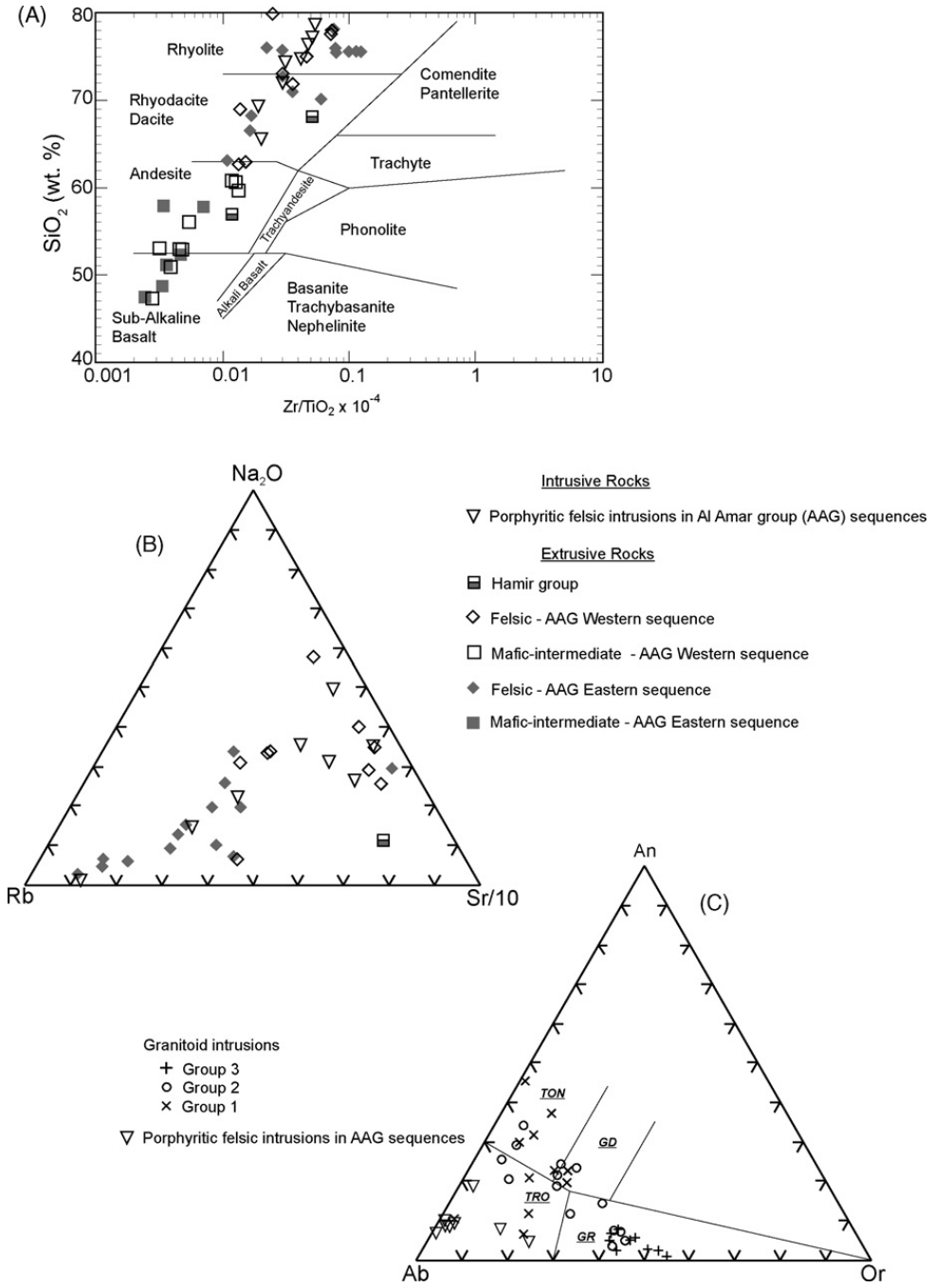

Fig. 5. Classification and discrimination diagrams for volcanic, subvolcanic, and granitoid intrusive rocks of the Ar Rayn terrane. Data from this study is combined with data from Le Bel and Laval (1986) and BRGM (2003) and all analytical data is presented in Appendix A. (A) Log Zr/TiO_2-Silica diagram showing the volatile-free compositions of Al Amar and Hamir group volcanic rocks. Boundaries are from Winchester and Floyd (1977). (B) Rb–Na_2O–Sr ternary diagram that discriminates eastern and western sequence felsic volcanic and intrusive rocks of the Al Amar group. (C) CIPW normative Ab–An–Or granitic rock classification of intrusive rocks from the Ar Rayn terrane (boundaries from Barker, 1979). TON: tonalite, GD: granodiorite, TRO: trondhjemite, GR: granite.

The age of the Hamir group has not been directly determined. Immediately west of the Jabal Idsas area (Figs. 3 and 4), a narrow elongated exposure of Hamir group basal conglomerate contains clasts of Jabal Idsas magnetite ore. This provides a lower age constraint of the Hamir group, i.e., post-magnetite-rich Fe-oxide Cu–Au mineralization (late- to post-group-1 plutonism; 632–616 Ma – see below). Hamir group rocks are intruded by a group-3 pluton southeast of Jabal as Sakhin at the southern end of the terrane. This provides an upper constraint as the oldest group-3 rocks have been dated at 607 ± 6 Ma (see below).

Author's personal copy

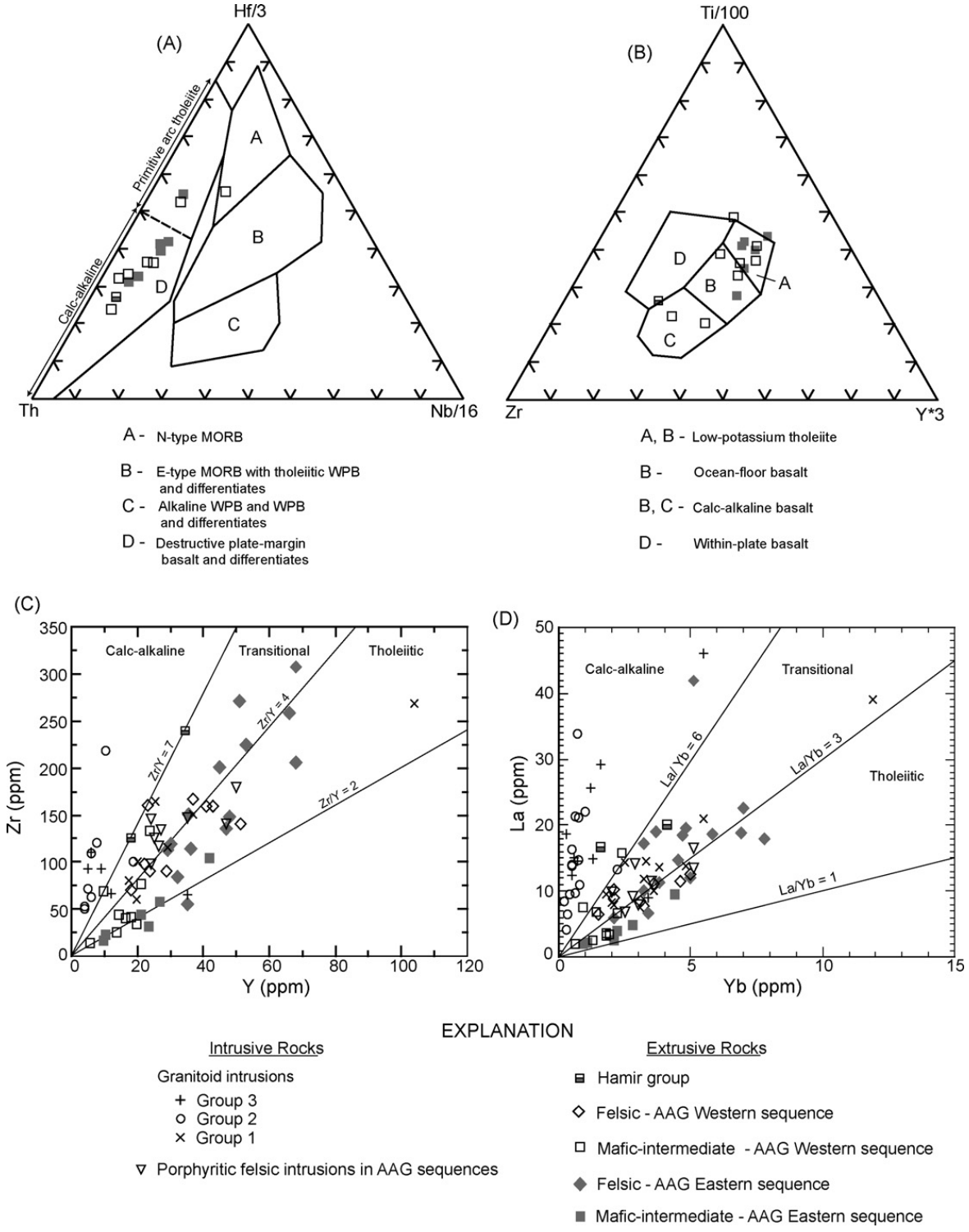

Fig. 6. Discrimination of calc-alkaline and tholeiitic affinities for igneous rocks of the Ar Rayn terrane. Data from this study is combined with data from Le Bel and Laval (1986) and BRGM (2003) and all analytical data is presented in Appendix A. (A) Th–Hf–Nb ternary discrimination diagram for Al Amar and Hamir group mafic-intermediate volcanic rocks. Boundaries are from Wood (1980). (B) Zr–Ti–Y ternary discrimination diagram for Al Amar and Hamir group mafic-intermediate volcanic rocks. Boundaries are from (Pearce and Cann, 1973). (C, D) Immobile trace element plots of Y–Zr (C) and Yb–La (D). Boundaries are from Lentz (1998) and Barrett et al. (1999).

Author's personal copy

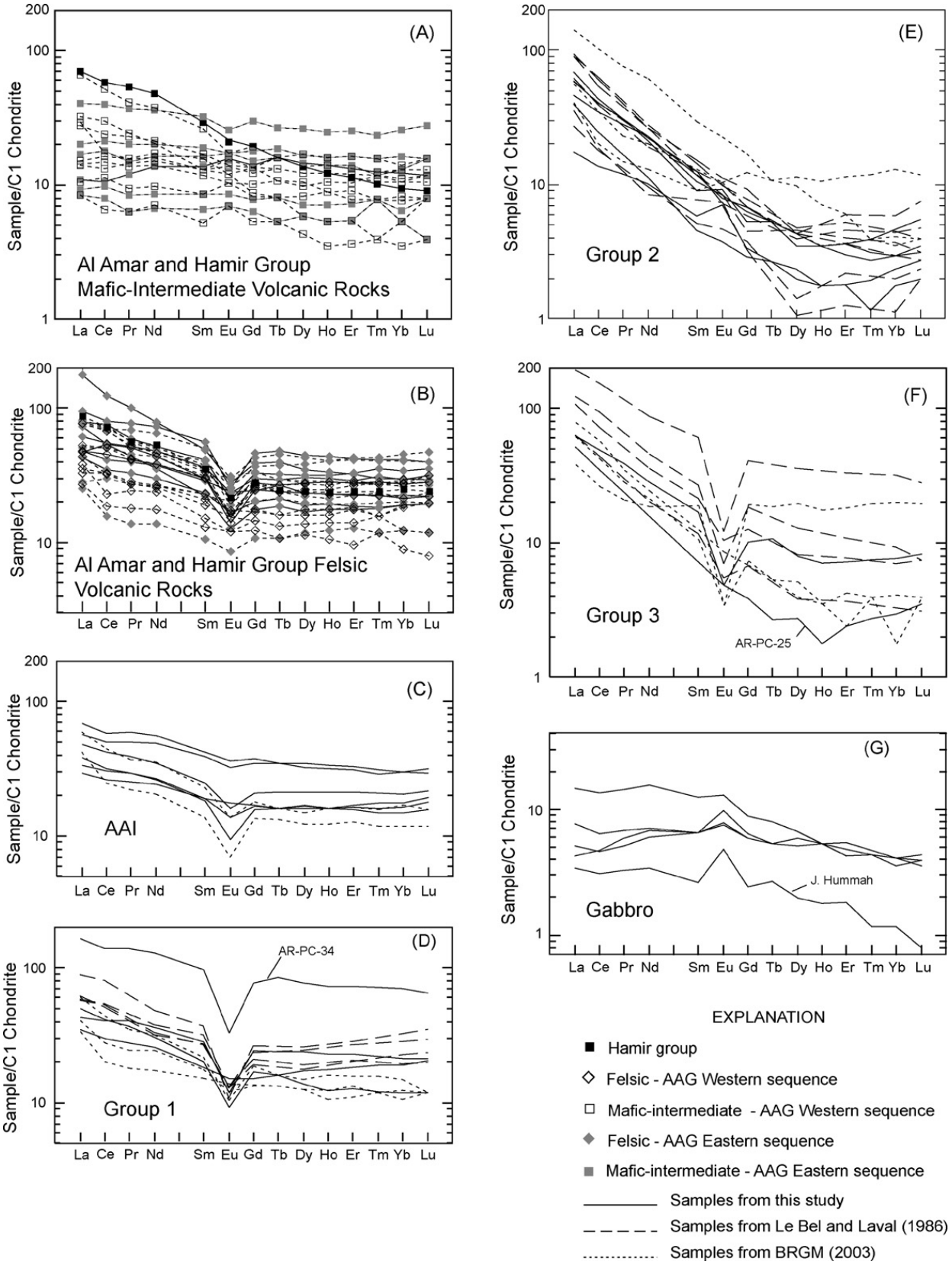

Fig. 7. Rare-earth element plots for igneous rocks of the Ar Rayn terrane. Data from this study is combined with data from Le Bel and Laval (1986) and BRGM (2003) and all analytical data is presented in Appendix A. Anomalous samples within a particular group are labeled for reference only. (A) Mafic to intermediate volcanic rocks, (B) Felsic volcanic rocks, (C) AAI: porphyritic felsic intrusions in Al Amar group, (D) Group-1 intrusions, (E) Group-2 intrusions, (F) Group-3 intrusions, (G) Gabbro.

Author's personal copy

Table 1
Geochronologic sample data for the Ar Rayn terrane

ID1 (AR-GC-#)[a]	ID2[b]	Age[c] (Ma)	Error (Ma)	Rock unit	Location or unit dated	Rock type	Analytical method[d]	Lower intercept[e]	Sample type and number of data points[f]	MSWD[g]	Initial Sr ratio	Latitude	Longitude	Data source[h]
4	AR-PC-7	616	±7	gp1	Jabal ar Ramadiyah	Trondhjemite	U–Pb(i)		Zircon 16			23.86875	45.06864	This study
5	AR-PC-8	632	±5	gp1	Jabal al Ashqar	Granodiorite	U–Pb(i)		Zircon 12			23.97520	45.00881	This study
11	AR-PC-20	617	±5	gp2	SE of Jabal Ruga'an	Granite	U–Pb(i)		Zircon 15			22.99936	45.48959	This study
14	AR-PC-25	583	±8	gp3	N. of Wadi Ghurrah	granite	U–Pb(i)		Zircon 8			23.23524	45.48540	This study
16	AR-PC-33	689	±10	gp2?	Jabal Umm Sharzah	Trondhjemite	U–Pb(i)		Zircon 10			24.00768	45.17218	This study
17	AR-PC-28	607	±6	gp3	N.of Ar Rayn town	Granite	U–Pb(i)		Zircon 8			23.56964	45.54191	This study
101		581	±6	gp3	Bitran pluton	Alkali granite	Rb–Sr		wr		0.7045	23.5167	45.1500	Abdel-Monem et al. (1982)
102		621	±17	gp1	Al Amar pluton	Tonalite	Rb–Sr		wr 8	0.60	0.7036	23.7500	45.1000	Calvez et al. (1984)
103		629	±7	gp2	Umm Dhaffar pluton	Tonalite	U–Pb(m)	15 ± 20	Zircon 3			23.5833	45.1167	Stacey et al. (1984)
104		631	±7	gp2	Quway'iyah pluton	Granodiorite	U–Pb(m)	15 ± 20	Zircon 2		0.7032	23.8833	45.1167	Stacey et al. (1984)
105		632	±25	gp2	Quway'iyah pluton	Trondhjemite	U–Pb(m)	15 ± 20	Zircon 4			23.9167	45.1500	Calvez and Delfour, 1986
106		633	±6	gp2	Ridah pluton	Tonalite	U–Pb(m)	15 ± 20	Zircon 4		0.7035	23.9500	45.2000	Calvez and Delfour, 1986
107		633	+5/-2	gp2	Umm Woraty pluton	Tonalite	U–Pb(m)	15 ± 20	Zircon 3		0.7032	23.5500	45.2500	Calvez and Delfour, 1986
108		633	±5	gp2	Quway'iyah pluton	Trondhjemite	U–Pb(c)		Zircon 4			23.9167	45.1333	Calvez et al. (1984)
109		634	±6	gp2	Umm Dhaffar pluton	Hornblende diorite	U–Pb(m)	15 ± 20	Zircon 2		0.7032	23.6000	45.1167	Stacey et al. (1984)
110		635	±6	gp1	Idsas pluton	Quartz diorite	U–Pb(m)	15 ± 20	Zircon 1		0.7032	23.3500	45.1833	Stacey et al. (1984)
111		641	±9	gp2	Bitran pluton	Tonalite	U–Pb(m)	15 ± 20	Zircon 3			23.5167	45.1167	Calvez and Delfour, 1986
112		648	±25	gp2	Mulayriqah pluton	Trondhjemite	U–Pb(m)	15 ± 20	Zircon 4			23.9500	45.1000	Calvez and Delfour, 1986
113		650	±9	gp2	Antariyah pluton	Tonalite gneiss	U–Pb(m)	15 ± 20	Zircon 1		0.7033	23.2833	45.3000	Stacey et al. (1984)
114		651	±43	aaw	Al Amar group	Rhyolite	Rb–Sr		wr 6	1.20	0.7052	23.7333	45.0833	Calvez and Delfour, 1986
115		2067	±74		Assaliyah complex (inherited zircons)	Gabbro/ trondhjemite	U–Pb(c)	645 ± 16 (age of complex)	Zircon 6			23.4500	45.1000	Calvez et al. (1985)

See Fig. 4 for sample locations and Appendix B for analytical data for samples collected for this study.
[a] Data for samples 101–115 from compilation by Johnson et al. (1997).
[b] Refers to corresponding lithogeochemical sample from this study. See Appendix A for lithogeochemical data.
[c] See Fig. 10 for concordia plots of samples 4 to 17 (this study).
[d] (i) ion probe (SHRIMP-RG); (c) conventional concordia/discordia; (m) model age, i.e., discordia forced through an assumed lower intercept([e])
[f] wr: whole rock.
[g] Mean standard weighted deviation.
[h] U–Pb isotope age determinations made during this study were conducted using the SHRIMP-RG at the Stanford-USGS Micro-Isotopic Analytical Center (SUMAC).

Author's personal copy

2.3. Plutonic rocks

Most of the Ar Rayn terrane consists of plutonic rocks that can be divided into three distinct compositional groups. This division was originally defined by Le Bel and Laval (1986) as (1) arc-related tonalite-trondhjemite, (2) synorogenic calc-alkaline granodiorite-granite, and (3) postorogenic alkali-feldspar granite. New petrographic, lithogeochemical, and geochronologic data on Ar Rayn terrane plutonic rocks build on the foundation set by Le Bel and Laval (1986). We maintain a 3-fold lithogeochemical classification which we refer to as group-1, -2 and -3 plutonism. However, our findings are not fully consistent with previous interpretations of the relative timing and tectonic classification of plutonism, which requires a re-interpretation of the sequence of events and the tectono-magmatic environment of plutonism.

2.3.1. Group-1 plutonic rocks

Group-1 plutonic rocks are a tonalite-trondhjemite suite of plutons (Fig. 5C) that are largely confined to a narrow belt along the western margin of the terrane (Fig. 4). This group includes the Jabal al Ashqar, Jabal ar Ramadiyah, and Umm ash Shalahib plutons (Figs. 3 and 4). In general, group-1 intrusive rocks are geographically coincident with exposures of Al Amar group western sequence volcanic rocks (Fig. 4) and share the sodic composition of western sequence felsic volcanic and porphyritic intrusive rocks. Group-1 intrusive rocks are characterized by weakly fractionated REE patterns with moderately negative to no Eu anomalies (Fig. 7). These rocks have similar geochemical enrichment-depletion patterns, when normalized to ocean-ridge granite, as volcanic arc granites (Fig. 8; Pearce et al., 1984) and classify as low-Al TTG (tonalite-trondhjemite-granodiorite) of Arth (1979) (Fig. 9A). The depleted Sr and elevated Y content of group-1 rocks relative to group-2 and -3 intrusions is distinct and discriminates group-1 as tholeiitic to calc-alkaline arc rocks (Fig. 9B) as defined by Defant and Drummond (1990) and Martin (1999). The lithogeochemistry of Al Amar group felsic extrusive and felsic porphyritic intrusive rocks show a strong compositional affinity with group-1 intrusive rocks and suggest a co-magmatic relationship (Figs. 7B–D; 8A and B; 9).

Two group-1 samples collected during this study yielded SHRIMP U–Pb zircon ages of 632 ± 5 and 616 ± 7 Ma (Figs. 4 and 10; Table 1). These ages are consistent (within error) with conventional U–Pb age determinations made on group-1 rocks in previous studies (635 ± 6 to 629 ± 7 Ma; Table 1).

2.3.2. Group-2 plutonic rocks

Group-2 rocks are a calc-alkaline suite of diorite, granodiorite, and granite plutons (Figs. 5C; 6C and D) that are exposed largely in the central and eastern parts of the terrane (Fig. 4), and represent the most voluminous suite of plutonic rock in the terrane. Rare-earth and trace element contents clearly discriminate group-1 and -2 rocks (Figs. 7–9) as two geochemically distinct plutonic suites. Group-2 rocks display depleted HREE patterns with no or positive Eu anomalies (Fig. 7) and are, on average, enriched in Rb, Sr, and depleted in Y and Yb, relative to group-1 rocks (Figs. 8 and 9). Geochemical enrichment-depletion patterns of group-2 rocks, normalized to ocean-ridge granite, are consistent with those of volcanic arc granite (Fig. 8; Pearce et al., 1984). Group-2 rocks partially plot in the high-Al TTG field of Arth (1979) (Fig. 9A), have high to very high Sr/Y ratios relative to all other plutonic and volcanic rocks in the terrane and plot clearly within the adakite fields of Defant and Drummond (1990), Martin (1999), and Martin et al., 2005) (Fig. 9B).

Geochronologic data indicate that crystallization of group-1 and -2 plutons was largely coeval, though much older group-2 plutons also exist. Two samples from group-2 intrusions collected during this study yield SHRIMP U–Pb zircon ages of 689 ± 10 Ma (the core of Jabal Umm Sharzah) and 617 ± 5 Ma (Figs. 3, 4 and 10). The 689 Ma age is the oldest age documented for the Ar Rayn terrane to date, and puts a further upper age constraint on Al Amar group eastern sequence rocks which are intruded by the Jabal Umm Sharzah pluton. Previous conventional U–Pb age dates on group-2 rocks range from 650 ± 9 to 631 ± 7 Ma (Table 1). The overlap in crystallization ages of group-1 (co-magmatic with arc volcanism) and -2 precludes that group-2 rocks are "syn-orogenic" as proposed by Le Bel and Laval (1986), because arc formation was still ongoing at the time of group-1 and -2 plutonism. Furthermore, there is no conclusive field evidence to support a synorogenic classification.

2.3.3. Group-3 plutonic rocks

Group-3 plutonic rocks are alkali-feldspar granites (Fig. 5C) that are exposed almost exclusively in a 25-km-wide, N.20 E.-trending belt that transects the eastern and southern parts of the terrane (Fig. 4). These rocks are generally more evolved and distinguished from group-1 and -2 plutonic rocks by their strongly fractionated REE patterns with strong negative Eu anomalies (Fig. 7) and their elevated K_2O, Rb, Th, and Nb contents (Figs. 8 and 9). Group-3 plutonic rocks have very distinctive geochemical enrichment-depletion patterns

Author's personal copy

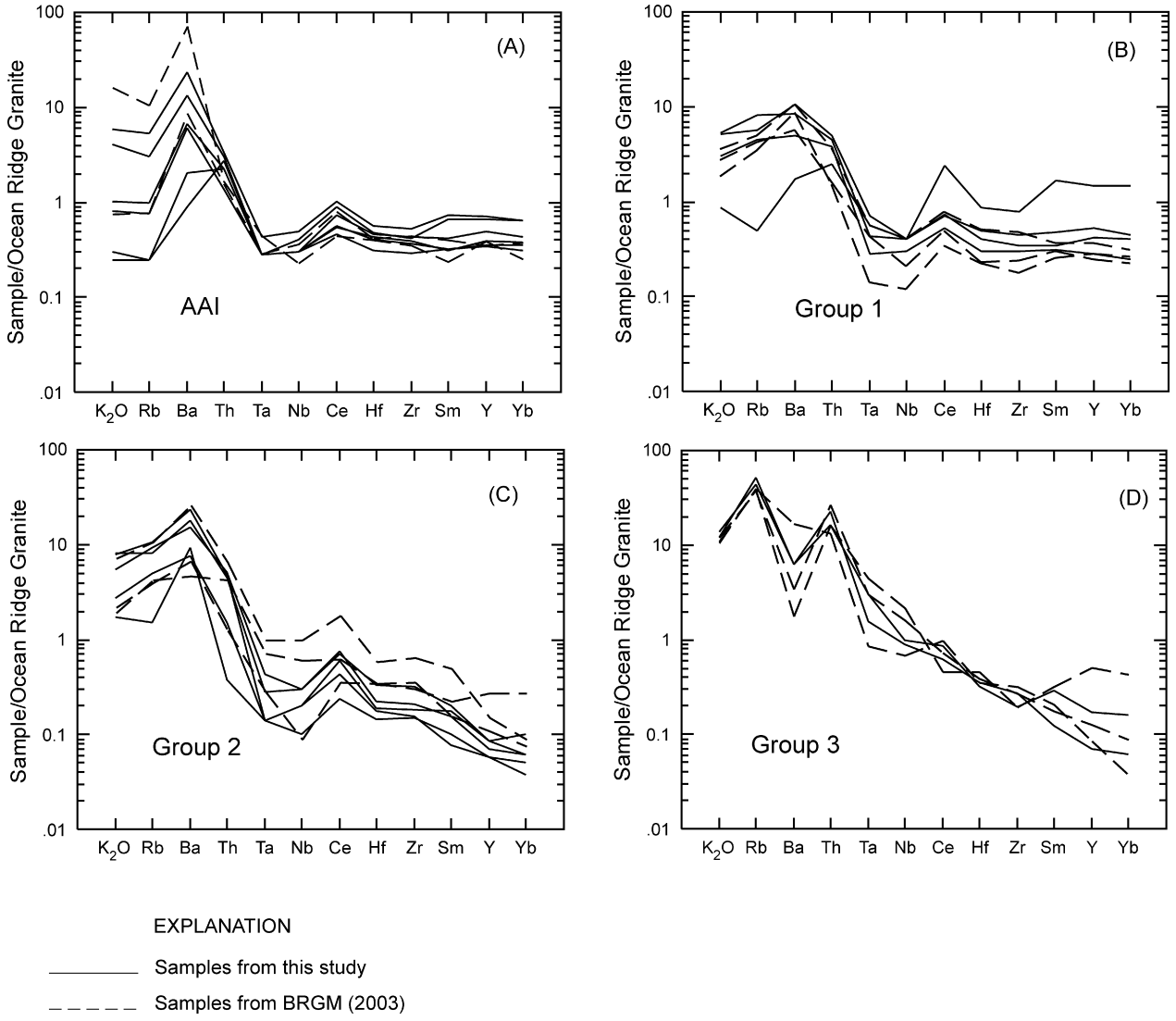

Fig. 8. Ocean-ridge granite normalized geochemical patterns for intrusive rocks of the Ar Rayn terrane. Data from this study is combined with data from BRGM (2003) and all analytical data is presented in Appendix A. Ocean-ridge granite data is from Pearce et al. (1984). Anomalous samples within a particular group are labeled for reference only. (A) AAI: porphyritic felsic intrusions in Al Amar group, (B) Group-1 intrusions, (C) Group-2 intrusions, (D) Group-3 intrusions.

(with Rb and Th peaks), normalized to ocean-ridge granite, which are similar to syn- and postorogenic granites (Fig. 8D; Pearce et al., 1984). In a Y–Nb discrimination plot, group-3 rocks plot mostly in the volcanic-arc granite/syn-collision granite field yet distinct from group-1 and -2 rocks (Fig. 9C).

These rocks represent the youngest plutonic rocks in the terrane, yet may overlap in age with some of the youngest group-1 and -2 plutons. Two samples from this study yielded SHRIMP U–Pb zircon ages of 607 ± 6 Ma and 583 ± 8 Ma (Figs. 4 and 10). Previous age determinations on group-3 rocks were by the Rb–Sr method and yielded an age of 581 ± 6 Ma on the Jabal Bitran pluton (Table 1). Le Bel and Laval (1986) classify group-3 plutons as postorogenic and emplaced into a cratonized region. The combined lithogeochemical, petrological, and geochronological data indicate group-3 plutons were late- to postorogenic intrusions.

2.3.4. Gabbro

Gabbro complexes, many compositionally layered, are exposed at scattered localities throughout the Ar Rayn terrane (Fig. 4). Field relations indicate that two generations of gabbro are present. Gabbro intrusions of the earlier group are more voluminous, generally are exposed as irregular elongated bodies (possibly sills) and are pre- to syn- group-1 and -2 plutonism. Gabbro intrusions of the latter group are generally smaller circular complexes that cut group-1 and -2 intrusions (e.g., Jabal Hummah, Figs. 3 and 4). Of the five gabbro samples collected for this study, the sample from J. Hummah (AR-PC-30) is significantly depleted in REE and has a

Author's personal copy

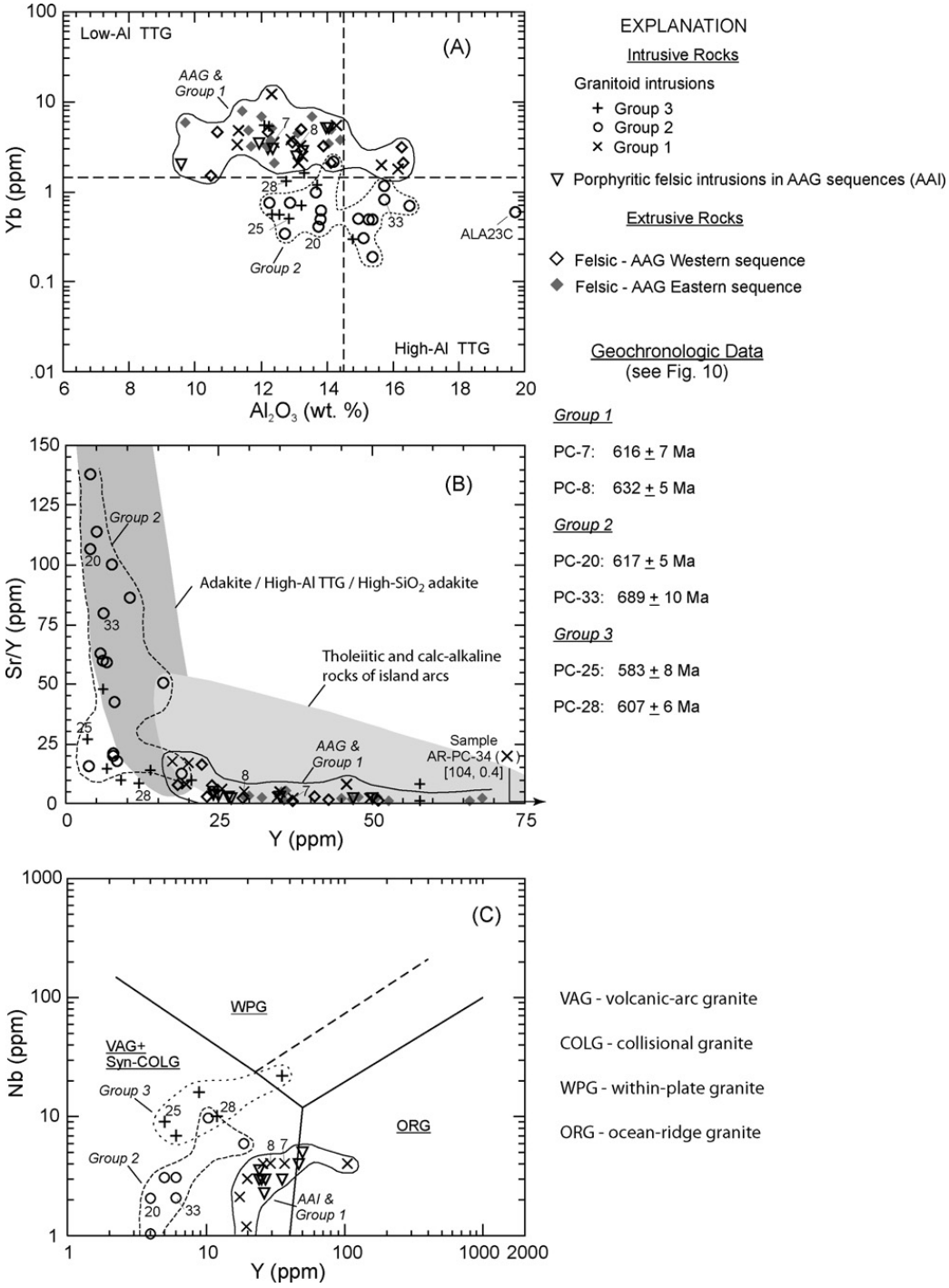

Fig. 9. Classification and tectonic discrimination diagrams for igneous rocks of the Ar Rayn terrane. Data from this study is combined with data from Le Bel and Laval (1986) and BRGM (2003) and all analytical data is presented in Appendix A. Samples dated for this study are labeled for reference. (A) Al_2O_3–Yb plot of all igneous rock samples, showing discrimination of Al Amar group (AAG) rocks and group-1 intrusions from group-2 intrusions. Subdivisions are from Arth (1979); TTG: trondhjemite-tonalite-granodiorite. (B) Y–Sr/Y plot showing the discrimination of AAG rocks and group-1 intrusions (island arc affinity) from group-2 intrusions (adakite affinity); shaded fields are from Martin (1999) and Martin et al. (2005). (C) Y–Nb plot showing discrimination between AAG rocks plus group-1 intrusions, group-2 intrusions, and group-3 intrusions; boundary lines are from Pearce et al. (1984).

large positive Eu anomaly relative to the other four earlier generation gabbro samples (Fig. 7G; Appendix A).

The Jabal Ruga'an layered mafic intrusive complex (Figs. 3 and 4) was explored for magmatic Cu–Ni resources. However, only magnetite-rich serpentinized ultramafic units with local concentrations of pyrrhotite were found, primarily near the base of the complex (Zubeir, 1976; Chevremont and Johan, 1982).

Author's personal copy

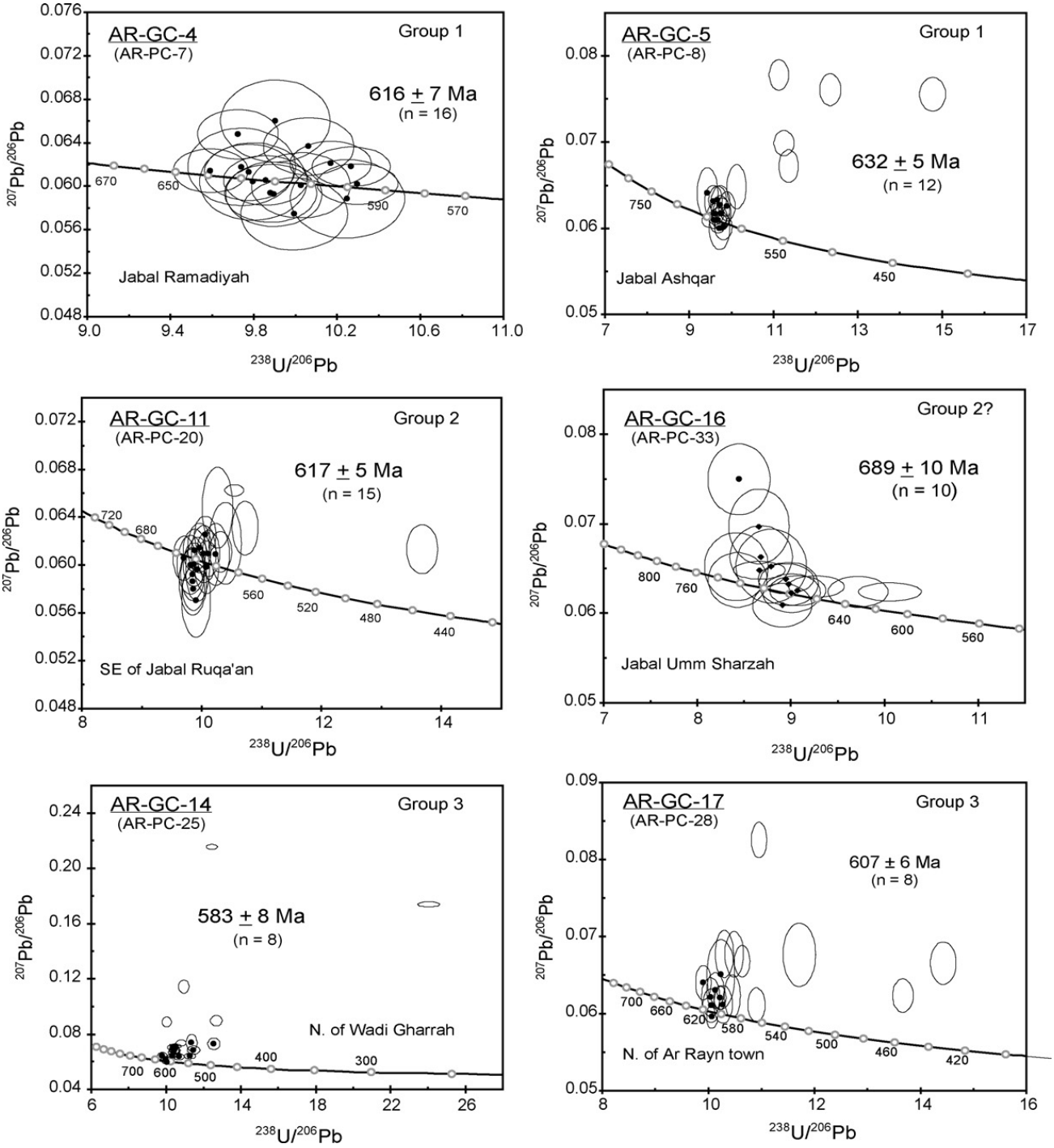

Fig. 10. Tera-Wasserburg concordia plots of SHRIMP zircon U–Pb isotope data. See Fig. 4 for location of sample sites, Table 1 for summary statistics, and Appendix B for analytical data. Error ellipses are equal to 2σ. Only data points shown were included in age calculation.

2.4. Structure

Important structural features in the terrane are north-trending folds, faults, foliation, and local schistosity that are cut by a northwest-trending set of sinistral trancurrent faults, which also had normal displacement. The earliest deformation in the terrane (D1) produced a north-striking foliation and local schistosity in Al Amar group eastern sequence rocks not seen in western sequence rocks. Western sequence rocks are characterized only by monoclinal folding and tilting, which affected both sequences, and is defined as D2 deformation. This implies that the eastern sequence is older than the western sequence, and is consistent with intrusion of the eastern sequence by the oldest dated rocks in the terrane (see above). D2 deformation corresponds to the east–west contraction

Author's personal copy

during amalgamation of the Ar Rayn and Ad Dawadimi terranes.

The most prominent faults in the terrane are the north-trending faults along and subparallel to the Al Amar fault zone and northwest-trending "Najd" faults that are present throughout the terrane and that divide it into a series of fault blocks (Fig. 4). Though many of these northwest-trending faults cross cut and offset the Al Amar fault and the magnetically-defined eastern margin of the terrane (Fig. 4), several major mapped northwest-trending faults (e.g. the Wadi Al Awj fault) trend more northerly as they approach the Al Amar fault and ultimately merge with the Al Amar fault zone (Fig. 4). Other northwest-trending faults terminate at the Al Amar fault (Fig. 4). The relative timing of faulting deduced from field relations indicates that strike-slip displacement along the Al Amar fault commenced prior to but also was coeval with transcurrent displacement on northwest-oriented faults. Though northwest-trending faults cut all rock units, including the Paleozoic platform sequence, discernible offset and truncation is seen only in rocks older than group-3 intrusions.

A D3 deformation event is manifested by Hamir group rocks tilted and folded into synclinoria, particularly in exposures in the southern part of the study area. This deformation would be syn- to late-orogenic and would have occurred late- or post-amalgamation of the Ar Rayn and Ad Dawadimi terranes, and perhaps during collision with a continental block from the east. This event would also correspond to formation of northwest-trending Najd transcurrent faults and translational displacement along the Al Amar fault zone. Emplacement of a group-3 intrusion into the folded Hamir rocks constrains the timing of amalgamation to between about 616 and 607 Ma.

Much of the displacement on northwest-striking faults has been sinistral; however, significant vertical displacement of fault blocks is indicated by correlation of magnetically-defined terrane in the southern part of the study area (Doebrich et al., 2005) and by the level of exposure of mineral systems in the terrane. Mineral deposit types are different across the Wadi al Awj fault (Fig. 11). Deposit types found north of the Wadi al Awj fault (epithermal Au–Ag–Zn–Cu-barite, porphyry Cu, hematite-rich Fe-oxide Cu–Au) were formed in shallower mineralizing environments, whereas deposit types found south of the fault (orogenic gold veins, magnetite-rich Fe-oxide Cu–Au systems) were formed in deeper environments. This may indicate that faulting has uplifted the southern part of the terrane relative to the northern part of the terrane, along the Wadi al Awj fault.

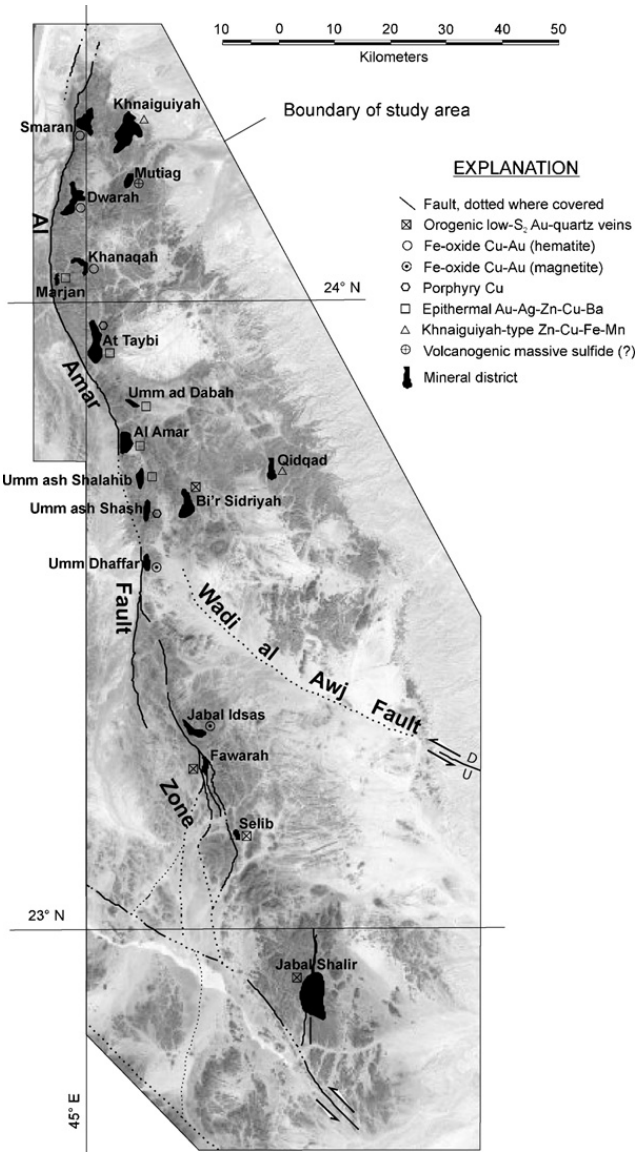

Fig. 11. Index map of the Ar Rayn terrane showing the distribution of major mineral districts. Symbols indicate dominant deposit type in each district.

3. Terrane metallogeny

A variety of mineral deposit types (Table 2) formed during a series of mineralizing episodes as the magmatic arc evolved and amalgamated within the East African orogen, and define the metallogeny of the Ar Rayn terrane. Khnaiguiyah-type Zn–Cu–Fe–Mn (enigmatic, stratiform; described below), epithermal Au–Ag–Zn–Cu-barite, and orogenic Au (low-sulfide gold-quartz) vein deposits (Table 2, Fig. 11) historically have attracted the most exploration attention in the terrane (Doebrich et al., 2005). Potential for porphyry Cu and Fe-oxide Cu–Au (IOCG) deposits in the Ar Rayn terrane (Table 2, Fig. 11) has recently been recognized

Author's personal copy

Table 2
Mineral deposit types identified in the Ar Rayn terrane with examples

Deposit type	Regional distribution and host rocks	Relative age	Morphology	Mineralogy	Alteration	Examples
Khnaiguiyah-type Zn–Cu–Fe–Mn	Found exclusively in Al Amar group eastern sequence rocks; concentrated along zones of carbonatization (locally converted to marble)	Syn- to late- Al Amar eastern sequence volcanism	Stratiform bodies and lenses; may be fault-controlled replacements and syn-deformational	Hematite, ilmenite, pyrite, sphalerite, chalcopyrite, rhodochrosite, rhodonite; Ag-, Pb-, and Bi-tellurides, barite	Carbonate, chloritic, calc-silicate	Khnaiguyiah, Qid Qad, Wadi Sidarah
Epithermal Au–Ag–Zn–Cu-barite	Found exclusively in Al Amar group western sequence rocks along the western margin of the terrane, and north of Wadi al Awj; located in volcanic centers, interpreted as westward-dipping tilted calderas; proximal to rhyodacite intrusive complexes	Probably syn-Al Amar group intrusive rocks	Veins and stockwork, massive barite lenses	Quartz, sphalerite, chalcopyrite, pyrite, galena, barite, gold, covellite, chalcocite, rutile, polybasite	Silicic, serictic, chloritic, carbonate, talc	Al Amar, Umm ash Shalahib, Umm adh Dabah
Porphyry Cu	Associated exclusively with porphyritic phases of group-1 intrusive rocks and Al Amar group western sequence rocks along the western margin of the terrane, and north of Wadi al Awj	Syn-group-1 intrusions	Current surface expression includes discrete veins and local stockworks	Malachite, chalcopyrite, magnetite, hematite	Potassic, phyllic, sodic, propylitic	Al Eitaby, Umm ash Shash
Fe-oxide Cu–Au (magnetite-rich)	Found primarily along the western margin of the terrane, mostly south of Wadi al Awj, in group-1 intrusions and Al Amar group western sequence volcanic and volcaniclastic rocks	Late- to post-group-1 intrusions and pre-Hamir group; Magnetite cobbles found in Hamir group conglomerate	Metasomatic replacement bodies of disseminated magnetite and smaller fault-controlled bodies of massive magnetite	Magnetite, apatite, hematite (martite), actinolite, chalcopyrite, chalcocite, covellite	Amphibole (actinolite), tourmaline, epidote, sericitic	Jabal Idsas
Fe-oxide Cu–Au (hematite-rich)	Found exclusively in the northern part of the terrane, and primarily along the northwest margin, in group-1 intrusive rocks, gabbro, and Al Amar group volcanic rocks (western and eastern sequences)	Late- to post- group-1 intrusions	Mineralized fault and breccia zones and replacement veins	Hematite, tourmaline, magnetite, rutile, apatite, chalcopyrite	Tourmaline, amphibole, carbonate, sericitic, silicic, epidote	Dwarah
Orogenic (low-S_2 quartz) Au veins	Found throughout the western part of the terrane, particularly in and near the Al Amar fault zone, and in the Bi'r Sidriyah and Jabal Shalir districts, in all rock units pre-group-3 plutonism in age	Post-group-1 and -2 plutonism, post-Al Amar group volcanism, pre-group-3 magmatism (syn-terrane amalgamation?)	Massive, tabular, and lensoid quartz veins emplaced in fault zones	Quartz, carbonate, pyrite, gold, malachite, chrysocolla	Carbonate, sericitic; also silicified and carbonate-altered serpentinite (listwaenite)	Selib, Fawarah, Jabal Shalir, Bi'r Sidriyah

Deposits types are listed in general geochronologic order, from earliest to latest. For more detailed descriptions see Doebrich et al. (2005).

Author's personal copy

(Doebrich et al., 2005) and represents new mineral exploration and research frontiers in the terrane.

Within the Arabian shield, Khnaiguiyah-type Zn–Cu–Fe–Mn deposits (Table 2, Fig. 11) are unique to the Ar Rayn terrane and represent a significant zinc resource. The four defined ore bodies of the Khnaiguiyah deposit contain mineable reserves ranging from 10.56 Mt averaging 7.41% Zn and 0.82% Cu to 2.66 Mt averaging 15.10% Zn and 0.80% Cu (BRGM, 1994). Khnaiguiyah-type deposit characteristics are consistent with deformation and metamorphism of volcanogenic massive sulfide (VMS) mineralization; the associated stratiform Mn-rich units are particularly indicative of a seafloor hydrothermal environment. The stratiform and shear-zone-hosted nature, base-metal sulfide and iron oxide mineralogy, alteration mineralogy, and geochemistry associated with these deposits (Table 2) are collectively enigmatic, and consequently their proposed genesis has been controversial, ranging from syngenetic, to syndeformational, to metasomatic (Elsass and Achard, 1979; Testard, 1983; Woldeabzghi and Prevot, 1983; BRGM, 1994). These deposits share similarities with the Archean magnetite-bearing VMS deposits of the Golden Grove district of Western Australia (Frater, 1983; Ashley et al., 1988; Barley and Large, 1992; Sharpe and Gemmell, 2001, 2002) as well as with the Perkoa zinc deposit in the Paleoproterozoic Birimian Supergroup of West Africa (Burkina Faso; Schwartz and Melcher, 2003).

Epithermal Au–Ag–Zn–Cu-barite vein deposits (Table 2, Fig. 11) represent significant resources of precious- and base-metals in the Ar Rayn terrane (Testard, 1982; Felenc, 1983a; Felenc et al., 1983; Lofts et al., 1986; Vadala et al., 1994; Leistel et al., 2000). Areas of epithermal-type mineralization are found proximal to volcanic centers that are localized along the Al Amar fault zone and display geologic characteristics consistent with a tilted caldera setting. The most significant resource of this type is at the Al Amar deposit which is scheduled to commence production in 2006 with reserves of 1.55 Mt @ 12.31 g/t Au, 6.16% Zn, 21.07 g/t Ag, and 0.92% Cu, (measured and indicated) plus 3.0 Mt @ 5.1 g/t Au (inferred) (Ma'aden, 2005). These deposits have characteristics similar to low-sulfidation epithermal vein deposits (Hayba et al., 1985; Heald et al., 1987) yet are sulfide-rich (sphalerite, chalocopyrite, and pyrite). The associated carbonatization, talc alteration, and sodic nature of proximal rhyodacitic domes may indicate a submarine epithermal environment of formation. At Al Amar, in addition to the main epithermal vein zones, submassive sulfide lenses locally are found in talc-barite-quartz rock that may have had an exhalative origin (Lofts, 1994).

Several copper–gold prospects along the northwest margin of the terrane (Table 2, Fig. 11) represent surface expressions of potential porphyry Cu systems. These areas contain copper-bearing vein and stockwork zones associated with porphyritic quartz monzodioritic intrusions, porphyry-type alteration assemblages, and proximal porphyry-related deposit types (Doebrich et al., 2005).

The Ar Rayn terrane contains the largest concentration of IOCG deposits in the Arabian shield. These deposits are either magnetite- or hematite-rich (Table 2; Doebrich et al., 2005) and most deposits are relatively small, fault-controlled bodies of magnetite and specularite. Magnetite-rich deposits are enriched in LREE, whereas hematite-rich deposits are more enriched in copper and gold. The magnetite deposits of the Jabal Idsas district (Fig. 11) represent the largest IOCG resource in the terrane, and are characterized by fault-controlled massive magnetite lenses (1.3–6.7 Mt @ 64–65% Fe) and extensive areas of disseminated replacement magnetite in andesitic volcanics (300 Mt @ 18–20% Fe) (Ashworth and Abdulaziz, 1978). Hematite-rich deposits exhibit a mineral paragenetic sequence of amphibole, followed successively by tourmaline, hematite, chalcopyrite, and gold. In mineralized breccias, tourmaline-altered fragments are cemented by specular hematite. Locally, hematite is derived from martitization of magnetite.

Orogenic gold vein deposits found in the terrane (Table 2) are typical greenstone-hosted low-sulfide gold-quartz veins found throughout the Arabian shield. The largest are found along the Al Amar fault zone (Fig. 11) and proximal to silicified and carbonatized serpentinite (listwaenite). Veins have average grades of 6–9 g/t gold, however exploration drilling has not identified significant tonnage (Coulomb, 1983). These deposits are often the source of significant local placer gold deposits (e.g. Selib, Fig. 11; Coulomb, 1983) which have not been systematically evaluated.

Age correlation of deposit-type formation with magmatic and tectonic events is shown in Fig. 12. In the absence of additional geochronologic data on the mineralizing systems themselves, preliminary correlations suggest that (1) Khnaiguiyah-type deposits formed before, during, or immediately subsequent to D1 deformation of Al Amar group eastern sequence rocks, (2) epithermal Au–Ag–Zn–Cu-barite, porphyry Cu, and IOCG deposits were temporally and genetically related to Al Amar group western sequence and group-1 magmatism, and (3) orogenic low-sulfide Au quartz veins were best developed along the Al Amar fault zone and subsidiary zones during amalgamation of the Ar Rayn and

Author's personal copy

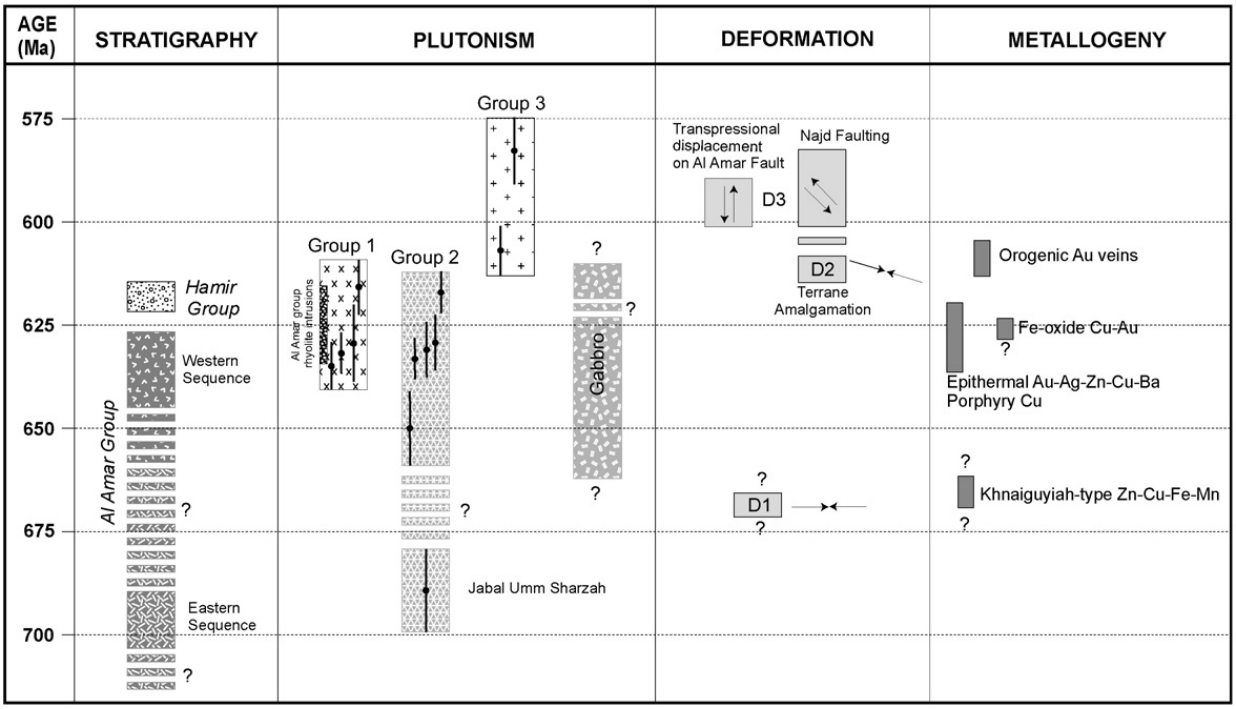

Fig. 12. Geologic history chart illustrating the temporal relationships between volcanic, plutonic, tectonic, and significant metallogenic events in the Ar Rayn terrane. Group-1, -2, and -3 intrusions show U–Pb zircon ages with error bars for selected samples representative of age range (see Table 1 for all geochronological data). Dashed events (broken bars) indicate possible continuation of event(s). Question marks indicate uncertainty in timing. Deformation arrows give directions of maximum compressive stress (colinear arrows) or simple shear (parallel arrows) with north up on the diagram.

Ad Dawadimi terranes and perhaps later during strike-slip rejuvenation of these fault zones (Fig. 12).

4. Discussion

Geologic, structural, and metallogenic characteristics of the Ar Rayn terrane are summarized in Fig. 12 and are synthesized here to discuss a geotectonic setting for the evolution of the terrane and its mineral systems. There is a clear lithogeochemical and spatial distinction between the (a) trondhjemitic, tholeiitic to calc-alkaline Al Amar group volcanic, subvolcanic and group-1 plutonic rocks and (b) the calc-alkaline adakitic group-2 plutonic rocks in the central and eastern parts of the terrane (Figs. 4; 6C and D; 7B–E; 9). Group-2 plutons represent a magmatic arc suite that was partially coeval with group-1 plutonism. The distribution of low-Al TTG plutons (group-1, west) versus high-Al TTG/adakite plutons (group-2, east) implies a west-dipping subducting slab, with the trench located somewhere east of the present margin of the Arabian shield (Fig. 13). When present in a subduction-related setting, the emplacement of adakitic rocks trenchward of the main volcanic arc is well documented in other parts of the world (Defant and Drummond, 1990, 1993; Drummond and Defant, 1990; Drummond et al., 1996; Bourdon et al., 2002; Samsonov et al., 2005). The high-Al TTG/adakite magmas are believed to represent slab melt under garnet amphibolite to eclogite facies that was generated by the subduction of young hot oceanic crust (possibly an oceanic ridge) or perhaps by high oblique subduction and related shear stresses (Drummond et al., 1996).

Geochronological data indicate some coeval emplacement of the group-1 and -2 plutonic suites, suggesting that they were generated from the same subducting slab but perhaps originated from different slab depths. However, the oldest intrusions are group-2 high-Al TTG/adakite in the eastern part of the terrane. This is consistent with an age progression of magmatism from trench to arc, with slab melting initially occurring proximal to the trench; as the slab cooled, melting migrated deeper and into the overlying mantle wedge to generate group-1 low Al-TTG in the arc.

In the arc-trench scenario described above, the Abt schist of the Ad Dawadimi terrane would correspond to either a deep-water back-arc basin sequence that accumulated between the Afif and Ar Rayn terranes or perhaps to a passive margin sedimentary sequence that formed along the Afif continental margin and on which the Ar Rayn magmatic arc was built. However, the Ad

Author's personal copy

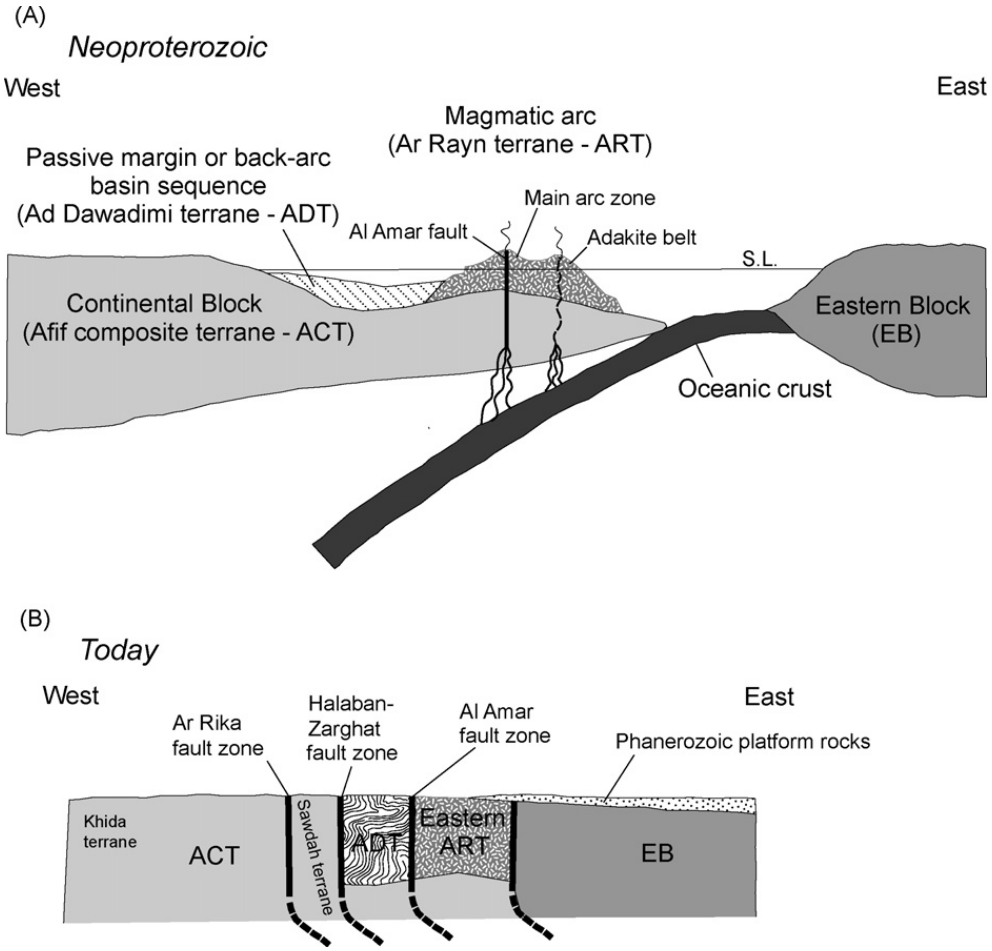

Fig. 13. Schematic section showing proposed subduction scenario for the Ar Rayn terrane and eastern Arabian shield. (A) Neoproterozoic configuration with west-directed subduction, formation of the adakite belt trenchward of the main arc zone, and formation of the Al Amar fault along the axis of the main arc zone. (B) Present-day configuration illustrating how the western segment of the Ar Rayn terrane has translated out of the section such that the Al Amar fault now separates the Ad Dawadimi and Ar Rayn terranes. The Afif composite terrane includes the Khida continental terrane (Stoeser et al., 2004; Stoeser and Frost, 2006) and the Sawdah terrane of Stoeser and Frost (2006) which either represents an older continental-margin arc (Al-Saleh and Boyle, 2001a) or is allochthonous and was translated into position along terrane-bounding faults.

Dawadimi terrane is bound by serpentinite-bearing faults and thus may instead be completely allochthonous and unrelated to the Afif and Ar Rayn terranes. This proposed scenario is consistent with findings of Al-Saleh et al. (1998) and Al-Saleh and Boyle (2001a,b) who have concluded that the Abt schist and ophiolite sequences of the Ad Dawadimi terrane (referred to as the Al Amar suture) represent a back-arc-basin suture above a west-dipping subduction complex along the eastern margin of the Afif continental terrane. Evidence of 2000-Ma inherited zircons from the 645 Ma Assaliyah plutonic complex that intrudes Abt schist along the Al Amar fault zone (Fig. 4, Table 1) suggests that older Proterozoic continental crust underlies this part of the eastern Arabian shield (Calvez et al., 1985).

What Al-Saleh et al. (1998) and Al-Saleh and Boyle (2001a,b) refer to as the Afif terrane or continental microplate corresponds to the Afif composite terrane (Stoeser and Camp, 1985; Stoeser and Stacey, 1988; Fig. 1). Earlier studies of common lead data for the Arabian shield (Stacey and Stoeser, 1983; Stoeser and Stacey, 1988) demonstrated a clear distribution of oceanic lead in the arc terranes of the western shield and continental lead, of at least early Proterozoic age, in rocks of the eastern shield, including the eastern Afif, Ad Dawadimi, and Ar Rayn terranes (Fig. 1). In a recent compilation of isotopic data for the Arabian shield, Stoeser and Frost (2006) have re-evaluated terrane delineation and conclude that the Khida terrane (Figs. 1 and 13), originally defined as part of the Afif composite terrane (Stoeser and Camp, 1985; Stoeser and Stacey, 1988; Fig. 1), is the only terrane composed of pre-Neoproterozoic continental crust and that both the western and eastern arc terranes are of oceanic arc affin-

Author's personal copy

ity. This leaves the Sawdah terrane, that separates the Khida and Ad Dawadimi terranes, in question as to its original tectonic setting. Either the Sawdah terrane represents an older continental margin arc (Al-Saleh and Boyle, 2001a) or it represents an allochthonous terrane that has translated into position along terrane-bounding faults to now separate the Ar Rayn-Ad Dawadimi continental arc-back-arc block from the Khida continental terrane.

The Al Amar fault has previously been interpreted as an ophiolitic suture zone between the Ad Dawadimi and Ar Rayn terranes (Al Shanti and Mitchell, 1976; Al-Saleh et al., 1998; Al-Saleh and Boyle, 2001a,b). However, the concentration of pre-amalgamation and syn-arc mineral deposits immediately east of the Al Amar fault (e.g., epithermal Au–Ag–Zn–Cu-barite, porphyry Cu, IOCG systems; Fig. 11) is not to be expected adjacent to an ophiolitic suture zone. Such deposits are typically formed along the axis of a magmatic arc and, for IOCG systems in particular, within continental-margin arc settings. Volcanic arcs are characterized by major trench-parallel intra-arc rifts and transpressional faults along which magma emplacement, volcanic centers, and hydrothermal systems are focused (Hamilton, 1979; Cembrano et al., 1996, 2000; Grocott and Taylor, 2002; Oyarzún et al., 2003). These deep-seated structures become major zones of transcurrent displacement during arc amalgamation and collision (McClelland et al., 2000). Our findings indicate that the Al Amar fault zone was an intra-arc fault zone, along which significant transcurrent displacement occurred (Fig. 13). The abrupt termination and apparent truncation of the Ar Rayn terrane at the Al Amar fault suggests that the western part of the Ar Rayn terrane was translated a significant distance along this major crustal structure. The western segment of the pre-faulted Ar Rayn arc is now likely concealed beneath the Phanerozoic platform sequence and may correspond to isolated magnetic anomalies centered at 21°N–46.5°E and (or) 17°N–46.5°E (Fig. 1). This would require sinistral displacement on the order of 300 km and 700 km, respectively. Such displacements along intra-arc transcurrent faults are not uncommon and have been well documented particularly along the North American cordillera (Gabrielse, 1985; Beck, 1992; McClelland et al., 2000). Though local kinematic indicators observed during this study suggest dextral displacement along the Al Amar fault south of Umm ash Shalahib, this may represent only the latest movement and not the original primary displacement.

The fault geometry of the Al Amar fault and the northwest-trending faults is analogous to well-documented intra-arc fault patterns due to oblique subduction, and particularly to intra-arc faults zones of the continental margin of the southern Cordillera of South America (Fig. 14; Brown et al., 1993; Taylor et al., 1998; Lavenu and Cembrano, 1999; Cembrano et al., 2000; Grocott and Taylor, 2002). Using this analogy, the Ar Rayn terrane fault pattern is consistent with oblique subduction from the east-southeast to the west-northwest resulting in sinistral transpressional displacement, with local transtensional domains. Serpentinized ultramafic rocks along the Al Amar fault zone need not indicate that it was the site of subduction that resulted in the collision of the two terranes. An alternative explanation is that back-arc or continental-margin rifting during formation of the Ad Dawadimi terrane gave rise to ophiolitic sequences and possible diapiric serpentinite seamounts (e.g., Boillot et al., 1980; Reston et al., 2004; Ueda et al., 2004) that were eventually juxtaposed to the Al Amar terrane during translation along the Al Amar fault zone late in the amalgamation process.

Globally, IOCG deposits are found in three general tectonic settings. These settings are characterized by (1) intra-continental orogenic collapse, (2) intra-continental anorogenic magmatism, or (3) extension along a subduction-related continental margin (Hitzman et al., 1992; Hitzman, 2000). The continental margin setting is the most plausible for the Ar Rayn terrane based on known geologic and lithogeochemical characteristics of the terrane geology and regional tectonic understanding. Therefore, the presence of IOCG deposits in the terrane is potentially diagnostic of the tectonic setting at the time of formation, and particularly when considered in conjunction with other geologic, geochronologic and lithogeochemical data.

A more recent analog to the Neoproterozoic tectonic setting of the Ar Rayn terrane, though of opposite subduction polarity, is that of the Andean margin of Chile, which is characterized by adakitic magmatic suites (Stern and Kilian, 1996; Bourdon et al., 2002), major intra-arc fault zones (e.g., the Atacama and Liquine-Ofqui fault zones; Scheuber and Gonzalez, 1999; Brown et al., 1993; Cembrano et al., 1996, 2000; Taylor et al., 1998; Lavenu and Cembrano, 1999; Grocott and Taylor, 2002), and epithermal gold, porphyry Cu, and IOCG systems localized along these fault zones (Colley et al., 1989; Espinoza, 1990; Camus et al., 1996; Oyarzún et al., 2003) (Fig. 14). In particular there are striking similarities with the Jurassic-early Cretaceous Coastal Range of northern Chile where the geotectonic setting at the beginning of the Jurassic was a north-trending magmatic arc with marine and subaerial volcanic rocks, and a marine back-arc basin overlapping the edge of the South American continental plate

Author's personal copy

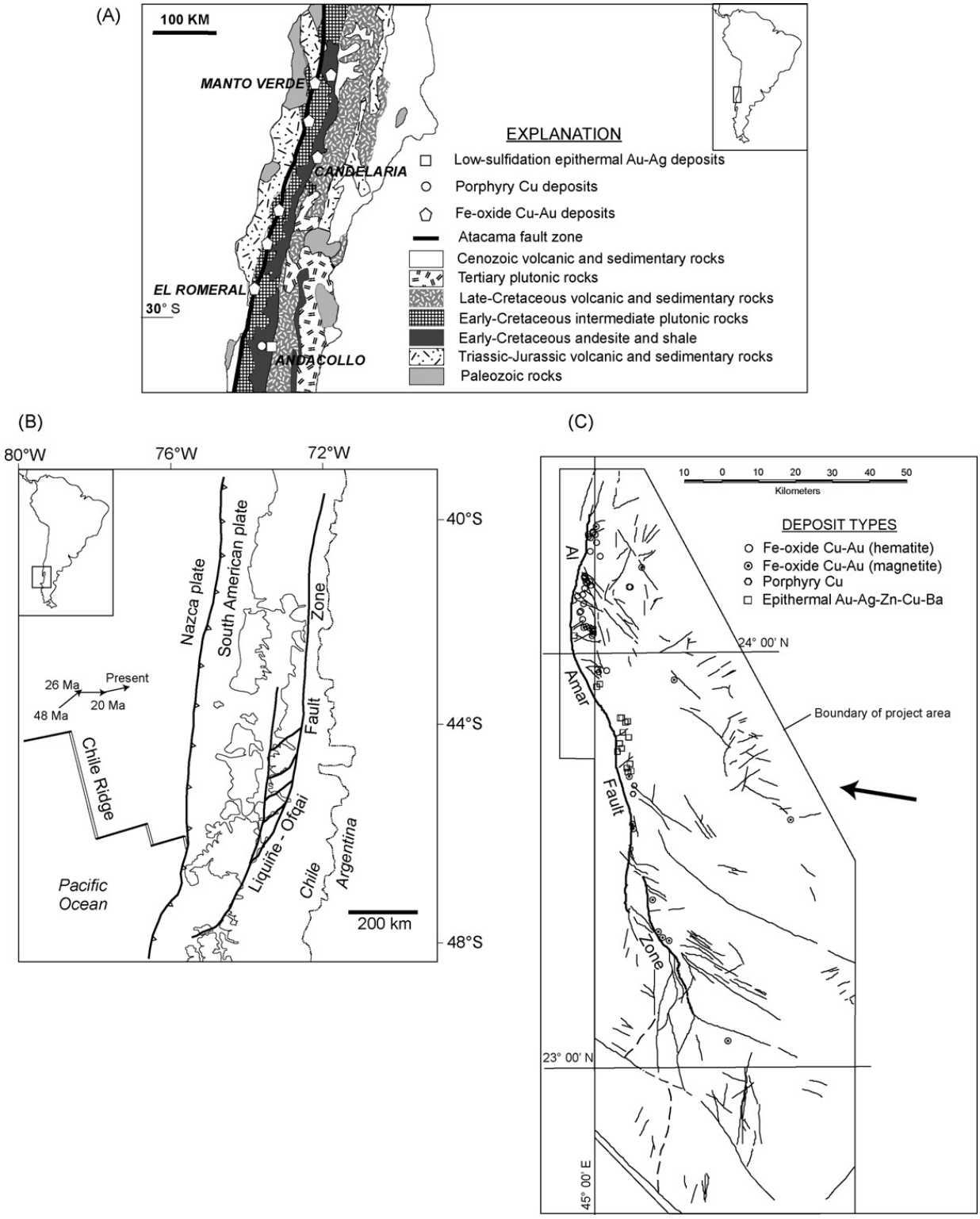

Fig. 14. Comparison of fault configurations and mineral deposit distributions between the Ar Rayn terrane and the Andean continental margin. (A) Generalized geologic map of the northern Chile coastal belt showing regional geology, the intra-arc Atacama fault, and spatially associated Fe-oxide Cu–Au, porphyry Cu, and epithermal Au deposits (modified from Espinoza, 1990); (B) Map of the southern Chilean continental margin showing the fault pattern of the Liquine-Ofqai intra-arc fault zone. Arrows refer to direction of Nazca plate motion through time (modified from Cembrano et al., 2000); (C) Distribution of faults and Fe-oxide Cu–Au, porphyry Cu, and epithermal Au deposits in the Ar Rayn terrane. Arrow represents proposed direction of eastern block plate motion, causing oblique subduction and transcurrent sinistral faulting along the Al Amar fault zone. Compare fault patterns and distribution of mineral deposits in the Ar Rayn terrane (C) with those of Chile (A and B) noting the opposite polarity of subduction in Chile vs. the Ar Rayn terrane.

Author's personal copy

(Espinoza et al., 1996). Transtensional and transpressional tectonic regimes within the arc gave rise to tholeiitic and calc-alkaline volcanic rocks, respectively (Espinoza et al., 1996). Likewise, in the Ar Rayn terrane, tholeiitic to transitional rocks formed along the central arc zone where transtensional regimes would have existed along the intra-arc Al Amar fault zone, and calc-alkaline group-2 intrusions were emplaced trenchward and presumably under a more transpressional environment.

The Afif composite terrane (the Khida continental terrane [≥1660 Ma] and adjacent continental-margin arcs and accreted terranes; Agar, 1985, 1988; Thieme, 1988; Stoeser et al., 2004; Johnson, 2005; Stoeser and Frost, 2006) was in place as a block by about 685–680 Ma (Al-Saleh et al., 1998; Doebrich et al., 2004). Collision of the Afif terrane with oceanic arc terranes of the western Arabian shield gave rise to the Nabitah orogeny, and was complete by about 640 Ma (Stacey and Agar, 1985; Stoeser and Stacey, 1988). Formation of the Ar Rayn terrane, between about 689 Ma to 616 Ma, occurred prior, during, and subsequent to the Nabitah orogeny, and corresponds to the final subduction zone that formed before complete closure of the Mozambique Ocean along what is now the eastern margin of the Arabian shield. Oblique subduction resulted in transcurrent faulting along the Al Amar fault zone and, ultimately, creation of northwest-oriented transcurrent faults. Syn- to postorogenic plutonism in the Ar Rayn terrane (607–583 Ma) followed very soon after arc plutonism, suggesting that the west-migrating land mass east of the subduction zone, which was presumably East Gondwana (the Eastern Block of Fig. 13) was not far from the continental margin at the time of Ar Rayn terrane arc formation.

Earlier studies (Stoeser and Stacey, 1988; Johnson and Kattan, 2001) have proposed that subduction and ocean basin closure in the Arabian shield culminated in the Nabitah orogeny between 680 and 640 Ma. Stern (1994) states that the consolidation of juvenile arcs in the East African orogen (EAO; Fig. 2) was complete by about 700 Ma and that tectonic escape in the northern EAO, which would have commenced only after terminal collision of East and West Gondwana, was underway by about 640 Ma. More recent studies of the East African orogen in Madagascar (Collins et al., 2003; Goncalves et al., 2003) Zimbabwe (Hargrove et al., 2003), the Nubian shield of East Africa (Abdelsalam et al., 2003) and the Sinai (Katz et al., 2004) provide evidence that subduction within the Mozambique Ocean and subsequent collision between East and West Gondwana transpired through the latest Neoproterozoic and into the Cambrian (Johnson and Woldehaimanot, 2003; Meert, 2003).

5. Conclusions

The Neoproterozoic Ar Rayn terrane is composed of the Al Amar group (AAG) volcanic arc complex and three distinct suites of plutonic rocks. The AAG volcanosedimentary rocks (>689 Ma to ~625 Ma) are divided into an eastern and western sequence based on difference in metamorphic and structural fabric and immobile trace-element lithogeochemistry (Figs. 4–6). The plutonic rocks of the terrane consist of (1) low-Al trondhjemite-tonalite-granodiorite (TTG) of arc affinity (632–616 Ma) in the western part of the terrane; these rocks have a spatial and lithogeochemical affinity with western sequence AAG rocks; (2) high-Al TTG/adakite of arc affinity (689–617 Ma) in the central and eastern part of the terrane, and (3) syn- to post-orogenic alkali granite (607–583 Ma) (Figs. 4, 7–10). The spatial distribution of high-Al TTG/adakitic rocks east of low-Al TTG within the arc is consistent with west-dipping subduction along a trench that is concealed under Phanerozoic platform rocks east of the Arabian shield (Fig. 13).

The structural fabric of the terrane is the result of three deformation events (Fig. 12). Event D1 produced foliation and local schistosity in eastern sequence AAG rocks. Amalgamation of the Ar Rayn and Ad Dawadimi terranes (D2) during oblique subduction resulted in monoclinal folding of western sequence AAG rocks. Finally, closure of the Mozambique Ocean through collision of the amalgamated terranes with a continental block from the east (D3) resulted in formation of northwest-trending Najd transcurrent faults and translational displacement along the Al Amar fault zone.

The Ar Rayn terrane is one of the most endowed terranes of the Arabian shield in terms of metallic mineral resources. Significant precious- and base-metal resources are found in epithermal Au–Ag–Zn–Cu-barite, enigmatic stratiform volcanic-hosted Khnaiguiyah-type Zn–Cu–Fe–Mn, and orogenic Au vein deposits, and the potential for significant resources exist in Fe-oxide Cu–Au (IOCG), and porphyry Cu deposits. A genetic model for Khnaiguiyah-type deposits is uncertain though may be that of a metamorphosed volcanogenic massive sulfide (VMS) deposit. There is a notable scarcity of classic VMS deposits in the terrane. The types and distribution of mineral deposits in the terrane are diagnostic of its tectonic setting. The concentration of epithermal, IOCG, and potential porphyry copper and related deposits immediately adjacent to the Al Amar fault zone (Fig. 11) suggests that this zone was a major intra-arc fault along which magmatism and mineral systems were focused. Furthermore, the presence of IOCG systems is

Author's personal copy

indicative of a magmatic arc that formed in a continental margin setting.

Geologic, structural, and metallogenic characteristics of the Ar Rayn terrane are analogous to the Andean continental margin of Chile (Fig. 14). Marine to subaerial, tholeiitic to calc-alkaline volcanic rocks, adakitic magmatic suites, major intra-arc fault zones and related epithermal, porphyry copper, and IOCG deposits are examples of shared characteristics between the Ar Rayn terrane and the Andean continental margin. We conclude that the Ar Rayn terrane represents a very similar continental margin setting above a west-dipping subduction zone along a continental block, presumably the Khida terrane or eastern margin of the Afif composite terrane (Fig. 13).

Our findings indicate that arc formation and accretionary processes in the eastern Arabian shield were still ongoing into the latest Neoproterozoic (Ediacaran), to about 620–600 Ma. Geologic evolution of the Ar Rayn terrane (arc formation, accretion, syn- to postorogenic plutonism) and associated metallogeny took place during the final stages of the assembly of the Gondwana supercontinent along the northeastern margin of the East African orogen.

Acknowledgements

This work was done under the terms of the Eleventh and Twelfth Extensions to the Work Agreement between the U.S. Geological Survey and the Saudi Arabian Ministry of Petroleum and Mineral Resources. The authors wish to thank Douglas B. Stoeser for constructive comment on this work as well as Klaus J. Schulz, Stephen G. Peters and two anonymous journal reviewers for technical review of manuscripts that helped improve the clarity of presentation.

Appendix A. Lithogeochemical data for igneous rocks: Ar Rayn Terrane

Major element oxides and elemental Fe and Na are in weight percent. All other analyses are in parts per million.

(*) no data

Unit label definitions:

- gb: gabbro
- grp3: group-3 intrusion
- grp2: group-2 intrusion
- grp1: group-1 intrusion
- hamir: Hamir group
- aai: Al Amar group felsic porphyritic intrusion
- aaaw: Al Amar group western sequence, intermediate to mafic volcanic rock
- aarw: Al Amar group western sequence, felsic volcanic rock
- aaae: Al Amar group eastern sequence, intermediate to mafic volcanic rock
- aare: Al Amar group eastern sequence, felsic volcanic rock

Data sources and analytical methods:

1. this study
   - Major element analyses, reported as oxides, by total digestion ICP-AES at Saudi Geological Survey (SGS) Lab, Jeddah
   - FeO analyses by colorimetric titration at SGS Lab, Jeddah
   - H_2O analyses by gravimetric technique at SGS Lab, Jeddah
   - Au, As, Br, Co, Cr, Fe, Ir, Na, Sb, Sc, and Se analyses by INAA ACTLABS-SKYLINE Lab, Tucson, AZ
   - All other analyses by fusion ICP/MS, ACTLABS-SKYLINE Lab, Tucson, AZ
2. Le Bel and Laval (1986)
   - All analyses by inductively coupled plasma atomic emission spectrometry
3. BRGM (2003)
   - Major elements by X-ray fluorescence
   - All other analyses by inductively coupled plasma mass spectrometry

Author's personal copy

Sample	AR-PC-01	AR-PC-02	AR-PC-03	AR-PC-04	AR-PC-05	AR-PC-06	AR-PC-07	AR-PC-08	AR-PC-09	AR-PC-10	AR-PC-11	AR-PC-12	AR-PC-13	AR-PC-14	AR-PC-15	AR-PC-16	AR-PC-17	AR-PC-18	AR-PC-19	AR-PC-20	AR-PC-21	AR-PC-22	AR-PC-23	AR-PC-24	AR-PC-25	AR-PC-26
Corresponding Geochron Sample							AR-GC-4	AR-GC-5												AR-GC-11					AR-GC-14	
Age (Ma)							616 ± 7	632 ± 5												617 ± 5					583 ± 8	
Unit	aai	aarw	aai	aaaw	aai	aai	grp1	grp1	aare	aai	aai	aare	aare	aaae	aare	aare	grp2	aare	gb	grp2	gb	grp2	hamir	gb	grp3	grp1
Data Source	1	1	1	1	1	1	1	1	1	1	1	1	1	1	1	1	1	1	1	1	1	1	1	1	1	1
Longitude	44.94642	44.97510	45.09008	45.04707	45.04877	45.06160	45.06864	45.00881	45.08947	45.07879	45.06631	45.11902	45.12558	45.31010	45.31364	45.51431	45.62163	45.55608	45.53773	45.48959	45.31207	45.25398	45.22457	45.29267	45.48540	45.17712
Latitude	24.04171	24.17500	23.71886	23.85857	23.85828	23.85614	23.86875	23.97520	24.27864	24.29151	24.28888	24.15862	24.21575	22.74249	22.73277	22.71432	23.01927	22.99486	22.99288	22.99936	23.07745	23.03977	23.10467	23.13854	23.23524	23.32694
Approx. location																										
SiO_2	60.68	71.30	75.30	51.20	72.80	74.90	76.00	71.60	68.80	70.00	67.91	74.50	70.00	56.25	76.30	76.00	72.00	78.40	51.25	75.50	51.75	71.60	56.00	41.15	75.50	62.15
Al_2O_3	12.10	12.85	11.64	11.23	12.95	11.98	12.19	13.02	12.73	13.60	13.80	11.87	13.50	13.80	12.25	12.40	15.00	11.75	14.20	13.80	16.60	15.00	16.40	16.15	12.80	15.50
Fe_2O_3T	4.84	4.56	1.90	10.80	2.59	2.25	1.93	3.86	4.82	3.87	5.36	4.35	6.00	12.15	2.80	3.00	2.40	1.75	9.90	0.80	8.40	2.25	8.50	11.60	1.36	8.25
TiO_2	0.45	0.47	0.28	0.88	0.29	0.27	0.29	0.30	0.55	0.58	0.73	0.33	0.51	1.26	0.40	0.22	0.26	0.15	0.44	0.06	0.61	0.26	1.05	0.72	0.18	0.70
CaO	7.90	1.60	1.12	16.12	1.40	1.40	1.42	3.05	1.43	0.70	1.22	1.60	2.80	6.20	1.46	1.10	2.80	2.00	9.90	2.00	10.80	3.40	6.50	9.80	0.70	5.10
MgO	1.42	1.00	1.62	4.00	0.71	0.92	0.40	1.11	1.12	0.88	1.10	0.40	0.55	3.10	0.42	0.18	1.18	0.60	9.50	0.40	7.60	0.96	3.80	6.15	0.44	2.60
Na_2O	4.94	7.46	5.60	2.83	6.34	6.34	5.87	3.71	5.80	5.26	6.07	4.56	6.23	4.23	5.37	4.41	4.36	4.22	1.83	4.69	2.70	5.13	4.05	0.97	3.80	3.71
K_2O	0.30	<0.05	0.12	<0.05	0.40	0.10	0.33	2.10	1.70	2.30	1.62	1.22	0.18	0.17	1.60	3.32	2.20	1.42	0.20	3.11	0.33	0.69	2.10	1.80	4.80	1.18
MnO	0.14	0.06	0.12	0.29	0.09	0.10	<0.05	0.10	0.11	0.21	0.30	0.18	0.09	0.23	0.12	0.09	0.06	0.10	0.17	<0.05	0.12	0.06	0.15	0.14	<0.05	0.10
P_2O_5	0.16	0.09	<0.05	0.10	0.05	<0.05	<0.05	<0.05	0.13	0.10	0.16	<0.05	0.10	0.31	0.07	<0.05	0.08	<0.05	<0.05	<0.05	0.06	0.11	0.32	0.06	0.05	0.16
L.O.I	7.77	0.96	1.70	2.03	1.47	1.08	0.82	1.08	1.18	1.33	1.20	0.84	0.48	2.01	0.58	0.31	0.71	0.66	1.20	0.41	0.30	1.16	2.03	11.10	1.00	1.91
Total	100.70	100.35	99.40	99.48	99.69	99.34	99.25	99.93	98.37	98.83	99.47	99.85	100.44	99.71	101.37	101.03	101.05	101.05	98.59	100.77	99.27	100.62	100.90	99.64	100.63	101.36
FeO	3.66	1.53	1.54	5.42	1.58	1.02	0.73	2.40	2.19	1.68	2.00	1.95	1.66	5.02	0.69	2.16	1.31	0.85	7.84	0.27	5.37	0.86	5.04	8.44	0.42	3.01
Fe_2O_3	0.77	2.86	0.19	4.78	0.83	1.12	1.12	1.19	2.39	2.00	3.14	2.18	4.16	6.57	2.03	0.60	0.94	0.81	1.19	0.50	2.43	1.29	2.90	2.22	0.89	4.91
H2O-	0.18	0.25	0.01	0.25	0.18	0.08	0.19	0.11	0.15	0.15	0.17	0.11	*	*	*	*	*	*	*	*	*	*	*	*	*	*
H2O+	1.72	0.63	0.98	1.28	0.68	0.47	0.64	0.41	1.11	1.09	0.50	0.34	*	*	*	*	*	*	*	*	*	*	*	*	*	*
Li	*	*	*	*	*	*	*	*	*	*	*	*	*	*	*	*	*	*	*	*	*	*	*	*	*	*
Na	3.92	5.51	4.17	2.05	4.79	5.12	4.37	2.82	4.37	4.24	4.73	3.48	4.55	2.87	3.52	2.95	3.12	2.69	0.95	3.27	1.69	3.57	2.83	0.4	2.59	2.32
Sc	15.4	15.4	8.3	36.7	9.8	9.9	8.5	14	15.5	16.9	18.3	11.6	14.8	44.2	10.2	7.9	4.3	6.1	39.4	1.1	31.8	3.2	22.3	42.7	3.1	24.6
V	47	52	13	349	20	18	22	67	44	<5	<5	<5	<5	322	10	<5	41	9	255	6	182	35	168	439	17	142
Cr	9	20	20	31	14	20	14	13	18	<5	<5	12	15	37	13	8	19	9	387	<5	221	8	104	38	7	16
Fe	3.84	3.4	1.55	8.22	2.08	1.79	1.52	3.02	3.83	3.17	4.33	3.32	4.45	9.18	1.74	2.25	1.84	1.29	7.57	0.57	6.82	1.64	6.74	9.62	1.02	6.15
Co	9	10	2	24	3	4	3	9	9	<1	3	2	10	28	<1	<1	8	2	48	2	52	6	30	56	3	20
Ni	<20	<20	<20	32	<20	<20	<20	<20	<20	<20	23	<20	<20	22	<20	<20	37	57	128	<20	106	<20	49	74	<20	20
Cu	25	69	108	343	<10	<10	<10	71	50	<10	<10	23	<10	43	<10	<10	13	<10	89	<10	80	234	97	659	426	13
Zn	36	<30	31	69	32	58	<30	44	90	148	67	48	<30	102	66	55	33	<30	75	<30	67	<30	74	89	38	38
Ga	12	15	11	15	14	12	12	14	16	19	16	17	19	15	12	19	16	11	15	12	17	15	19	16	19	16
Ge	<1	1	<1	3	<1	<1	<1	1	1	1	1	1	<1	2	1	<1	<1	<1	1	<1	1	<1	1	1	1	1
As	4.5	9.8	3.7	58.4	4.4	3.9	5.5	12.6	2.9	1.6	2	2	1.7	3.4	1.5	1.3	1.9	2.5	1.6	3.8	1.5	3	23.9	2	1.6	4.5
Se	<3	<3	<3	<3	<3	<3	<3	<3	<3	<3	<3	<3	<3	<3	<3	3	<3	<3	<3	<3	<3	<3	<3	<3	<3	<3
Ile	<0.5	<0.5	<0.5	<0.5	<0.5	<0.5	1.6	2.3	<0.5	<0.5	<0.5	<0.5	<0.5	<0.5	<0.5	<0.5	<0.5	<0.5	<0.5	<0.5	<0.5	1	<0.5	<0.5	3.2	<0.5
Rb	3	<2	<2	<2	4	<2	2	33	15	21	12	10	<2	5	20	53	37	20	2	42	<2	6	25	48	206	18
Sr	121	45	96	290	79	56	83	144	95	111	101	87	138	123	98	140	567	91	409	424	830	549	642	361	106	336
Y	24	37	35	18	25	27	37	29	45	50	47	66	68	21	30	51	5	29	7	4	8	4	18	7	5	20
Zr	98	167	147	41	126	134	150	115	201	179	141	259	207	44	119	271	72	113	10	53	13	51	126	9	93	101
Nb	3	5	3	2	3	3	4	4	5	5	4	6	7	1	3	12	3	5	<1	2	<1	1	4	<1	9	3
Mo	<2	<2	<2	3	<2	<2	<2	<2	<2	<2	<2	2	<2	<2	<2	3	<2	<2	<2	<2	<2	<2	<2	<2	25	<2
Ag	<0.5	<0.5	<0.5	<0.5	<0.5	<0.5	<0.5	<0.5	<0.5	<0.5	<0.5	<0.5	<0.5	<0.5	<0.5	<0.5	<0.5	<0.5	<0.5	<0.5	<0.5	<0.5	<0.5	<0.5	<0.5	<0.5
In	<0.2	<0.2	<0.2	<0.2	<0.2	<0.2	<0.2	<0.2	<0.2	<0.2	<0.2	<0.2	<0.2	<0.2	<0.2	<0.2	<0.2	<0.2	<0.2	<0.2	<0.2	<0.2	<0.2	<0.2	<0.2	<0.2
Sn	<1	2	<1	<1	<1	<1	1	1	20	13	10	8	8	5	5	4	3	3	2	2	2	2	2	1	3	2
Sb	1.5	<0.1	0.7	2.5	0.6	<0.1	0.2	0.7	0.2	0.3	0.4	0.2	0.3	<0.1	<0.1	<0.1	<0.1	0.2	0.3	0.7	0.3	0.4	1.4	0.6	0.2	0.6
Cs	<0.5	<0.5	<0.5	<0.5	<0.5	<0.5	<0.5	0.7	<0.5	<0.5	<0.5	<0.5	<0.5	<0.5	<0.5	<0.5	1.2	<0.5	<0.5	1.3	<0.5	0.5	<0.5	0.7	4.0	1.1
Ba	304	29	103	37	339	45	87	418	452	1,170	669	649	75	67	642	1,100	768	630	81	1,150	160	469	594	143	309	249
Hf	2.8	4.8	4.2	1.2	3.7	3.9	4.4	3.7	5.5	5.1	4.3	7.3	8.4	1.3	3.4	7.4	2.0	3.2	0.4	1.6	0.5	1.3	3.5	0.3	3.2	2.7
Ta	0.2	0.3	0.2	<0.1	0.2	0.2	0.4	0.3	0.3	0.3	0.2	0.3	0.4	<0.1	0.2	0.9	0.3	0.3	<0.1	0.1	<0.1	<0.1	0.3	<0.1	1.1	0.2
W	<1	<1	<1	<1	<1	<1	<1	<1	<1	<1	<1	<1	<1	<1	<1	<1	<1	<1	<1	<1	<1	<1	<1	2	2	<1
Ir	<5	<5	<5	<5	<5	<5	<5	<5	<5	<5	<5	<5	<5	<5	<5	<5	<5	<5	<5	<5	<5	<5	<5	<5	<5	<5
Au	<2	<2	<2	<2	9	<2	<2	<2	<2	<2	<2	<2	<2	5	2	6	6	6	<2	11	10	22	<2	28	<2	<2
Tl	0.1	<0.1	<0.1	<0.1	0.2	<0.1	<0.1	0.2	0.2	0.2	<0.1	<0.1	<0.1	<0.1	0.1	0.2	0.2	<0.1	<0.1	0.2	<0.1	<0.1	0.1	0.2	1.4	0.2
Pb	<5	13	<5	11	<5	<5	41	<5	6	38	15	<5	<5	<5	6	6	18	14	<5	12	5	<5	5	<5	28	<5
Bi	<0.4	<0.4	<0.4	<0.4	<0.4	<0.4	<0.4	<0.4	<0.4	<0.4	<0.4	<0.4	<0.4	<0.4	<0.4	<0.4	<0.4	<0.4	<0.4	<0.4	<0.4	<0.4	<0.4	<0.4	<0.4	<0.4
Th	1.1	4.4	1.8	0.2	1.8	2.2	2.0	3.6	2.4	2.7	2.4	3.1	3.1	0.3	1.6	6.5	4.1	4.2	0.3	3.8	0.2	0.3	2.9	<0.1	18.0	3.0
U	1.0	2.4	0.8	0.5	0.7	0.9	0.7	1.7	1.1	1.1	1.0	1.3	1.3	0.1	0.5	0.9	2.7	0.9	<0.1	1.0	<0.1	0.1	1.2	<0.1	4.9	0.6
La	6.9	11.2	11.5	3.3	9.1	8.0	10.1	11.8	14.7	16.5	13.5	18.8	22.6	2.6	10.1	41.9	16.3	17.3	1.8	9.5	3.5	4.2	16.6	1.0	12.3	8.3
Ce	16.0	33.0	25.7	8.1	19.5	18.8	24.8	25.4	33.6	35.8	30.8	43.2	49.0	6.5	21.5	76.2	26.7	32.8	3.9	15.3	8.2	8.4	35.5	2.9	21.5	18.3
Pr	2.42	4.85	3.68	1.38	2.78	2.77	3.84	3.49	4.95	5.63	4.79	6.56	7.28	1.14	3.13	9.49	2.95	4.16	0.64	1.62	1.37	1.14	5.10	0.56	2.25	2.65
Nd	11.3	20.5	16.3	7.1	12.5	12.2	16.9	14.3	22.6	26.3	23.0	30.4	34.0	6.4	14.1	37.1	9.9	16.5	3.3	5.3	7.3	4.7	22.5	3.2	7.3	12.1
Sm	2.9	4.6	3.8	2.0	2.9	2.8	4.3	3.1	5.5	6.5	6.0	7.7	8.5	2.1	3.6	7.5	1.4	3.4	1.0	0.7	1.9	0.9	4.5	1.0	1.1	2.8
Eu	1.02	0.81	0.93	0.80	0.80	0.55	0.68	0.54	1.37	2.10	1.88	1.74	1.47	0.91	0.97	1.61	0.54	0.74	0.45	0.22	0.76	0.41	1.27	0.44	0.28	0.87
Gd	3.5	5.1	4.3	2.5	3.4	3.2	5.0	3.5	6.1	7.8	7.1	8.8	9.6	2.9	4.1	8.0	1.1	3.6	1.2	0.6	1.8	0.7	4.0	1.2	0.8	3.1
Tb	0.6	0.9	0.8	0.5	0.6	0.6	0.9	0.6	1.1	1.3	1.2	1.7	1.8	0.6	0.8	1.5	0.2	0.7	0.2	<0.1	0.3	0.1	0.6	0.2	0.1	0.6
Dy	4.2	5.9	5.4	3.1	4.1	4.3	6.1	4.4	7.3	8.8	8.2	11.0	11.4	3.7	5.0	8.9	0.9	4.3	1.3	0.5	1.7	0.6	2.5	1.3	0.7	3.5
Ho	0.9	1.3	1.2	0.7	0.9	0.9	1.3	1.0	1.6	1.9	1.8	2.3	2.5	0.8	1.1	1.9	0.2	1.0	0.3	0.1	0.3	0.1	0.7	0.3	0.1	0.7
Er	2.6	3.7	3.5	1.9	2.7	2.8	3.8	3.0	4.6	5.4	5.1	6.9	7.0	2.2	3.1	5.3	0.5	2.9	0.8	0.3	0.9	0.3	1.9	0.7	0.4	2.1
Tm	0.38	0.57	0.53	0.27	0.41	0.45	0.56	0.48	0.70	0.79	0.74	1.03	1.06	0.32	0.47	0.77	0.07	0.46	0.11	0.05	0.12	<0.05	0.26	0.11	0.07	0.31
Yb	2.5	3.6	3.5	1.8	2.8	3.0	3.6	3.2	4.5	5.1	5.1	6.9	7.0	2.1	3.2	5.1	0.5	3.2	0.7	0.4	0.7	0.3	1.6	0.6	0.5	2.0
Lu	0.40	0.56	0.55	0.27	0.46	0.49	0.54	0.52	0.68	0.80	0.75	1.01	1.02	0.30	0.49	0.74	0.09	0.49	0.11	0.07	0.10	0.05	0.23	0.10	0.09	0.30

Author's personal copy

Sample	AR-PC-27	AR-PC-28	AR-PC-29	AR-PC-30	AR-PC-31	AR-PC-32	AR-PC-33	AR-PC-34	AR-PC-35	1214	1222	1238	1252	1256	1281	1292	1211A	1211B	1212A	1235A	1235D	1255A	1287D	1339A	ALA03B	ALA05A
Corresponding Ge		AR-GC-17					AR-GC-16																			
Age (Ma)		607 ± 6					689 ± 10																			
Unit	grp2	grp3	aarw	gb	aaow	aaco	grp2	grp1?	gb	grp2	grp1	grp2	grp2	grp1	grp2	grp3	grp3	grp3	grp3	grp2	grp2	grp1	grp2	grp1	aarw	aarw
Data Source	1	1	1	1	1	1	1	1	1	2	2	2	2	2	2	2	2	2	2	2	2	2	2	2	3	3
Longitude	45.31663	45.54191	45.10878	45.22761	45.08484	45.04713	45.17218	45.16477	45.14328	45.4718137	45.1348039	45.4044118	45.4595588	45.1286765	45.5392157	45.4901961	45.557598	45.557598	45.4779412	45.3063726	45.3063726	45.122549	45.3615196	45.0122549	44.9975	45.0677
Latitude	23.96265	23.56964	23.51730	23.61514	23.69739	24.01101	24.00768	24.02167	24.06764	23.2359551	23.488764	23.4494382	23.0280899	23.6797753	22.8876405	23.3932584	23.1123596	23.1123596	23.1011236	23.6179775	23.6179775	23.7078652	23.2078652	24.0505618	23.9086	23.7783
Approx. location																										
SiO_2	74.10	77.00	77.25	46.50	58.50	67.70	71.50	77.25	46.85	76.92	78.32	74.66	71.79	77.05	71.98	76.83	76.89	74.68	74.70	69.00	77.00	72.40	76.10	73.48	61.40	70.50
Al_2O_3	14.10	12.90	12.10	18.50	15.80	14.30	15.50	12.30	16.40	12.89	11.31	13.67	15.37	11.26	13.82	12.11	12.34	13.7	13.3	15.25	12.72	12.93	12.25	14.28	15.9	13.7
Fe_2O_3T	1.62	0.60	2.00	6.60	7.40	5.90	1.82	1.90	8.80	1.17	1.58	1.63	2.11	2.05	2.05	1.13	0.79	1.81	2	3.22	0.82	4.33	1.09	2.6	7.56	3.54
TiO_2	0.20	0.10	0.22	0.15	0.58	0.66	0.19	0.13	0.41	0.18	0.27	0.26	0.31	0.17	0.2	0.08	0.07	0.21	0.23	0.28	0.11	0.38	0.1	0.22	0.63	0.52
CaO	1.66	0.75	0.80	12.20	6.30	2.29	2.65	0.80	14.15	0.84	4.88	0.97	2.58	1.31	1.71	0.29	0.15	0.34	0.96	3.27	0.41	3.11	0.59	2.17	2.7	0.4
MgO	0.58	0.20	0.60	10.75	2.80	0.79	0.55	0.20	9.40	0.15	0.15	0.02	0.71	0.26	0.47	0.09	0.22	0.09	0.46	1.26	*	0.93	0.09	0.51	1.6	1.4
Na_2O	4.60	3.81	6.05	1.78	3.85	5.15	5.25	5.15	1.19	3.61	2.6	4.04	4.61	4.34	3.64	3.82	2.85	3.03	4.07	4.3	3.96	3.83	3.63	3.67	5.3	5.7
K_2O	3.26	5.60	0.10	0.10	1.46	2.62	1.09	2.05	0.33	4.2	0.09	4.34	2.38	1.68	3.4	4.31	5.04	4.96	4.3	2.16	4.27	1.8	4.41	2.17	2.21	0.66
MnO	<0.05	<0.05	0.06	0.10	0.14	0.07	0.12	<0.05	0.18	0.03	0.02	0.05	0.04	0.04	0.04	0.02	0.03	0.06	0.04	0.07	0.02	0.08	0.02	0.06	0.13	0.17
P_2O_5	0.07	<0.05	<0.05	<0.05	0.10	0.22	0.06	<0.05	0.11	*	*	*	0.08	*	*	0.34	0.04	0.06	0.09	*	*	*	*	*	0.14	0.11
LOI	0.54	0.42	0.84	2.23	2.62	0.27	0.92	0.55	1.58	0.09	0.43	0.09	0.46	0.63	2.05	0.18	1.21	1.52	0.07	0.63	0.27	0.31	0.4	0.63	2.1	2
Total	100.73	101.38	100.02	98.91	99.55	99.79	99.65	100.33	99.40	100.08	99.65	99.73	100.44	98.79	99.36	99.20	99.63	100.46	100.22	99.44	99.58	100.10	98.68	99.79	99.67	99.10
FeO	0.85	0.20	1.40	4.95	5.10	2.74	0.92	0.21	6.73	*	*	*	*	*	*	*	*	*	*	*	*	*	*	*	*	*
Fe_2O_3	0.68	0.38	0.44	1.10	1.73	2.86	0.80	1.67	1.32	*	*	*	*	*	*	*	*	*	*	*	*	*	*	*	*	*
H2O-	*	*	*	*	*	*	*	*	*	*	*	*	*	*	*	*	*	*	*	*	*	*	*	*	*	*
H2O+	*	*	*	*	*	*	*	*	*	*	*	*	*	*	*	*	*	*	*	*	*	*	*	*	*	*
Li	*	*	*	*	*	*	*	*	*	*	*	*	*	*	*	*	*	*	*	*	*	*	*	*	<10	<10
Na	3.36	2.63	4.21	0.92	2.51	3.68	4.64	4.59	1.1	*	*	*	*	*	*	*	*	*	*	*	*	*	*	*	*	*
Sc	2.5	2.4	10.6	20.8	28.5	18.8	2.4	1.5	78.6	*	*	*	*	*	*	*	*	*	*	*	*	*	*	*	*	*
V	19	5	6	69	170	18	20	<5	122	16	119	*	172	12	42	12	*	36	35	*	*	83	12	38	148	40
Cr	9	8	11	431	25	12	<5	<5	427	*	*	*	*	*	*	*	*	*	*	*	*	*	*	*	22	19
Fe	1.24	0.48	1.55	5.25	5.89	4.35	1.52	1.68	8.26	*	*	*	*	*	*	*	*	*	*	*	*	*	*	*	*	*
Co	4	1	3	66	23	3	6	<1	55	*	*	*	*	*	*	*	*	*	*	*	*	*	*	*	16	6
Ni	<20	<20	<20	246	22	<20	<20	<20	80	*	*	*	*	*	*	*	*	*	*	*	*	*	*	*	<10	<10
Cu	<10	<10	<10	47	64	<10	<10	18	38	*	*	*	*	*	*	*	*	*	*	*	*	*	*	*	*	*
Zn	<30	<30	<30	<30	44	<30	<30	<30	37	*	*	*	*	*	*	*	*	*	*	*	*	*	*	*	*	*
Ga	16	17	12	12	15	16	16	24	12	*	*	*	*	*	*	*	*	*	*	*	*	*	*	*	*	*
Ge	<1	1	1	<1	1	1	<1	1	1	*	*	*	*	*	*	*	*	*	*	*	*	*	*	*	*	*
As	2.2	2.1	9	2	2.8	3.4	6.7	8.2	1	*	*	*	*	*	*	*	*	*	*	*	*	*	*	*	*	*
Se	<3	<3	<3	<3	<3	<3	<3	<3	<3	*	*	*	*	*	*	*	*	*	*	*	*	*	*	*	*	*
Br	2.4	<0.5	<0.5	2.9	<0.5	<0.5	<0.5	2.7	<0.5	*	*	*	*	*	*	*	*	*	*	*	*	*	*	*	*	*
Rb	32	173	<2	<2	26	27	20	23	3	164	*	123	64	48	148	147	169	177	149	63	96	55	99	31	42	7
Sr	351	97	81	736	316	188	475	80	264	152	373	149	888	91	336	66	98	197	198	389	59	169	161	110	363	60
Y	6	12	43	3	21	36	6	104	8	7.7	45.8	8.3	2.1	34.5	7.9	57.8	6.6	13.8	20.6	6.6	3.8	34.9	7.7	49.6	22.2	23
Zr	109	67	160	6	77	114	63	268	8	*	*	*	*	*	*	*	*	*	*	*	*	*	*	*	98	161
Nb	3	10	4	<1	2	3	2	4	<1	*	*	*	*	*	*	*	*	*	*	*	*	*	*	*	2.4	4.1
Mo	<2	<2	<2	<2	<2	<2	<2	<2	<2	*	*	*	*	*	*	*	*	*	*	*	*	*	*	*	*	*
Ag	<0.5	<0.5	<0.5	<0.5	<0.5	<0.5	<0.5	<0.5	<0.5	*	*	*	*	*	*	*	*	*	*	*	*	*	*	*	*	*
In	<0.2	<0.2	<0.2	<0.2	<0.2	<0.2	<0.2	<0.2	<0.2	*	*	*	*	*	*	*	*	*	*	*	*	*	*	*	*	*
Sn	1	2	2	<1	1	2	<1	4	<1	*	*	*	*	*	*	*	*	*	*	*	*	*	*	*	*	*
Sb	<0.1	1	0.4	<0.1	1.5	0.5	<0.1	<0.1	0.3	*	*	*	*	*	*	*	*	*	*	*	*	*	*	*	*	*
Cs	<0.5	4.3	<0.5	<0.5	0.6	<0.5	<0.5	<0.5	<0.5	*	*	*	*	*	*	*	*	*	*	*	*	*	*	*	*	*
Ba	890	314	102	41	276	754	385	531	63	364	55	554	1220	553	887	107	917	1186	438	646	805	318	517	391	518	443
Hf	3.0	2.9	4.5	0.2	2.3	3.2	1.7	7.9	0.3	*	*	*	*	*	*	*	*	*	*	*	*	*	*	*	2.6	4.1
Ta	0.2	2.1	0.2	<0.1	0.1	0.2	0.1	0.5	<0.1	*	*	*	*	*	*	*	*	*	*	*	*	*	*	*	0.2	0.2
W	<1	<1	<1	<1	<1	<1	<1	<1	<1	*	*	*	*	*	*	*	*	*	*	*	*	*	*	*	*	*
Ir	<5	<5	<5	<5	<5	<5	<5	<5	<5	*	*	*	*	*	*	*	*	*	*	*	*	*	*	*	*	*
Au	12	<2	<2	8	<2	<2	30	37	<2	*	*	*	*	*	*	*	*	*	*	*	*	*	*	*	*	*
Tl	0.1	0.6	<0.1	<0.1	0.2	<0.1	0.1	0.2	<0.1	*	*	*	*	*	*	*	*	*	*	*	*	*	*	*	*	*
Pb	8	11	<5	<5	<5	<5	<5	<5	<5	*	*	*	*	*	*	*	*	*	*	*	*	*	*	*	*	*
Bi	<0.4	<0.4	<0.4	<0.4	<0.4	<0.4	<0.4	<0.4	<0.4	*	*	*	*	*	*	*	*	*	*	*	*	*	*	*	*	*
Th	3.6	13.2	2.2	0.2	1.4	2.6	1.2	4.0	0.2	*	*	*	*	*	*	*	*	*	*	*	*	*	*	*	2.2	1.4
U	0.5	3.4	0.8	<0.1	0.7	1.0	0.7	1.7	<0.1	*	*	*	*	*	*	*	*	*	*	*	*	*	*	*	0.6	0.3
La	14.0	14.9	11.5	0.8	6.6	11.3	10.9	39.1	1.2		13.9	22.1	8.4	14.5	21.4	46	15.1	25.7	29.2	13.8	6.5	13.6	21.2	21	10.3	9
Ce	25.0	29.9	27.8	1.9	14.6	25.4	21.2	84.6	2.8	23.7	32.7	37.2	11.4	31.1	33.1	95	27.1	44.7	58.3	24.9	10.9	32.4	38.5	49.2	19.8	14
Pr	2.98	3.73	3.94	0.31	2.17	3.78	2.71	13.24	0.49	*	*	*	*	*	*	*	*	*	*	*	*	*	*	*	2.6	2.3
Nd	10.7	13.3	17.9	1.6	10.0	17.5	10.7	60.5	2.8	8.8	17.6	12.3	3.9	14.7	12.3	41.6	9.5	16.8	21.6	10.3	4.5	15.3	12.9	22.4	12.1	11.1
Sm	1.8	2.6	4.6	0.4	2.6	4.4	1.6	14.8	1.0	1.9	4.82	2.3	0.07	4.2	1.8	9.4	1.8	3.3	4.2	1.9	0.79	4.1	2.2	5.6	2.9	2.3
Eu	0.46	0.28	0.96	0.28	0.81	1.38	0.49	1.91	0.57	0.42	0.76	0.65	0.43	0.76	0.49	0.71	0.32	0.61	0.41	0.58	0.27	0.74	0.57	0.62	0.9	0.7
Gd	1.4	2.1	5.5	0.5	2.8	5.0	1.3	16.0	1.3	1.2	4.8	1.9	0.67	4.3	0.92	8.5	1.4	2.6	3.8	1.4	0.78	3.9	1.6	5.4	3	3
Tb	0.2	0.4	1.0	<0.1	0.6	1.0	0.2	3.2	0.2	*	*	*	*	*	*	*	*	*	*	*	*	*	*	*	0.5	0.5
Dy	1.1	2.0	7.1	0.5	3.5	6.0	0.9	19.7	1.5	1	6.2	1.1	0.27	4.8	1.16	9.2	0.98	2.1	3.3	1.1	0.36	4.5	1.2	6.5	3.5	3.5
Ho	0.2	0.4	1.6	0.1	0.8	1.3	0.2	4.1	0.3	*	*	*	*	*	*	*	*	*	*	*	*	*	*	*	0.8	0.8
Er	0.6	1.2	4.6	0.3	2.2	3.8	0.6	12.0	0.8	0.76	4.4	0.99	0.21	3.4	0.66	5.6	0.61	1.3	1.8	0.96	0.36	3.3	0.87	4.7	2.3	2.3
Tm	0.08	0.19	0.72	<0.05	0.32	0.56	0.10	1.83	0.11	*	*	*	*	*	*	*	*	*	*	*	*	*	*	*	0.4	0.4
Yb	0.5	1.3	4.6	0.2	2.2	3.8	0.8	11.9	0.7	0.75	4.8	1	0.19	3.3	0.63	5.5	0.56	1.2	1.6	0.5	0.34	3.8	0.76	5.5	2.1	2.1

Author's personal copy

Sample	ALA05C	ALA06A	ALA06B	ALA06C	ALA07A	ALA07B	ALA13	ALA14	ALA15	ALA16	ALA19A	ALA19B	ALA19C	ALA22A	ALA23C	ALA27A	ALA27B	JL 94-39	JL 94-40	JL 94-41	JL 94-42	JL 94-43	JL 94-49	JL 94-55	JL 94-56	JL 94-57
Corresponding Ge																										
Age (Ma)																										
Unit	aarw	grp3	grp3	grp3	grp2	grp2	aab	grp1	grp1	hanir	grp1	aaaw	aare	aaiw	grp2	aai	aaaw	aarw	aaaw	aarw	aaaw	aarw	aaaw	aare	aaac	aarw
Data Source	3	3	3	3	3	3	3	3	3	3	3	3	3	3	3	3	3	3	3	3	3	3	3	3	3	3
Longitude	45.0677	45.4793	45.4793	45.4793	45.4239	45.4239	45.1757	45.1139	45.0822	43.0572	45.3849	45.3849	43.3849	45.0833	45.2323	45.0677	45.0677	*	*	*	*	*	*	*	*	*
Latitude	23.7783	23.2083	23.2083	23.2083	23.1103	23.1103	23.3259	23.6104	23.7523	23.8187	22.9133	22.9133	22.9133	23.7167	23.8858	23.7783	23.7783	*	*	*	*	*	*	*	*	*
Approx. location																		Marjar	Marjar	Marjar	Umm Ash Shalahit	Umm Ash Shalahit	Umm Ash Shalahit	Mighza	Mighza	Mighza
SiO_2	78.80	75.30	73.00	74.10	59.70	70.30	58.50	73.60	63.40	66.70	74.80	42.40	73.60	76.50	61.90	72.20	48.70	60.00	53.97	66.86	51.99	73.99	49.51	75.56	49.50	77.50
Al_2O_3	10.3	13.2	14.6	13	16	14.1	15.2	13.2	15.9	15.8	13	13.4	12	9.3	19.6	12	15.2	15.56	16.43	13.43	16.19	13	17.67	11.57	17.95	10.64
Fe_2O_3T	2.13	0.55	1.5	1.6	5.56	4.79	9.22	3.22	6.46	4.85	2.7	10.97	2.93	1.25	3.68	3.92	11.19	4.15	10.43	5.52	12.16	2.16	10.56	2.06	10.09	1.47
TiO_2	0.28	0.05	0.2	0.17	1.09	0.27	0.97	0.32	0.67	0.43	0.24	0.45	0.24	0.21	0.46	0.45	0.86	0.65	0.71	0.64	1.06	0.3	0.63	0.15	0.62	0.22
CaO	1	0.7	1.1	0.8	4	3.9	5.6	2.9	4.6	1.9	3.3	10.9	4	0.3	6.1	0.9	5.1	4.66	4.02	2.69	4.06	0.93	8.04	2.01	8.96	1.23
MgO	0.3	<.2	0.5	0.4	2.7	1	3.7	0.6	1.8	1.3	0.4	11.1	0.4	3.1	1.3	2.2	6.7	1.83	4.25	1.44	4.04	2.14	5.59	0.54	4.95	*
Na_2O	5.5	4.2	3.8	3.6	4.3	4.3	3.5	4.4	4.4	6.2	3.9	<.2	2.6	0.4	5.4	5.1	2.5	8.53	5.83	5.7	6.32	5.54	4.08	4.33	3.89	6.34
K_2O	0.2	4.38	4.26	4.77	2.74	0.76	0.96	1.44	1.08	0.56	0.73	<.05	1.04	6.16	0.87	0.28	1.12	0.17	0.22	0.33	1.55	0.38	0.75	1.05	0.56	0.09
MnO	0.08	<.02	0.03	0.04	0.09	0.12	0.11	0.05	0.19	0.08	0.06	0.19	0.04	0.14	0.05	0.18	0.52	0.11	0.19	0.19	0.49	0.15	0.22	0.05	0.14	0.05
P_2O_5	0.06	<.05	0.08	0.06	0.40	0.07	0.23	0.08	0.20	0.09	0.06	0.09	0.06	<.05	0.16	0.09	0.11	0.19	0.09	0.17	0.15	0.05	0.08	*	0.07	*
L.O.I	0.7	0.6	1.2	0.6	2.3	0.5	1.4	0.4	1.3	2.1	1.6	10	3	1.8	0.5	1.8	7.5	4.15	4.34	3.68	2.39	2.08	3.21	2.53	3.6	1.25
Total	99.35	98.98	100.27	99.14	99.28	100.11	99.39	100.21	100.00	100.01	100.79	99.50	99.91	99.16	100.02	99.12	99.50	100.00	100.48	100.65	100.40	100.72	100.34	99.85	100.33	98.79
FeO	*	*	*	*	*	*	*	*	*	*	*	*	*	*	*	*	*	*	*	*	*	*	*	*	*	*
Fe_2O_3	*	*	*	*	*	*	*	*	*	*	*	*	*	*	*	*	*	*	*	*	*	*	*	*	*	*
H2O-	*	*	*	*	*	*	*	*	*	*	*	*	*	*	*	*	*	*	*	*	*	*	*	*	*	*
H2O+	*	*	*	*	*	*	*	*	*	*	*	*	*	*	*	*	*	*	*	*	*	*	*	*	*	*
Li	<10	<10	20	21	12	<10	<10	<10	11	20	<10	<10	<10	<10	<10	<10	14	*	*	*	*	*	*	*	*	*
Na	*	*	*	*	*	*	*	*	*	*	*	*	*	*	*	*	*	*	*	*	*	*	*	*	*	*
Sc	*	*	*	*	*	*	*	*	*	*	*	*	*	*	*	*	*	*	*	*	*	*	*	*	*	*
V	12	<10	19	17	119	44	204	22	78	62	<10	355	16	<10	82	39	371	72	274	62	356	12	264	13	264	*
Cr	15	<10	10	11	60	12	61	13	19	18	<10	501	11	19	21	23	70	*	*	*	*	*	66	10	25	13
Fe	*	*	*	*	*	*	*	*	*	*	*	*	*	*	*	*	*	*	*	*	*	*	*	*	*	*
Co	<5	<5	7	<5	19	7	25	5	12	8	<5	47	<5	<5	11	6	33	7	18	9	18	*	31	*	30	*
Ni	<10	<10	<10	<10	26	<10	13	<10	<10	<10	<10	178	<10	<10	<10	<10	25	15	22	*	12	16	35	16	25	15
Cu	*	*	*	*	*	*	*	*	*	*	*	*	*	*	*	*	*	*	*	*	*	*	*	*	*	*
Zn	*	*	*	*	*	*	*	*	*	*	*	*	*	*	*	*	*	*	*	*	*	*	*	*	*	*
Ga	*	*	*	*	*	*	*	*	*	*	*	*	*	*	*	*	*	*	*	*	*	*	*	*	*	*
Ge	*	*	*	*	*	*	*	*	*	*	*	*	*	*	*	*	*	*	*	*	*	*	*	*	*	*
As	*	*	*	*	*	*	*	*	*	*	*	*	*	*	*	*	*	*	*	*	*	*	*	*	*	*
Se	*	*	*	*	*	*	*	*	*	*	*	*	*	*	*	*	*	*	*	*	*	*	*	*	*	*
Br	*	*	*	*	*	*	*	*	*	*	*	*	*	*	*	*	*	*	*	*	*	*	*	*	*	*
Rb	2	153	158	149	42	17	15	20	17	9	14	<1	19	41	16	3	15	3	4	5	11	5	13	29	10	1
Sr	141	48	287	87	896	232	292	159	309	413	163	164	158	55	760	86	101	185	261	64	120	61	205	124	234	107
Y	18.1	35.3	6	8.9	10.4	18.8	23.8	25.5	17.4	34.6	19.6	5.8	35.2	26.5	7.6	24.1	14.3	23.9	16.5	28.8	19.7	51.1	13.7	47.8	10.5	40.7
Zr	70	66	110	93	218	101	133	164	81	239	61	14	56	117	121	146	44	90	40	90	34	140	25	148	21	159
Nb	1.5	21.9	6.9	16.2	9.9	6	5.2	4	2.1	5.9	1.2	0.2	1	2.2	0.9	3.5	1	2.7	1.2	2.9	1.2	2.7	0.7	3.1	0.7	3.2
Mo	*	*	*	*	*	*	*	*	*	*	*	*	*	*	*	*	*	*	*	*	*	*	*	*	*	*
Ag	*	*	*	*	*	*	*	*	*	*	*	*	*	*	*	*	*	*	*	*	*	*	*	*	*	*
In	*	*	*	*	*	*	*	*	*	*	*	*	*	*	*	*	*	*	*	*	*	*	*	*	*	*
Sn	*	*	*	*	*	*	*	*	*	*	*	*	*	*	*	*	*	*	*	*	*	*	*	*	*	*
Sb	*	*	*	*	*	*	*	*	*	*	*	*	*	*	*	*	*	*	*	*	*	*	*	*	*	*
Cs	*	*	*	*	*	*	*	*	*	*	*	*	*	*	*	*	*	*	*	*	*	*	*	*	*	*
Ba	288	89	849	170	1276	234	374	521	287	290	435	20	440	3500	337	417	455	3500	157	173	1351	37	181	80	101	*
Hf	2	4.1	3.2	3.5	5.3	3.1	3.5	4.6	2.1	6.5	2	0.3	1.9	3.5	3.1	3.6	1.2	2.2	1	2.2	0.8	3.1	0.6	3.3	0.5	3.5
Ta	0.1	3.1	0.6	2.1	0.7	0.5	0.6	0.4	0.3	0.5	0.1	0.1	0.3	0.3	0.2	0.2	0.1	0.2	*	0.2	*	0.2	*	0.2	*	0.2
W	*	*	*	*	*	*	*	*	*	*	*	*	*	*	*	*	*	*	*	*	*	*	*	*	*	*
Ir	*	*	*	*	*	*	*	*	*	*	*	*	*	*	*	*	*	*	*	*	*	*	*	*	*	*
Au	*	*	*	*	*	*	*	*	*	*	*	*	*	*	*	*	*	*	*	*	*	*	*	*	*	*
Tl	*	*	*	*	*	*	*	*	*	*	*	*	*	*	*	*	*	*	*	*	*	*	*	*	*	*
Pb	*	*	*	*	*	*	*	*	*	*	*	*	*	*	*	*	*	*	*	*	*	*	*	*	*	*
Bi	*	*	*	*	*	*	*	*	*	*	*	*	*	*	*	*	*	*	*	*	*	*	*	*	*	*
Th	0.7	12.9	10.7	21.6	5.2	3.4	3.4	2.9	1.3	4.7	1.2	0.2	0.8	1.3	1	1.2	0.3	1.4	0.5	2.1	0.4	1.9	0.4	3.3	0.3	7.6
U	0.2	5.1	2.4	12.8	1.3	0.3	0.8	0.8	0.2	2.3	0.1	<.1	<.1	0.6	0.4	0.3	<.1	0.6	0.2	1	0.3	0.8	0.2	1.5	0.2	1.4
La	6.4	9	18.6	14.6	33.8	13.2	15.7	14.3	9.6	20	7.9	2	6	9.9	9.7	14.1	6.9	8.4	3.4	7.8	3.6	12.5	2.5	19.5	2.2	18.4
Ce	11.3	16.1	35	25.7	63.4	21.5	31.8	27	17	42.7	12.2	4	9.7	15.3	12.4	27.4	10.6	20.3	9	20	10	31	7	43.8	6	41.2
Pr	1.7	2	3.3	2.7	7.2	2.2	3.9	3.3	2.3	5.2	1.7	0.6	1.3	2.1	1.4	3.5	1.5	2.7	1.3	2.7	1.5	4	0.9	5.4	0.8	5
Nd	8.2	8.7	11.4	9.9	28.8	9.4	17.4	14.7	11.3	24.1	8.1	3.3	6.4	9.6	6.1	16.5	7.5	12.5	6.5	12.5	8.1	17.9	4.6	23.7	4	21.5
Sm	2	2.9	1.9	1.6	4.5	2	4	3.3	2.7	5.2	2.3	0.8	1.6	2.1	1.4	3.5	2	3.2	1.8	3.5	2.4	4.7	1.3	5.8	1.3	5.1
Eu	0.7	0.2	0.5	0.2	1.3	0.6	1	0.6	0.7	1.2	0.8	0.4	0.5	0.4	0.6	0.8	0.9	1.2	0.6	1	0.7	0.9	0.6	1.1	0.5	0.9
Gd	2.5	4	1.4	1.5	3.5	2.5	4	3.8	2.7	5.6	2.8	1.1	2.2	2.8	1.4	3.7	2.8	3.6	2.1	3.5	2.8	5.7	1.7	6.2	1.6	5.3
Tb	0.4	0.7	0.2	0.2	0.4	0.4	0.6	0.6	0.5	0.9	0.5	0.2	0.4	0.5	0.2	0.6	0.4	0.6	0.4	0.6	0.5	1	0.3	1.1	0.3	0.9
Dy	2.9	5	1	1.3	2.5	2.9	4.3	3.8	2.2	5.9	3.2	1.1	3	3.1	1.1	3.8	2.7	4.1	2.5	4.5	3.1	6.9	2.1	7	1.8	6.3
Ho	0.6	1	0.2	0.2	0.4	0.6	0.9	0.9	0.6	1.3	0.7	0.2	0.7	0.7	0.2	0.9	0.5	0.9	0.6	1	0.7	1.5	0.5	1.6	0.4	1.4
Er	1.6	3	0.4	0.7	1	1.9	2.7	2.6	1.8	3.9	2.2	0.6	2.1	2.1	0.6	2.7	1.5	2.9	1.7	3	2	4.8	1.3	4.6	1.2	4.4
Tm	0.3	0.5	0.1	0.1	0.1	0.3	0.4	0.4	0.3	0.6	0.3	0.1	0.3	0.3	0.1	0.4	0.2	0.4	0.3	0.4	0.3	0.7	0.2	0.7	0.2	0.7
Yb	1.5	3.4	0.3	0.7	0.7	2.2	2.4	2.5	1.8	4.1	2.1	0.6	2.1	2	0.6	2.9	1.4	3.1	1.9	3.2	1.8	5	1.3	4.8	1.1	4.7
Lu	0.2	0.5	0.1	0.1	0.1	0.3	0.4	0.3	0.3	0.6	0.3	0.1	0.3	0.3	0.1	0.4	0.2	0.5	0.3	0.5	0.3	0.8	0.2	0.7	0.2	0.8

Author's personal copy

Sample	JL 94-58	JL 94-59	JL 94-65	JL 94-66	JL 94-67	JL 94-69	JL 94-71	JL 94-72	JL 94-73	JL 94-74
Corresponding Ge										
Age (Ma)										
Unit	aaae	aaaw	aare	aaae	aare	aare	aaae	aaae	aare	aare
Data Source	3	3	3	3	3	3	3	3	3	3
Longitude	*	*	*	*	*	*	*	*	*	*
Latitude	*	*	*	*	*	*	*	*	*	*
Approx. location	Mighza	W-Bitrar	Muthiaş	Muthiaş	Muthiaş	Muthiaş	Muthiaş	Khnaiyguiyal	Khnaiyguiyal	Khnaiyguiyal
SiO_2	46.46	58.95	75.80	47.78	61.38	75.50	51.19	56.80	70.16	66.00
Al_2O_3	18.32	16.3	11.39	20.5	13.64	9.67	16.13	13.02	11.82	13.98
Fe_2O_3T	12.29	5.42	2.49	8.92	8.17	3.12	12.92	13.67	5.37	6.95
TiO_2	1.28	0.56	0.27	0.5	0.75	0.2	1.22	1.44	0.49	0.82
CaO	10.54	5.75	0.69	10.72	2.89	2.46	8.9	3.33	0.88	1.53
MgO	4.79	4.08	0.28	5.98	2.87	0.75	3.66	2.78	1.73	0.81
Na_2O	1.91	4.51	6.39	2.72	1.97	2.54	2.85	4.35	2.08	7.2
K_2O	1.66	1.16	0.76	0.67	5.28	2.72	0.68	2.05	3.36	1.4
MnO	0.43	0.09	0.06	0.17	0.21	0.15	0.21	0.58	0.55	0.24
P_2O_5	0.19	0.17	*	0.05	0.16	*	0.14	0.22	0.1	0.22
L.O.I	1.9	2.31	0.74	1.97	2.66	2.32	2.15	1.63	1.63	1.24
Total	99.77	99.30	98.87	99.98	99.98	99.43	100.05	99.87	98.17	100.39
FeO	*	*	*	*	*	*	*	*	*	*
Fe_2O_3	*	*	*	*	*	*	*	*	*	*
H2O-	*	*	*	*	*	*	*	*	*	*
H2O+	*	*	*	*	*	*	*	*	*	*
Li	*	*	*	*	*	*	*	*	*	*
Na	*	*	*	*	*	*	*	*	*	*
Sc	*	*	*	*	*	*	*	*	*	*
V	374	118	*	212	114	*	329	312	99	10
Cr	21	142	15	67	*	*	*	*	50	10
Fe	*	*	*	*	*	*	*	*	*	*
Co	26	20	*	30	15	*	29	27	5	*
Ni	33	92	30	61	*	13	20	20	46	24
Cu	*	*	*	*	*	*	*	*	*	*
Zn	*	*	*	*	*	*	*	*	*	*
Ga	*	*	*	*	*	*	*	*	*	*
Ge	*	*	*	*	*	*	*	*	*	*
As	*	*	*	*	*	*	*	*	*	*
Se	*	*	*	*	*	*	*	*	*	*
Br	*	*	*	*	*	*	*	*	*	*
Rb	35	13	7	11	67	29	11	22	37	12
Sr	195	783	54	218	79	51	230	276	67	86
Y	23.3	9.7	68	9.6	32	52.8	26.8	41.8	35.5	46.8
Zr	32	69	206	17	84	225	58	104	151	135
Nb	1.1	1.4	4.7	0.6	2.5	5.6	1.9	2.9	8.2	3.3
Mo	*	*	*	*	*	*	*	*	*	*
Ag	*	*	*	*	*	*	*	*	*	*
In	*	*	*	*	*	*	*	*	*	*
Sn	*	*	*	*	*	*	*	*	*	*
Sb	*	*	*	*	*	*	*	*	*	*
Cs	*	*	*	*	*	*	*	*	*	*
Ba	203	360	75	33	187	525	83	1014	3423	796
Hf	0.8	1.4	4.6	0.5	2	4.8	1.4	2.4	3.3	2.9
Ta	*	*	0.3	*	0.2	0.3	0.1	0.2	0.5	0.2
W	*	*	*	*	*	*	*	*	*	*
Ir	*	*	*	*	*	*	*	*	*	*
Au	*	*	*	*	*	*	*	*	*	*
Tl	*	*	*	*	*	*	*	*	*	*
Pb	*	*	*	*	*	*	*	*	*	*
Bi	*	*	*	*	*	*	*	*	*	*
Th	0.3	0.8	3.3	0.2	1	3.5	0.6	1.6	6.2	2.6
U	0.2	0.6	1.6	0.1	0.5	1.6	0.3	0.8	2.6	1.9
La	4	7.6	18	2	6.7	18.6	4.8	9.6	19.1	12.1
Ce	10.9	18.4	42.4	4.9	18.5	46.4	13	24.3	45.5	31.1
Pr	1.4	2.3	4.8	0.6	2.6	5.6	1.9	3.5	5.3	4.3
Nd	7.6	9.6	22	3.1	12.3	24.3	9.4	17	22.5	20.3
Sm	2.5	2	6.2	1	3.5	6.3	2.9	4.9	5.3	4.8
Eu	1	0.7	1.5	0.4	1.1	1.2	1	1.5	1.2	1.8
Gd	3.1	1.8	7.6	1.3	4.2	6.8	3.7	6.1	5.6	6.9
Tb	0.6	0.3	1.4	0.2	0.8	1.2	0.7	1	0.9	1.1
Dy	3.7	1.5	9.8	1.5	4.8	8.1	4.2	6.6	5.6	7.7
Ho	0.8	0.3	2.3	0.3	1.1	1.8	0.9	1.4	1.2	1.7
Er	2.3	0.9	7.1	0.9	3.2	5.4	2.7	4.2	3.7	4.8
Tm	0.3	0.1	1.1	0.2	0.5	0.9	0.4	0.6	0.6	0.8
Yb	2.2	0.9	7.8	0.9	3.4	5.8	2.8	4.4	3.7	5
Lu	0.4	0.2	1.2	0.1	0.5	0.9	0.4	0.7	0.6	0.8

Author's personal copy

Appendix B. Analytical and calculated data for SHRIMP analyses on zircon from plutonic rocks in the Ar Rayn terrane

Samples were collected during this study. Analyses were conducted using the SHRIMP-RG at the Stanford-USGS Micro-Isotopic Analytical Center (SUMAC), Palo Alto, California. Each row represents a spot analysis on a separate zircon grain. Stikethrough indicates analysis was not included in the final age calculation due to high common lead contents and presumed lead loss. See Fig. 4 for sample localities, Fig. 10 for concordia plots, and Table 1 for summary data.

Spot analysis No. (ARGC###)	%Common ^{206}Pb	ppm U	ppm Th	^{232}Th/^{238}U	^{207}Pb- corrected ^{206}Pb/^{238}U Age (Ma)	1 sigma error (Ma)	Total ^{238}U/^{206}Pb	1 sigma error (%)	Total ^{207}Pb/^{206}Pb	1 sigma error (%)	^{204}Pb-corrected ^{207}Pb/^{235}U	1 sigma error (%)	^{204}Pb-corrected ^{206}Pb/^{238}U	1 sigma error (%)	Error correlation
4-1	0.00	176	104	0.61	638.9	7.7	9.59	1.2	.0614	2.2	0.88	2.5	.1042	1.2	.497
4-2	3.98	1214	1036	0.88	471.6	5.0	~~12~~.57	~~1~~.0	.0935	~~2~~.3	0.65	6.8	.0764	1.1	.166
4-3	0.00	71	20	0.28	621.4	9.5	9.90	1.5	.0593	3.3	0.83	3.6	.1010	1.5	.424
4-4	0.00	70	25	0.37	613.0	9.4	10.03	1.6	.0601	3.3	0.83	3.6	.0997	1.6	.429
4-5	0.00	50	16	0.33	629.1	10.9	9.74	1.8	.0618	3.8	0.87	4.2	.1026	1.8	.419
4-6	0.83	192	91	0.49	597.7	7.1	10.27	1.2	.0618	1.9	0.73	4.1	.0966	1.2	.300
4-7	0.00	49	16	0.34	600.9	10.5	10.25	1.8	.0589	4.1	0.79	4.4	.0976	1.8	.399
4-8	0.00	94	41	0.45	627.3	8.9	9.78	1.4	.0613	2.8	0.86	3.1	.1023	1.4	.459
4-9	0.66	55	18	0.33	616.8	10.3	9.99	1.7	.0575	3.8	0.71	8.3	.0994	1.7	.211
4-10	0.84	57	16	0.29	626.6	10.8	9.80	1.7	.0604	3.9	0.75	7.4	.1012	1.8	.241
4-11	0.45	46	14	0.32	615.9	10.7	9.90	1.8	.0660	3.8	0.87	5.8	.1005	1.8	.308
4-12	0.25	86	34	0.41	622.3	9.0	9.88	1.5	.0594	3.0	0.80	4.1	.1010	1.5	.361
4-13	0.00	195	112	0.59	597.1	7.3	10.30	1.2	.0602	2.0	0.81	2.4	.0971	1.2	.520
4-14	0.00	158	85	0.56	603.1	7.5	10.17	1.3	.0621	2.2	0.84	2.5	.0983	1.3	.505
4-15	0.17	137	64	0.49	627.9	8.1	9.72	1.3	.0648	2.3	0.90	3.1	.1027	1.3	.433
4-16	0.00	119	46	0.40	622.9	8.3	9.86	1.3	.0606	2.5	0.85	2.8	.1014	1.3	.478
4-17	0.22	104	47	0.47	608.1	8.5	10.06	1.4	.0637	2.7	0.85	3.7	.0991	1.4	.391
5-1	0.09	236	71	0.31	632.4	8.7	9.67	1.4	.0633	1.7	0.89	2.3	.1033	1.4	.603
5-2	0.28	76	25	0.34	647.6	11.1	9.43	1.7	.0641	3.1	0.90	4.3	.1058	1.8	.405
5-3	0.00	275	93	0.35	633.4	8.6	9.68	1.4	.0609	1.6	0.87	2.1	.1033	1.4	.660
5-4	0.35	155	51	0.34	639.1	9.2	9.57	1.5	.0631	2.0	0.87	4.4	.1041	1.5	.344
5-5	1.81	384	117	0.31	~~490~~.7	~~6~~.6	~~12~~.34	~~1~~.4	.0761	~~1~~.6	0.68	5.3	.0795	1.4	.265
5-6	0.79	191	71	0.38	~~603~~.9	~~8~~.9	~~10~~.12	~~1~~.5	.0648	~~2~~.6	0.79	5.3	.0980	1.5	.288
5-7	0.00	257	75	0.30	626.1	8.5	9.81	1.4	.0601	1.6	0.84	2.1	.1019	1.4	.656
5-8	0.52	145	35	0.25	629.1	9.2	9.74	1.5	.0618	2.2	0.81	5.5	.1021	1.5	.278
5-9	1.29	359	153	0.44	~~538~~.2	~~7~~.1	~~11~~.36	~~1~~.4	.0672	~~1~~.9	0.68	4.5	.0869	1.4	.307
5-10	0.23	360	141	0.40	636.7	8.4	9.62	1.3	.0617	1.3	0.85	2.1	.1037	1.3	.647
5-11	2.34	282	69	0.25	~~541~~.9	~~7~~.3	~~11~~.13	~~1~~.4	.0778	~~1~~.5	0.71	6.1	.0878	1.4	.235
5-12	0.00	603	199	0.34	639.4	12.5	9.59	2.0	.0609	1.0	0.88	2.3	.1043	2.0	.895
5-13	0.96	326	134	0.42	~~541~~.6	~~7~~.4	~~11~~.25	~~1~~.4	.0699	~~1~~.4	0.76	3.6	.0881	1.4	.395
5-14	0.44	695	356	0.53	619.0	7.9	9.90	1.3	.0625	1.8	0.82	2.7	.1006	1.3	.482
5-15	2.72	388	82	0.22	~~411~~.7	~~5~~.6	~~14~~.78	~~1~~.4	.0756	~~1~~.7	0.49	8.9	.0658	1.5	.168
5-16	0.28	145	43	0.30	632.0	10.1	9.72	1.6	.0600	2.7	0.82	4.1	.1026	1.6	.398
5-17	0.00	126	45	0.37	628.5	9.6	9.74	1.6	.0627	2.4	0.89	2.8	.1027	1.6	.548
5-18	0.15	185	63	0.35	627.3	9.0	9.77	1.5	.0617	2.0	0.85	2.9	.1022	1.5	.509

Author's personal copy

11-1	0.00	56	33	0.61	622.4	9.9	9.91	1.6	.0571	3.6	0.79	3.9	.1009	1.6	.412
11-2	0.12	170	72	0.44	632.2	7.7	9.71	1.2	.0606	2.0	0.85	2.6	.1029	1.2	.468
11-3	0.68	5645	4928	0.90	579.2	5.6	10.55	1.0	.0663	0.5	0.79	1.4	.0942	1.0	.732
11-4	49.08	77	25	0.33	1088.2	19.7	2.93	1.3	.4389	0.8			.1737	5.9	
11-5	0.27	119	39	0.34	624.5	8.1	9.85	1.3	.0592	2.4	0.80	3.2	.1013	1.3	.418
11-6	0.00	113	55	0.50	609.8	8.0	10.08	1.3	.0598	2.4	0.82	2.8	.0992	1.3	.480
11-7	9.89	1761	1151	0.68	307.6	3.2	18.31	1.0	.1379	0.8	0.40	10.1	.0492	1.2	.123
11-8	0.00	67	53	0.81	590.5	10.0	10.40	1.7	.0618	3.7	0.82	4.0	.0962	1.7	.422
11-9	0.00	70	36	0.53	624.6	9.4	9.85	1.5	.0586	3.2	0.82	3.6	.1015	1.5	.428
11-10	0.00	287	233	0.84	609.2	7.2	10.06	1.2	.0625	1.7	0.86	2.0	.0994	1.2	.590
11-11	0.00	195	121	0.64	620.8	7.8	9.88	1.3	.0612	1.9	0.85	2.3	.1012	1.3	.554
11-12	1.45	58	23	0.42	595.7	9.7	10.26	1.7	.0648	3.5	0.70	12.1	.0960	1.8	.149
11-13	0.00	165	63	0.40	607.4	7.5	10.11	1.3	.0610	2.1	0.83	2.5	.0989	1.3	.510
11-14	0.21	94	58	0.64	625.6	9.4	9.82	1.5	.0600	2.7	0.82	3.7	.1016	1.5	.414
11-15	0.00	133	67	0.52	615.7	7.8	9.96	1.3	.0614	2.2	0.85	2.6	.1004	1.3	.501
11-16	0.11	181	164	0.94	624.2	7.5	9.87	1.2	.0580	2.0	0.80	2.6	.1012	1.2	.468
11-17	0.14	176	92	0.54	452.0	5.6	13.68	1.3	.0613	2.2	0.61	2.9	.0730	1.3	.436
11-18	0.27	143	51	0.37	571.9	7.4	10.73	1.3	.0631	2.4	0.78	3.9	.0930	1.3	.339
11-19	0.15	205	58	0.29	622.4	7.4	9.87	1.2	.0600	2.0	0.82	2.5	.1011	1.2	.485
11-20	0.00	117	58	0.51	611.8	8.3	10.04	1.4	.0609	2.6	0.84	3.0	.0996	1.4	.467
11-21	0.10	232	49	0.22	595.5	7.0	10.32	1.2	.0611	1.8	0.81	2.4	.0968	1.2	.504
11-22	0.16	134	69	0.53	618.9	8.1	9.93	1.3	.0596	3.0	0.81	3.6	.1005	1.3	.366
11-23	0.00	100	47	0.49	600.0	8.5	10.24	1.4	.0609	2.8	0.82	3.2	.0977	1.4	.453
14-1	1.19	136	108	0.82	582.1	10.6	10.47	1.9	.0682	2.1	0.76	6.4	.0944	1.9	.299
14-2	0.14	209	216	1.07	613.2	10.4	10.00	1.7	.0621	1.8	0.84	2.6	.0999	1.7	.669
14-3	1.20	474	357	0.78	484.3	8.1	12.56	1.7	.0731	3.9	0.69	5.7	.0787	1.7	.298
14-4	1.14	78	29	0.38	531.8	10.1	11.48	1.9	.0685	2.9	0.70	4.5	.0861	1.9	.436
14-5	39.70	1204	1397	1.20	93.9	1.9	40.24	1.7	.3821	0.7	0.13	51.8	.0150	4.4	.086
14-6	0.57	151	128	0.87	544.2	9.5	11.27	1.8	.0642	2.1	0.72	3.5	.0882	1.8	.515
14-7	0.30	452	342	0.78	623.7	10.2	9.80	1.7	.0640	2.9	0.86	3.4	.1017	1.7	.482
14-8	14.16	1015	608	0.62	223.6	3.7	24.04	1.6	.1739	0.7	0.30	17.2	.0357	2.1	.120
14-9	3.20	762	655	0.89	469.5	7.7	12.69	1.6	.0898	2.8	0.68	6.2	.0763	1.7	.272
14-10	0.82	100	100	1.02	585.0	10.8	10.43	1.9	.0668	2.6	0.79	6.5	.0951	1.9	.297
14-11	1.45	150	105	0.73	585.9	10.3	10.37	1.8	.0705	2.0	0.77	6.9	.0951	1.8	.269
14-12	1.24	332	205	0.64	533.2	9.3	11.37	1.7	.0737	5.4	0.76	10.0	.0868	1.8	.182
14-13	7.60	412	318	0.80	525.2	8.9	10.95	1.7	.1144	2.8	0.61	17.6	.0844	2.0	.113
14-14	18.37	846	1018	1.24	402.2	6.6	12.45	1.6	.2155	0.5	0.63	18.6	.0656	2.3	.122
14-15	1.17	507	145	0.29	582.2	9.5	10.46	1.7	.0688	3.0	0.77	6.4	.0945	1.7	.264
14-16	1.37	368	359	1.01	576.0	9.4	10.54	1.7	.0712	1.2	0.78	4.3	.0936	1.7	.392
14-17	3.18	430	262	0.63	591.0	9.8	10.04	1.7	.0888	2.8	0.84	7.0	.0965	1.7	.246
14-18	0.11	404	188	0.48	611.6	10.6	10.05	1.8	.0598	1.4	0.81	2.4	.0994	1.8	.758
14-19	0.53	248	94	0.39	590.7	9.9	10.36	1.7	.0643	1.6	0.80	3.2	.0960	1.7	.540
14-20	68.19	736	157	0.22	219.6	7.3	9.07	1.6	.6083	0.5			.0351	10.5	
14-21	0.17	138	127	0.95	573.6	10.3	10.69	1.8	.0636	2.4	0.80	3.4	.0934	1.8	.543
14-22	2.10	534	342	0.66	560.3	9.2	10.81	1.7	.0735	2.0	0.71	6.7	.0906	1.7	.256
16-1	0.00	21	6	0.31	722.2	18.9	8.42	2.7	.0652	3.9	1.07	4.7	.1188	2.7	.571
16-2	0.00	74	20	0.27	678.6	14.9	9.01	2.3	.0623	2.3	0.95	3.2	.1110	2.3	.703
16-3	0.19	397	178	0.46	659.3	13.5	9.27	2.1	.0630	1.3	0.91	2.6	.1077	2.1	.797
16-4	0.74	22	9	0.45	692.4	19.2	8.79	2.8	.0653	4.2	0.92	7.3	.1129	2.9	.392

Author's personal copy

Appendix B (*Continued*)

Spot analysis No. (ARGC###)	%Common ^{206}Pb	ppm U	ppm Th	^{232}Th/^{238}U	^{207}Pb- corrected ^{206}Pb/^{238}U Age (Ma)	1 sigma error (Ma)	Total ^{238}U/^{206}Pb	1 sigma error (%)	Total ^{207}Pb/^{206}Pb	1 sigma error (%)	^{204}Pb-corrected ^{207}Pb/^{235}U	1 sigma error (%)	^{204}Pb-corrected ^{206}Pb/^{238}U	1 sigma error (%)	Error correlation
16-5	0.62	118	56	0.49	681.8	14.5	8.95	2.2	.0638	1.7	0.90	5.0	.1111	2.2	.438
16-6	0.00	56	16	0.30	680.1	15.4	8.97	2.3	.0633	2.5	0.97	3.4	.1114	2.3	.677
16-7	0.00	116	41	0.36	673.7	14.4	9.07	2.2	.0626	1.8	0.95	2.8	.1102	2.2	.779
16-8	0.00	53	19	0.36	687.1	15.7	8.91	2.3	.0609	2.6	0.94	3.5	.1123	2.3	.666
16-9	1.77	23	6	0.26	711.3	18.2	8.45	2.6	.0750	3.5	0.97	6.6	.1163	2.6	.398
16-10	0.00	131	11	0.09	630.3	13.4	9.72	2.2	.0624	1.8	0.89	2.8	.1029	2.2	.769
16-11	0.18	334	145	0.45	702.7	14.4	8.66	2.1	.0648	1.0	1.01	2.6	.1152	2.1	.798
16-12	0.22	339	9	0.03	609.3	13.1	10.06	2.2	.0624	1.1	0.83	2.9	.0992	2.2	.771
16-13	1.07	31	9	0.30	698.7	16.9	8.66	2.5	.0697	4.0	0.96	9.9	.1143	2.5	.256
16-14	0.00	25	13	0.56	699.9	17.4	8.68	2.5	.0663	3.4	1.05	4.3	.1152	2.5	.595
16-15	0.00	29	17	0.58	722.4	17.4	8.43	2.5	.0637	3.2	1.04	4.0	.1186	2.5	.615
17-1	0.33	419	318	0.78	587.0	3.5	10.45	0.6	0.06	1.8	0.79	2.1	.0954	0.6	.286
17-2	0.93	474	314	0.69	574.0	3.3	10.64	0.6	0.07	1.3	0.78	4.0	.0933	0.6	.153
17-3	-0.08	795	697	0.91	610.8	2.6	10.07	0.4	0.06	1.0	0.80	1.2	.0992	0.4	.346
17-4	0.26	793	774	1.01	600.2	2.7	10.22	0.4	0.06	1.0	0.80	2.1	.0975	0.5	.222
17-5	2.95	469	255	0.56	547.2	3.6	10.95	0.5	0.08	1.1	0.73	7.2	.0888	0.7	.092
17-6	0.10	352	190	0.56	610.8	3.9	10.05	0.6	0.06	1.5	0.82	2.1	.0993	0.7	.316
17-7	0.99	305	161	0.54	591.6	4.1	10.30	0.7	0.07	1.9	0.75	5.4	.0958	0.7	.139
17-8	1.21	345	139	0.42	521.9	5.6	11.72	1.1	0.07	2.5	0.77	2.8	.0852	1.1	.381
17-9	0.45	381	168	0.46	617.4	3.7	9.91	0.6	0.06	1.4	0.81	3.3	.1003	0.6	.192
17-10	0.16	321	193	0.62	597.6	4.1	10.28	0.7	0.06	1.6	0.82	1.8	.0973	0.7	.389
17-11	0.78	511	179	0.36	451.7	2.6	13.67	0.6	0.06	1.4	0.58	2.9	.0728	0.6	.209
17-12	0.27	401	212	0.55	564.1	3.4	10.91	0.6	0.06	1.5	0.73	2.4	.0914	0.6	.258
17-13	1.38	376	182	0.50	426.1	3.0	14.43	0.7	0.07	1.7	0.52	5.7	.0684	0.8	.132
17-14	1.02	324	252	0.81	581.4	4.0	10.49	0.7	0.07	1.8	0.79	4.1	.0945	0.7	.174
17-15	0.24	347	235	0.70	610.6	4.2	10.04	0.7	0.06	1.7	0.81	2.9	.0992	0.7	.247
17-16	0.64	163	81	0.51	597.2	6.3	10.24	1.0	0.07	2.9	0.79	6.1	.0970	1.1	.182
17-17	0.36	399	418	1.08	604.7	4.0	10.13	0.7	0.06	1.5	0.82	2.2	.0984	0.7	.311

Author's personal copy

References

Abdel-Monem, A.A., Radain, A.A., Gazzaz, M.A., 1982. Rb-Sr dating and petrology of the Jabal Bitran granite, Idsas area, Saudi Arabia. Precamb. Res. 16, A3 (Abstract).

Abdelsalam, M.G., Abdel-Rahman, E.M., El-Faki, E.M., Al-Hur, B., El-Bashier, F.M., Stern, R.J., Thurmond, A.K., 2003. Neoproterozoic deformation in the northeastern part of the Saharan Metacraton, northern Sudan; evolution of the East African and related orogens, and the assembly of Gondwana. Precamb. Res. 123, 203–221.

Agar, R.A., 1985. Stratigraphy and paleogeography of the Siham group: direct evidence for a late Proterozoic continental microplate and active continental margin. J. Geol. Soc. Lond. 142, 1205–1220.

Agar, R.A., 1988. Geologic map of the Zalm quadrangle, sheet 22F, Kingdom of Saudi Arabia. Saudi Arabian Directorate General of Mineral Resources Geoscience Map GM-89C, scale 1:250,000.

Al-Saleh, A.M., Boyle, A.P., Mussett, A.E., 1998. Metamorphism and $^{40}Ar/^{39}Ar$ dating of the Halaban Ophiolite and associated units; evidence for a two-stage orogenesis in the eastern Arabian Shield. J. Geol. Soc. Lond. 155, 165–175.

Al-Saleh, A.M., Boyle, A.P., 2001a. Neoproterozoic ensialic back-arc spreading in the eastern Arabian Shield; geochemical evidence from the Halaban Ophiolite. J. Afr. Earth Sci. 33 (1), 1–15.

Al-Saleh, A.M., Boyle, A.P., 2001b. Structural rejuvenation of the eastern Arabian Shield during continental collision: $^{40}Ar/^{39}Ar$ evidence from the Ar Ridayniyah ophiolitic mélange. J. Afr. Earth Sci. 33 (1), 135–141.

Al Shanti, A.M.S., Mitchell, A.H.G., 1976. Late Precambrian subduction and collision in the Al Amar-Idsass region, Kingdom of Saudi Arabia. Tectonophysics 30, T41–T47.

Arth, J.G., 1979. Some trace elements in trondhjemites—their implications to magmas genesis and tectonic setting. In: Barker, F. (Ed.), Trondhjemites, Dacites, and Related Rocks. Elsevier, New York, pp. 123–132.

Ashley, P.M., Dudley, R.J., Lesh, R.H., Marr, J.M., Ryall, A.W., 1988. The Scuddles Cu–Zn prospect, an Archean volcanogenic massive sulfide deposit, Golden Grove District, Western Australia. Econ. Geol. 83, 918–951.

Ashworth, K.L., Abdulaziz, M.I., 1978. Economic geology and evaluation of the Jabal Idsas magnetite deposits. Saudi Arabian Directorate General Resources Open-File Report DGMR-664.

Barker, F., 1979. Trondhjemite—definition, environment, and hypothesis of origin. In: Barker, F. (Ed.), Trondhjemites, Dacites, and Related Rocks. Elsevier, Amsterdam, pp. 1–12.

Barley, M.E., Large, R.R., 1992. A review of Archean volcanic-hosted massive sulfide and sulfate mineralization in Western Australia; a special issue devoted to Australian volcanic-hosted massive sulfide (VHMS) deposits and their volcanic environment. Econ. Geol. 87, 855–872.

Barrett, T.J., MacLean, W.H., Barrie, C.T., Hannington, M.D., 1999. Volcanic sequences, lithogeochemistry, and hydrothermal alteration in some bimodal volcanic-associated massive sulfide systems; volcanic-associated massive sulfide deposits; processes and examples in modern and ancient settings. Rev. Econ. Geol. 8, 101–131.

Beck Jr., M.E., 1992. Tectonic significance of paleomagnetic results for the western conterminous United States. In: Burchfiel, B.C., Lipman, P.W., Zoback, M.L. (Eds.), The Cordilleran Orogen: Conterminous U.S. Geological Society of America. The Geology of North America G-3, pp. 683–697.

Boillot, G., Grimaud, S., Mauffret, A., Mougenot, D., Kornprobst, J., Mergoil-Daniel, J., et al., 1980. Ocean-continent boundary off the Iberian margin; a serpentinite diapir west of the Galicia bank. Earth Plan. Sci. Lett. 48 (1), 23–34.

Bourdon, E., Eissen, J., Monzier, M., Robin, C., Martin, H., Cotten, J., 2002. Adakite-like lavas from Antisana volcano (Ecuador); evidence from slab melt metasomatism beneath the Andean northern volcanic zone. J. Petrol. 43 (2), 199–217.

BRGM, 1994. Khnaiguiyah zinc-copper deposit prefeasibility study. Saudi Arabian Directorate General of Mineral Resources Technical Report BRGM-TR-13-4.

BRGM, 2003. Geochemistry, accessed 3 October 2003 at URL: http://gisarabia.brgm.fr/geochemi.htm.

Brown, M., Diaz, F., Grocott, J., 1993. Displacement history of the Atacama fault system 25°00′S–27°00′S, northern Chile. Geol. Soc. Am. Bull. 105, 1165–1174.

Calvez, J.Y., Alsac, C., Delfour, J., Kemp, J., Pellaton, C., 1984. Geologic evolution of western, central, and eastern parts of the northern Precambrian Shield. Kingdom of Saudi Arabia, vol. 6. King Abdulaziz University, Faculty of Earth Sciences Bulletin, pp. 23–48.

Calvez, J.Y., Delfour, J., 1986. Geochronology of the Ar Rayn structural province. Saudi Arabian Deputy Ministry for Mineral Resources Open-File Report BRGM-OF-06-14.

Calvez, J.Y., Delfour, J., Feybesse, J.L., 1985. 2000-million-years old inherited zircons in plutonic rocks from the Al Amar region: new evidence for an early Proterozoic basement in the eastern Arabian Shield? Saudi Arabian Deputy Ministry for Mineral Resources Open-File Report BRGM-OF-05-11.

Camus, F., Sillitoe, R.H., Petersen, R. (Eds.), 1996. Andean copper deposits: new discoveries, mineralization, styles, and metallogeny. Society of Economic Geologists Special Publication, p. 5.

Cembrano, J., Herveĭ, F., Lavenu, A., 1996. The Liquine–Ofqui fault zone: a long-lived intra-arc fault system in southern Chile. Tectonophysics 259, 55–66.

Cembrano, J., Schermer, E., Lavenu, A., Sanhueza, A., 2000. Contrasting nature of deformation along an intra-arc shear zone, the Liquine-Ofqui fault zone, south Chilean Andes. Tectonophysics 319 (2), 129–149.

Chevremont, P., Johan, Z., 1982. Mafic-ultramafic layered complexes of the Jabal Ruga'an type. Saudi Arabian Deputy Ministry for Mineral Resources Open-File Report BRGM-OF-02-7.

Colley, H., Treloar, P.J., Diaz, F., 1989. Gold-silver mineralization in the El Salvador region, northern Chile. In: Keays, R.R., Ramsay, W.R., Groves, D.I. (Eds.), The Geology of Gold Deposits: The Perspective in 1988, vol. 6. Economic Geology Monograph, pp. 208–217.

Collins, A.S., Fitzsimons, I.C.W., Hulscher, B., Razakamanana, T., 2003. Structure of the eastern margin of the East African Orogen in central Madagascar; evolution of the East African and related orogens, and the assembly of Gondwana. Precamb. Res. 123, 111–133.

Coulomb, J. J., 1983. Exploration for gold in the southern part of the Al 'Amar belt; Selib, Fawarah, and Chelir prospects. Saudi Arabian Deputy Ministry for Mineral Resources Open-File Report BRGM-OF-03-27.

Defant, M.J., Drummond, M.S., 1990. Derivation of some modern arc magmas by melting of young subducted oceanic lithosphere. Nature 347, 662–665.

Defant, M.J., Drummond, M.S., 1993. Mount S. Helens: potential example of the partial melting of the subducted lithosphere in a volcanic arc. Geology 21, 547–550.

Delfour, J. (compiler), 1979. Geologic map of the Halaban Quadrangle, sheet 23G (without topographic base). Saudi Arabian Deputy

Author's personal copy

Ministry of Mineral Resources, Geoscience Map GM-46-C, scale 1:250,000.

Delfour, J., 1981. Geologic, tectonic and metallogenic evolution of the northern part of the Arabian Shield (Kingdom of Saudi Arabia). Bulletin du BRGM (deuxieme series), 1–19, sec II, no 1–2.

Delfour, J., Dhellemmes, R., Elsass, P., Vaslet, D., Brosse, J., Le Nindre, Y., Dottin, O., 1982. Geologic map of the Ad Dawadimi quadrangle, sheet 24 G, Kingdom of Saudi Arabia. Saudi Arabian Deputy Ministry of Mineral Resources, Geoscience Map GM-60A, scale 1:250,000.

Doebrich, J.L., Al-Jehani, A.M., Siddiqui, A.A., Hayes, T.S., Saleh, Y., Wooden, J.L., Johnson, P.R., Kattan, F.H., Shaikan, B., Basahl, M., Zahran, H., Al-Shammari, A., 2005. Geology and mineral resources of the Ar Rayn terrane, eastern Arabian Shield, Kingdom of Saudi Arabia. Saudi Geological Survey Technical Report SGS-TR-2005-2.

Doebrich, J.L., Zahony, S.G., Leavitt, J.D., Portacio Jr., J.S., Siddiqui, A.A., Wooden, J.L., Fleck, R.J., Stein, H.J., 2004. Ad Duwayhi, Saudi Arabia: geology and geochronology of a Neoproterozoic intrusion-related gold system in the Arabian shield. Econ. Geol. 99, 713–741.

Drummond, M.S., Defant, M.J., 1990. A model for trondhjemite-tonalite-dacite genesis and crustal growth via slab melting: archean to modern examples. J. Geophys. Res. 95 (B13), pp. 21, 503–21, 521.

Drummond, M.S., Defant, M.J., Kepezhinskas, P.K., 1996. Petrogenesis of slab-derived trondhjemite-tonalite-dacite/adakite magmas. Transactions of the Royal Society of Edinburgh, Earth Sciences 87, 205–215.

Elsass, P., Achard, D., 1979. Qidqad prospect (23/45 A), preliminary investigation results. Bureau de Recherches Geologiques et Minieres Open-File Report JED-OR 79-1.

Espinoza, S., 1990. The Atacama-Coquimbo ferriferous belt, northern Chile. In: Fontboté, L., Amstutz, G.C., Cardozo, M., Cedillo, E., Fruto, J. (Eds.), Stratabound ore deposits in the Andes. Spinger-Verlag, Berlin, pp. 353–364.

Espinoza, S.R., Véliz, H.G., Esquivel, J.L., Arias, J.F., Moraga, A.B., 1996. The cupriferous province of the coastal range, northern Chile. In: Camus, F., Sillitoe, R.H., Petersen, R. (Eds.), Andean copper deposits: new discoveries, mineralization, styles, and metallogeny., vol. 5. Society of Economic Geologists Special Publication, pp. 19–32.

Felenc, J., 1983a. Mineral exploration in the Marjan prospect. Saudi Arabian Deputy Ministry for Mineral Resources Open-File Report BRGM-OF-03-21.

Felenc, J., 1983b. Microgranitic sill, volcanic apophyses, and carbonatization as an ore-forming process (Au, Ag, Zn, Ba) in the Al Amar belt. Saudi Arabian Deputy Ministry for Mineral Resources Open-File Report BRGM-OF-03-26.

Felenc, J., Woldeabzhi, T., Vaillant, F., 1983. Mineral exploration in the Umm ad Dabah prospect. Saudi Arabian Deputy Ministry for Mineral Resources Open-File Report BRGM-OF-03-43.

Fleck, R.J., Coleman, R.G., Cornwall, H.R., Greenwood, W.R., Hadley, D.G., Prinz, W.C., Ratte, J.S., Schmidt, D.L., 1976. Potassium-argon geochronology of the Arabian Shield, Kingdom of Saudi Arabia. Geol. Soc. Am. Bull. 87, 9–21.

Frater, K.M., 1983. Geology of the Golden Grove prospect, Western Australia; a volcanogenic massive sulfide-magnetite deposit. Econ. Geol. 78, 875–919.

Gabrielse, H., 1985. Major dextral transcurrent displacements along the Northern Rocky Mountain Trench and related lineaments in north-central British Columbia. Geol. Soc. Am. Bull. 96, 1–14.

Goncalves, P., Nicollet, C., Lardeaux, J., 2003. Finite strain pattern in Andriamena unit (north-central Madagascar); evidence for late Neoproterozoic-Cambrian thrusting during continental convergence; evolution of the East African and related orogens, and the assembly of Gondwana. Precamb. Res. 123, 135–157.

Grocott, J., Taylor, G.K., 2002. Magmatic arc fault systems, deformation partitioning and emplacement of granitic complexes in the Coastal Cordillera, north Chilean Andes (25°30′S to 27°00′S). J. Geol. Soc. Lond. 159 (4), 425–442.

Hamilton, W., 1979. Tectonics of Indonesian region. U.S. Geological Survey Professional Paper 1078.

Hargrove, U.S., Hanson, R.E., Martin, M.W., Blenkinsop, T.G., Bowring, S.A., Walker, N., Munyanyiwa, H., 2003. Tectonic evolution of the Zambezi orogenic belt; geochronological, structural, and petrological constraints from northern Zimbabwe; evolution of the East African and related orogens, and the assembly of Gondwana. Precamb. Res. 123, 159–186.

Hayba, D.O., Bethke, P.M., Heald, P., Foley, N.K., 1985. Geologic, mineralogic, and geochemical characteristics of volcanic-hosted epithermal precious-metal deposits. In: Berger, B.R., Bethke, P.M. (Eds.), Geology and Geochemistry of Epithermal Systems. Rev. Econ. Geol. vol. 2, 129–162.

Heald, P., Foley, N.K., Hayba, D.O., 1987. Comparative anatomy of volcanic-hosted epithermal deposits: acid-sulfate and adularia-sericite types. Econ. Geol. 82, 1–26.

Hitzman, M.W., 2000. Iron oxide Cu–Au deposits: what, where, when, and why. In: Porter, T.M. (Ed.), Hydrothermal Iron Oxide Copper-Gold & Related Deposits: A Global Perspective 1. PGC Publishing, Adelaide, pp. 9–25.

Hitzman, M.W., Oreske, N., Einaudi, M.T., 1992. Geological characteristics and tectonic setting of Proterozoic iron oxide (Cu–U–Au–REE) deposits. Precamb. Res. 58, 241–287.

Johnson, P.R., 1996. Proterozoic geology of western Saudi Arabia, east-central sheet: description of Proterozoic map units. Saudi Arabian Deputy Ministry for Mineral Resources Open-File Report USGS-OF-96-4.

Johnson, P.R., 2005. Proterozoic geology of western Saudi Arabia, east-central sheet: (revised, digital edition). Notes on Proterozoic stratigraphy. Saudi Geological Survey Open-File Report SGS-OF-2004-9.

Johnson, P.R., Carten, R.B., Jastaniah, A., 1997. Tabulation of previously published U–Pb, Pb–Pb, Rb–Sr, and Sm–Nd numerical age data for the Precambrian of northeast Africa and Arabia (Second Edition). Saudi Arabian Deputy Ministry for Mineral Resources Open-File Report USGS-OF-97-1.

Johnson, P.R., Kattan, F.H., 2001. Oblique sinistral transpression in the Arabian shield: the timing and kinematics of a Neoproterozoic suture zone. Precamb. Res. 107, 117–138.

Johnson, P.R., Stewart, I.C.F., 1995. Magnetically inferred basement structure in central Saudi Arabia. Tectonopysics 245, 37–52.

Johnson, P.R., Vranas, G. J., 1984. The origin and development of late Proterozoic rocks of the Arabian shield; an analysis of terranes and mineral environments. Saudi Arabian Deputy Ministry for Mineral Resources Open-File Report RF-OF-04-32.

Johnson, P.R., Woldehaimanot, B., 2003. Development of the Arabian-Nubian Shield; perspectives on accretion and deformation in the northern East African Orogen and the assembly of Gondwana; Proterozoic East Gondwana; supercontinent assembly and breakup, vol. 206. Geological Society Special Publications, pp. 289–325.

Katz, O., Beyth, M., Miller, N., Stern, R., Avigad, D., Basu, A., Anbar, A., 2004. A late Neoproterozoic (approximately 630 Ma) high-magnesium andesite suite from southern Israel; implications for

Author's personal copy

the consolidation of Gondwanaland. Earth Plan. Sci. Lett. 218, 475–490.

Lavenu, A., Cembrano, J., 1999. Compressional- and transpressional-stress pattern for Pliocene and Quaternary brittle deformation in fore arc and intra-arc zones, Andes of Central and Southern Chile. J. Struct. Geol. 21, 1669–1691.

Le Bel, L., Laval, M., 1986. Felsic plutonism in the Al Amar-Idsas area, Kingdom of Saudi Arabia. J. Afr. Earth Sci. 4, 87–98.

Leistel, J.M., Saleh, Y., Khalil, I., Al-Jahdali, N., Itard. Y., Kattu, G., with the collaboration of Eberlé, J.M., Siddiqui, A.A., 2000. Results of precious-metal exploration in the Umm ash Shalahib prospect. Saudi Geological Survey Technical Report BRGM TR-99-19.

Lentz, D.R., 1998. Petrogenetic evolution of felsic volcanic sequences associated with Phanerozoic volcanic-hosted massive sulphide systems; the role of extensional geodynamics. Ore Geol. Rev. 12, 289–327.

Lofts, P.G., 1994. Al 'Amar gold deposit. In: Collenette, P., Grainger, D.J. (Eds.), Mineral Resources of Saudi Arabia. Saudi Arabian Directorate General of Mineral Resources Special Publication SP-2, pp. 95–99.

Lofts, P.G., Bognar, B., Howes, D.R., McHugh, J.J., Saleh, Y.T., 1986. Exploration of the Al Amar Prospect. Saudi Arabian Deputy Ministry of Mineral Resources Open-File Report RF-OF-06-1.

Ma'aden, 2005. Press release, Ma'aden signs an engineering procurement & construction management (EPCM) contract for development of Al-Amar mine in Reiyadgh region accessed 3 October 2005 at URL: http://www.maaden.com.sa/press.html.

Manivit, J., Pellaton, C., Vaslet, D., Le Nindre, Y., Brosse, J., Fourniguet, J., 1985a. Geologic map of the Wadi al Mulayh quadrangle, sheet 22H, Kingdom of Saudi Arabia. Saudi Arabian Deputy Ministry of Mineral Resources, Geoscience Map GM-92A, scale 1:250,000.

Manivit, J., Pellaton, C., Vaslet, D., Le Nindre, Y., Brosse, J., Fourniguet, J., 1985b. Geologic map of the Darma quadrangle, sheet 24H, Kingdom of Saudi Arabia. Saudi Arabian Deputy Ministry of Mineral Resources, Geoscience Map GM-101C, scale 1:250,000.

Martin, H., 1999. Adakitic magmas; modern analogues of Archaean granitoids; granites; crustal evolution and associated mineralization. Lithos 46, 411–429.

Martin, H., Smithies, R.H., Rapp, R., Moyen, J., Champion, D., 2005. An overview of adakite, tonalite-trondhjemite-granodiorite (TTG), and sanukitoid; relationships and some implications for crustal evolution; Geodynamic controls on adakite, TTG and sanukitoid genesis; implications for models of crust formation. Lithos 79, 1–24.

McClelland, W.C., Tikoff, B., Manduca, C.A., 2000. Two-phase evolution of accretionary margins: examples from the North American Cordillera. Tectonophysics 326 (1–2), 37–55.

Meert, J.G., 2003. A synopsis of events related to the assembly of eastern Gondwana; Paleomagnetism applied to tectonics; a tribute to Rob Van der Voo. Tectonophysics 362, 1–40.

Oyarzún, R., Oyarzún, J., Ménard, J.J., Lillo, J., 2003. The Cretaceous iron belt of northern Chile: role of oceanic plates, a superplume event, and a major shear zone. Miner. Depos. 38 (5), 640–646.

Pearce, J.A., Cann, J.R., 1973. Tectonic setting of basic volcanic rocks determined using trace element analyses. Earth Plan. Sci. Lett. 19, 290–300.

Pearce, J.A., Harris, N.B.W., Tindle, A.G., 1984. Trace element discrimination diagrams for the tectonic interpretation of granitic rocks. J. Petrol. 25, 956–983.

Reston, T.J., Gaw, V., Pennell, J., Klaeschen, D., Stubenrauch, A., Walker, I., 2004. Extreme crustal thinning in the South Porcupine Basin and the nature of the Porcupine median high: implications for the formation of non-volcanic rifted margins. J. Geol. Soc. Lond. 161 (5), 783–798.

Samsonov, A.V., Bogina, M.M., Bibikova, E.V., Petrova, A.Yu., Shchipansky, A.A., 2005. The relationship between adakitic, calc-alkaline volcanic rocks and TTGs: implications for the tectonic setting of the Karelian greenstone belts, Baltic Shield. Lithos 79, 83–106.

Scheuber, E., Gonzalez, G., 1999. Tectonics of the Jurassic-Early Cretaceous magmatic arc of the north Chilean Coastal Cordillera (22°–26°S): a story of crustal deformation along a convergent plate boundary. Tectonics 18 (5), 895–910.

Schwartz, M.O., Melcher, F., 2003. The Perkoa zinc deposit, Burkina Faso. Econ. Geol. 98, 1463–1485.

Sharpe, R., Gemmell, J.B., 2001. Alteration characteristics of the Archean Golden Grove Formation at the Gossan Hill Deposit, Western Australia; induration as a focusing mechanism for mineralizing hydrothermal fluids; a special issue devoted to alteration associated with volcanic-hosted massive sulfide deposits, and its exploration significance. Econ. Geol. 96, 1239–1262.

Sharpe, R., Gemmell, J.B., 2002. The Archean Cu–Zn magnetite-rich Gossan Hill volcanic-hosted massive sulfide deposit, Western Australia; genesis of a multistage hydrothermal system. Econ. Geol. 97, 517–539.

Stacey, J.S., Agar, R.A., 1985. U–Pb isotopic evidence for the accretion of a continental microplate in the Zalm region of the Saudi Arabian shield. J. Geol. Soc. Lond. 142, 1189–1203.

Stacey, J.S., Stoeser, D.B., 1983. Distribution of oceanic and continental leads in the Arabian-Nubian shield. Contrib. Min. Petrol. 84, 91–105.

Stacey, J.S., Stoeser, D.B., Greenwood, W.R., Fischer, L.B., 1984. U–Pb zircon geochronology and geologic evaluation of the Halaban-Al Amar region of the eastern Arabian Shield. J. Geol. Soc. Lond. 141, 1043–1055.

Stern, R.J., 1994. Arc assembly and continental collision in the Neoproterozoic East African Orogen: implications for consolidation of Gondwanaland. Annu. Rev. Earth Planet. Sci. 22, 319–351.

Stern, C.R., Kilian, R., 1996. Role of the subducted slab, mantle wedge and continental crust in the generation of adakites from the Andean Austral Volcanic Zone. Contrib. Min. Petrol. 123, 263–281.

Stoeser, D.B., Camp, V.E., 1985. Pan-African microplate accretion of the Arabian Shield. Geol. Soc. Am. Bull. 96, 817–826.

Stoeser, D.B., Frost, C.D., 2006. Nd, Pb, Sr, and O isotopic characterization of Saudi Arabian shield terranes. Chem. Geol. 226, 163–188.

Stoeser, D.B., Stacey, J.S., 1988. Evolution, U–Pb geochronology, and isotope geology of the Pan-African Nabitah orogenic belt of the Saudi Arabian shield. In: El-Gaby, S., Greiling, R.O. (Eds.), The Pan-African Belt of Northeast Africa and Adjacent Areas. Vieweg and Sohn, Braunschweig/Weisbaden, pp. 227–288.

Stoeser, D.B., Whitehouse, M.J., Stacey, J.S., 2004. Neoproterozoic evolution of the Khida terrane, Saudi Arabia: a detached microplate in the Arabian craton. In: Proceedings of 32nd International Geologic Congress, Florence, Italy.

Taylor, G.K., Grocott, J., Pope, A., Randall, D.E., 1998. Mesozoic fault systems, deformation and fault block rotation in the Andean forearc: A crustal scale strike-slip duplex in the Coastal Cordillera of northern Chile. Tectonophysics 299 (1–3), 93–109.

Testard, J., 1982. At Taybi prospect. Saudi Arabian Deputy Ministry for Mineral Resources Open-File Report BRGM-OF-02-1.

Author's personal copy

Testard, J., 1983. Khnaiguiyah, a synsedimentary hydrothermal deposit comprising Cu–Zn–Fe sulfides and Fe oxides in an ignimbritic setting. Saudi Arabian Deputy Ministry of Mineral Resources Open-File Report BRGM-OF-03-9.

Thieme, J., 1988. Geologic map of the Jabal Khida quadrangle, sheet 21 G, Kingdom of Saudi Arabia. Saudi Arabian Directorate General of Mineral Resources Geologic Map GM-90, scale 1:250,000.

Ueda, H., Usuki, T., Kuramoto, Y., 2004. Intraoceanic unroofing of eclogite facies rocks in the Omachi seamount, Izu-Bonin frontal arc. Geology 32 (10), 849–852.

Unrug, R., 1996. The assembly of Gondwanaland. Episodes 19, 11–19.

Vadala, P., Beziat, P., Saleh, Y., Ralay, F., Siddiqui, A.A., Shanti, M., with the collaboration of Lemiere, B., 1994. Reconnaissance for precious metals in the Al Amar belt and its environs. Saudi Arabian Directorate General of Mineral Resources Technical Report BRGM-TR-12-8.

Vaslet, D., Manivit, J., Le Nindre, Y., Brosse, J., Fourniguet, J., Delfour, J., 1983. Geologic map of the Wadi Ar Rayn quadrangle, sheet 23 H, Kingdom of Saudi Arabia. Saudi Arabian Deputy Ministry of Mineral Resources Geoscience Map GM-63A, scale 1:250,000.

Winchester, J.A., Floyd, P.A., 1977. Geochemical discrimination of different magma series and their differentiation products using immobile elements. Chem. Geol. 20, 323–343.

Woldeabzghi, T., Prevot, J. C., 1983. Mineral exploration of the Wadi Sidarah prospect. Saudi Arabian Deputy Ministry for Mineral Resources Open-File Report BRGM-OF-03-44.

Wood, D.A., 1980. The application of a Th-Hf-Ta diagram to problems of tectonomagmatic classification and to establishing the nature of crustal contamination of basaltic lavas of the British Tertiary volcanic province. Earth Planet. Sci. Lett. 50, 11–30.

Zubeir, M.O., 1976. Geological, petrological, and geochemical study of the Ruga'an mafic-ultramafic layered intrusion. M.Sc. Thesis, Institute of Applied Geology, King Abdulaziz University, Jiddah.